INFORMATION TO USERS

This manuscript has been reproduced from the microfilm master. UMI films the text directly from the original or copy submitted. Thus, some thesis and dissertation copies are in typewriter face, while others may be from any type of computer printer.

The quality of this reproduction is dependent upon the quality of the copy submitted. Broken or indistinct print, colored or poor quality illustrations and photographs, print bleedthrough, substandard margins, and improper alignment can adversely affect reproduction.

In the unlikely event that the author did not send UMI a complete manuscript and there are missing pages, these will be noted. Also, if unauthorized copyright material had to be removed, a note will indicate the deletion.

Oversize materials (e.g., maps, drawings, charts) are reproduced by sectioning the original, beginning at the upper left-hand corner and continuing from left to right in equal sections with small overlaps. Each original is also photographed in one exposure and is included in reduced form at the back of the book.

Photographs included in the original manuscript have been reproduced xerographically in this copy. Higher quality 6" x 9" black and white photographic prints are available for any photographs or illustrations appearing in this copy for an additional charge. Contact UMI directly to order.

UMI

A Bell & Howell Information Company
300 North Zeeb Road, Ann Arbor MI 48106-1346 USA
313/761-4700 800/521-0600

THE ROLE OF ELECTRIC FIELDS IN THE OCCURRENCE, STRUCTURE, AND DRIFT OF THIN METALLIC ION LAYERS IN THE HIGH-LATITUDE IONOSPHERE

A

THESIS

Presented to the Faculty
of the University of Alaska Fairbanks
in Partial Fulfillment of the Requirements
for the Degree of

DOCTOR OF PHILOSOPHY

By
David Franklin Bedey, B.S., M.S., M.A.

Fairbanks, Alaska
May 1996

THE ROLE OF ELECTRIC FIELDS IN THE OCCURRENCE, STRUCTURE, AND DRIFT OF THIN METALLIC ION LAYERS IN THE HIGH-LATITUDE IONOSPHERE

By

David Franklin Bedey

RECOMMENDED:

Advisory Committee Chair

Department Head

APPROVED:

Dean, College of Natural Sciences

Dean of the Graduate School

4-12-96

Date

ABSTRACT

Metallic ions deposited in the upper atmosphere through the process of meteoroid ablation can, on occasion, be forced into dense layers at altitudes of 90-120 km with a thickness of <2 km. These layers result from a combination of appropriately directed neutral winds and electric fields. The objective of this thesis is to gain new insights into several poorly understood aspects of these atmospheric structures.

An experimental program has been developed to determine layer morphology and temporal occurrence in relation to ionospheric electric fields. These metallic ion structures have been found to be often spatially limited, and highly variable in both their location and time of occurrence. Simultaneous electric field measurements confirmed the dominant role of these fields in the formation of thin layers at high latitudes.

A time-dependent numerical model was used to simulate data, in an attempt to understand why layers tend to be observed at lower altitudes than theoretically predicted. It was found that adopting a reduced value for the ion-neutral collision frequency brings observations and theory into agreement. Empirical determinations of the collision frequency indicated values that are about a factor of ten smaller than predicted by the induced-dipole model now used in other ionospheric studies.

Observations indicate a greater rate of layer occurrence during the summer months. An explanation for this seasonal effect is proposed that invokes an annual variation in large-scale electric fields, suggested by an empirical model of the high-latitude convection pattern.

The large-scale circulation of metallic ions has been investigated. This examination suggests that the structure of the convection pattern controls the redistribution of metallic ions, which in turn defines where and when layers may occur. The results of this analysis explain the limited times of layer occurrence, as well as the absence of layers even when appropriate formation conditions exist.

Finally, a theoretical analysis indicated that layers can drift horizontally at speeds exceeding 100 m/s. Observations confirmed this result. This suggests that advection may be important when interpreting observations of evolving metal layers.

TABLE OF CONTENTS

LIST OF FIGURES

LIST OF TABLES

PREFACE

Over the past few years, the study of thin metallic layers in the upper atmosphere has received increasing attention in large part due to observations of neutral layers made with lidars, and of ion layers made with incoherent-scatter radars. Layers, both neutral and ionic, have been observed at middle latitudes and at high latitudes. Formation of ion layers at mid-latitudes is associated with the neutral wind (tides and gravity waves), while at high latitudes the convective electric field often controls layer formation. The formation mechanism for neutral layers remains an open question, one complicated by the current imprecise knowledge of gas-phase metallic chemistry. A connection (if any exists) between neutral layers and ion layers is yet to be established. Thus, much work, both theoretical and observational, remains to be accomplished. This subject is of importance, because the explication of the nature of these small-scale structures tests our understanding of the dynamics of the upper atmosphere. It is hoped that this thesis will contribute to advancing our knowledge of thin layer phenomena.

I owe a debt of gratitude to my advisor and friend, Professor Brenton Watkins, who introduced me to this exciting field and treated me as a colleague throughout the accomplishment of this research program. I look forward to a continuing professional relationship with Brent; we make a good team. I also appreciate the support lent me by the other members of my advisory committee, Dean Joseph Kan, Professor John Pender, and Professor Daniel Swift. I especially wish to acknowledge Dr. Swift's acute criticisms of early drafts of this thesis; he taught me to question my assumptions and in doing so open my mind to new possibilities.

This effort would not have been possible without the support of my best friend (and wife), Deborah. She put me back on track whenever my concentration waned. Finally, I dedicate this thesis to our daughter, Karis Alise. Accomplishments are made sweeter when shared with those you love. I am indeed lucky.

D.F.B.

CHAPTER 1
INTRODUCTION

1.1 General

Metallic ion structures of thickness less than 2 km, occurring in a nominal altitude range of 90-120 km, have long been connected to the mid-latitude sporadic-E detected by ionosondes (Whitehead, 1961; Axford, 1963; Axford and Cunnold, 1966). Following the general theoretical development of Dungey [1959], these authors showed that a shear in the neutral wind could lead to vertical convergence of ions, since ion motion is strongly influenced both by the inclination of the geomagnetic field, and by collisional coupling with the neutral component of the atmosphere. Thin ion structures have been observed at middle latitudes using a variety of instruments, including ionosondes, rocket-borne mass spectrometers, and incoherent-scatter radars. These observations have generally confirmed the wind-shear mechanism. Layer formation by the action of neutral winds is reviewed in the next section of this chapter.

As one moves to higher latitudes the wind-shear mechanism becomes less effective, due to the increase in the dip angle of the geomagnetic field. Additionally, at high latitudes, strong electric fields of magnetospheric origin map into the ionosphere. It has been shown that such electric fields can often dominate the effects of the neutral wind, and when appropriately directed should cause layers to form (Nygrén et al., 1984a; Kirkwood and von Zahn, 1991; Bristow and Watkins, 1991). At high latitudes, incoherent-scatter radars (one is located at Sondrestrom in Greenland, another near Tromsø, Norway) have been the instruments of choice, since the signature of auroral precipitation on ionograms is sometimes difficult to differentiate from that of a thin layer. Observations (reviewed later in this chapter) show that the relationship of electric field direction to the occurrence of thin layers is not as simple as suggested by the prevailing theory of layer formation. Layers often form at lower altitudes than predicted, while those expected to form at low altitudes tend to be thinner than anticipated. Quite dense thin

structures suddenly appear, and just as abruptly disappear with no obvious change in the electric field. Moreover, layers often appear to drift across the field of view. This complicated situation suggests that proper electric field direction may be a necessary, but not sufficient, condition for metallic ion layers to form *and persist*. An additional complication is that even at high latitudes the wind-shear mechanism can dominate, if electric fields are weak, necessitating care to discriminate between layers formed by the action of the neutral wind and those due to convective electric fields.

The purpose of this study is to reevaluate the role of electric fields in the formation of thin metallic ion layers, with the aim of reconciling theory with observation. In the next two sections of this chapter, the wind-shear and electric field mechanisms are reviewed. Then the scope of this investigation is outlined, and its objectives presented in the form of a series of scientific questions. The chapter concludes with a description of the organization of the balance of this work.

1.2 Formation of Thin Ion Layers at Middle Latitudes

Although this thesis focuses on metallic layers at high latitudes, where electric fields often control the dynamics of their formation, it is useful to begin the study of thin ion-structures with a review the phenomenon at temperate latitudes, where shears in the large-scale neutral winds dominate. This is so for two reasons. First, the conceptual development is virtually identical; much of the earlier work carries over directly to the present study. Second, it is important from an observational standpoint to be able to differentiate between layers formed by the two processes, since either might occur at higher latitudes, depending on the magnitude of the convective electric field. The coverage is not meant to be exhaustive, but rather is tailored to support the specific questions being examined in this thesis. For a good review on mid-latitude sporadic-E (and by extension, metallic thin layers), see Whitehead [1989].

The early history of research on metallic ion layers is inextricably tied to the study of sporadic-E (E_s). Understanding the nature of E_s was a subject of considerable interest to

those involved in the design and operation of high frequency radio systems. E_s had been observed in some detail since the 1940s using ionosondes, most of which were located at temperate latitudes. The resultant ionograms showed that sporadic E is a quite complicated phenomenon (Piggott and Rawer, 1961). Whitehead [1961] offered the first explanation for features often seen at mid-latitudes. He argued that the observed dependence of the occurrence of E_s on the horizontal component of the geomagnetic field could be explained by Dungey's [1959] wind-shear mechanism. Briefly, vertical motion of ions in the presence of an inclined magnetic field can arise due to shears in the horizontal neutral wind. At relatively high altitudes, where the ratio of ion-neutral collision frequency to gyrofrequency is low, ions will be forced to move along magnetic field lines under the influence of magnetically meridional winds. A sheared meridional wind with northward flow above southward flow will yield convergence of ions at the null in the wind profile. At lower altitudes, where the collision frequency is greater, the ions tend to be dragged across magnetic field lines by the horizontal neutral wind. In this case, the magnetically zonal neutral wind is most influential; ions moving with it will experience a Lorentz force with a vertical component. In this case, westward winds over eastward winds yield convergence. Extending this argument to lower altitudes, the collision frequency can become so large that the ions are constrained to follow the neutral wind with very little Lorentz deflection (in this region the usually negligible vertical component of the wind can dominate the effects of wind shear). The specific altitudes dividing these three regimes depend upon such parameters as magnetic dip and the assumed model for the collision frequency. As an representative example (Chimonas and Axford, 1968), the uppermost region is above 120 km, while the lowest is below 95 km.

Several theoretical papers appeared over the next few years which expanded upon Whitehead's work (e.g., Axford, 1963; Whitehead, 1966; Axford and Cunnold, 1966; Chimonas and Axford, 1968). There was some debate on whether the ions forming the layers are predominantly molecular (i.e., O_2^+ and NO^+) or meteoric metallics (e.g., Fe^+ and Mg^+). This was settled in favor of the metallic ions from the results of a number of

observations made with rocket-borne mass spectrometers (e.g., Istomin, 1963; Narcisi and Bailey, 1965), which have since been supported by incoherent-scatter radar observations (e.g., Behnke and Vickrey, 1975; Huuskonen et al., 1988). Since the lifetimes of the metallic ions are much greater than that of the molecular ions, this finding also suggests that layer lifetimes are controlled by diffusion rather than recombination.

The sources of wind-shear structures were assumed to be atmospheric tides and atmospheric gravity waves (Axford, 1963; Chimonas and Axford, 1968). A layer forms at a node in the tidal or gravity-wave structure, then moves downward, following the phase progression of the wave, until the collision frequency becomes so great that the wind-shear mechanism is no longer effective. Chimonas and Axford dubbed this altitude, at which the ions are totally controlled by collisions with the neutral wind, the "dumping altitude." This behavior has been often observed (e.g., Constantinides and Bedinger, 1971; Geller et al., 1975; Mathews and Bekeny, 1979); in fact, marked downward motion can be considered a distinguishing characteristic of layers formed by the wind-shear mechanism. While direct connection of layers to gravity waves remains somewhat speculative (the problem being to show that gravity waves are indeed present), the evidence in support of a tidal source is quite compelling (Miller, 1995).

Studies conducted with rocket-borne mass spectrometers have yielded much useful information beyond confirmation of the metallic composition of the thin ion layers. There is strong evidence that on average there exists globally a broad metallic ion layer with a density peak at around 95 km (half-width of 5-10 km), primarily composed of Na^+, Mg^+, and Fe^+ with ionic iron being most abundant at a peak density of $\sim 5 \times 10^3$ cm^{-3} (e.g., Narcisi, 1971; Zbinden et al., 1975). Thinner layers with density an order of magnitude greater than the background layer have also been observed to form, superimposed on the background layer, presumably from relatively localized redistribution of ions. By comparison, well above the world-wide layer (>110 km), mid-latitude thin layers tend to follow the scheme of downward drift to a dumping altitude, where the peak density is often as low as 10^2 to 10^3 cm^{-3}. The appearance of two apparently different

types of thin layers, dependent on altitude, has led some to speculate that the wind-shear mechanism is not the primary cause for those observed at low altitudes (Smith and Mechtly, 1972). However, an alternate explanation is that the wind-shear mechanism operates in both cases: at the lower altitudes gravity waves with relatively large shears drive layer formation; higher up atmospheric tides can play the ascendant role

Several aspects of the morphology of thin layer phenomena cannot be adequately addressed by the wind-shear theory by itself, and remain open to interpretation. Some of these issues are discussed below. For example, the horizontal extent of thin layers at temperate latitudes seem to be on the order of hundreds of kilometers, based of rocket observations (Whitehead, 1989). However, within a layer there often appear patches of increased ionization (e.g., Miller and Smith, 1975). Such structure within a layer has been attributed to horizontal variation in the wind-shear system (From and Whitehead, 1978), or to interaction between tides and gravity waves (Chimonas, 1971). Another well-established fact is that the occurrence of E_s, equatorward of a geomagnetic latitude of 60°, has a strong seasonal dependence, with most being observed during the summer months (Smith, 1978; Whitehead, 1989). This behavior does not appear to be correlated to periodic variations in the meteoric influx (Trísková, 1974; Smith, 1978; Baggaley and Steel, 1984). The cause of the seasonal variation in E_s remains a mystery, but may well be determined by world-wide transport of metallic ions.

1.3 Formation of Thin Ion Layers at High Latitudes

The study of thin ionization structures at auroral latitudes has begun more recently. Here layers can form under the action of wind-shear, the convective electric field, or a combination of the two. In an extension of the basic approach used for developing the wind-shear theory, Nygrén et al. [1984a] showed that an electric field directed in the magnetic northwest quadrant (in the Northern Hemisphere) could force ions to converge from above and below at a null in their vertical velocity profile. This process is detailed in Chapter 3, but is easy to understand in a qualitative sense. At high altitudes a mag-

netically westward component of the electric field drives ions downward through **ExB** drift. Lower down, where ion-neutral collisions are more frequent, the component of the field normal to the magnetic field and directed to the north gives rise to an upward Pederson drift. The altitude of the *convergent null* in the vertical velocity profile of the ions is determined by the altitudinal variation of the ion-neutral collision frequency. Nygrén and his coworkers noted that layers observed in the morning and late afternoon at high latitudes might well be caused by wind shear, but that those seen near local midnight were most likely associated with the structure of the convective electric field. Bristow and Watkins [1991] used a one-dimensional simulation to show that measurable layers should form when the electric field is directed to the southwest, as a consequence of uniformly downward motion toward a dumping altitude. They argued that such layers should appear at lower altitudes than those forming when the field is to the northwest. Kirkwood and von Zahn [1991] extended this reasoning further, demonstrating that broad layers could form for electric fields directed to the southeast as well, since this would create downward ion motion below the altitude of a *divergent null* in the vertical ion velocity profile. They pointed out that layers forming for southerly electric fields should have asymmetric profiles, in contrast to the case of NW fields. In a later theoretical analysis, Kirkwood and von Zahn [1993] argued that southward electric fields should enhance tidal E_s, while northward fields, even weak ones, should interfere with the formation of tidal E_s.

All of these studies indicate that layers, caused by an appropriately directed electric field, should form in a matter of tens of minutes for fields magnitudes exceeding 30-50 mV/m (the actual time decreasing with increasing electric field magnitude). Those layers formed by an electric field to the northwest would form above 120 km, but would not drift downward (assuming that the field direction did not change). Those forming due to southerly fields would appear below 105 km, and would show slight downward motion. Also, for a given electric field magnitude and ion column density, the layers formed by a southward field should be thicker, less symmetric, and less dense than those forming

when the field is to the northwest. It should be noted that the simulations of layer formation assumed a substantial population of metallic ions above background metallic ion layer which resides at 85-105 km (Kirkwood and von Zahn used an initial Gaussian ion profile centered at 105 km with a width of 40 km (full-width at half maximum), while Bristow and Watkins used a profile peaked at an altitude of 120 km tapering off above and below). The availability of metallic ions at relatively high altitudes is essential for layer formation above 100 km (how ions get there will be discussed in Chapter 3).

Accompanying the theoretical developments concerning the role of electric fields in the formation metallic thin layers, there have been a number of incoherent-scatter radar observations of thin layers at high latitudes. A review of the literature revealed seven studies made using the European Incoherent Scatter Facility (EISCAT) radar near Tromsø, Norway (69.58° N, 19.23° E; invariant latitude, 66.2° N; dip angle, 78.1°). Another was made with the National Science Foundation (NSF) supported radar at Sondrestrom in Greenland (66.99° N, 309.05° E; invariant latitude 73.9° N; dip angle, 80.5°). In all, over 20 layers were observed at EISCAT (an exact count is somewhat subjective, since some papers report what appear to be single layers as a series of "events" which vary according to the behavior of the layer), and 12 at Sondrestrom. Some found layers which were much like those seen at mid-latitudes (and thus deduced to have formed due to wind-shear), others were attributed to the action of electric fields. As a whole, what emerges is a series of partial validations of the theory. The results of each study are summarized below.

Turunen et al. [1985] observed one layer at EISCAT on 16 November 1983. The radar was operating with a vertical beam and a spatial resolution of 450 m. This layer was over the radar for six minutes (1800-1806 UT) at an altitude of 106 km. Its thickness was 1-1.5 km and the peak density was 4×10^5 cm^{-3}. Simultaneous measurement of the electric field by the STARE radar (the STARE radar is described in Greenwald et al. [1978]) indicated a field strength of 25-30 mV/m. The field over the radar was directed to the SW until 1802 UT, at which point it turned to the NW. The authors offered this

observation as plausible validation of the theory of Nygrén et al. [1984a], but acknowledged that the layer may have formed elsewhere, then drifted over the radar. The layer observed here displayed the characteristics of one formed by a NW electric field, except for one. It formed far lower than theoretically expected for such a field. On the other hand the layer was thinner than one predicted for a southerly field.

Turunen et al. [1988] observed another layer at EISCAT on 14 August 1986. The radar operated with a vertical beam and spatial resolution of 300 km. The layer had been in existence for several hours (presumably based on ionosonde measurements), but was only observed from 1145-1250 UT with the radar. It had a thickness of 2 km, and a peak density of $3x10^5$ cm^{-3}. It was initially at an altitude of 102 km, but rose to 105 km while under observation. Electric fields were not measured. The authors noted that E_s should only move downward with the descending nodes of tides, or remain stationary at the dumping altitude. They speculated that the electric field may have a role in the uplift of the layer.

Huuskonen et al. [1988] reported eight events at EISCAT, which upon further examination appear to represent four thin layers, all with peak density ~10^5 cm^{-3}. The radar was directed vertically with a range resolution of 600 m (the primary objective of the experiment was to determine the ion composition of E_s). The first layer occurred on 18 August 1984, 0410-0530 UT. This layer was first at 114 km, then dropped to 108 km in approximately 15 min. The second layer occurred on 18 August 1984, from 2150 to 2310 UT. This layer was initially at an altitude of 100 km with a thickness of 2 km. It then descended to 96 km before vanishing. The third layer occurred on 19 August 1984, 0025-0150 UT. It was initially at 100 km, but fell to 96 km in 20 minutes, where it remained until vanishing from the beam of the radar. The fourth layer was also observed on 19 August 1984. It lasted one hour (0200-0300 UT), and remained at a constant altitude of 97 km. No electric fields were observed for this experiment, and therefore the electric field mechanism cannot be evaluated in this case. The authors were careful to suggest that horizontal motion (not measured) of the layers may influence the apparent

lifetimes. Three of the four layers described in this study were at or below 100 km, while one appeared above 110 km. Downward layer motion was a common feature, but was generally limited to a few kilometers.

Kirkwood and Collis [1989] observed two layers at EISCAT on 12-13 August 1986. The first appeared at 98 km from 2240 to 2315 UT, with a density well over 10^5 cm^{-3}. It was followed by a very weak layer at about 95 km from 2325 to 2350 UT, descending to 92 km where it lasted until 0150 UT. The electric field was observed to be directed to the SE, and was weak (usually less than 5 mV/m). Kirkwood and Collis attributed these layers to the passage of a gravity wave.

Kirkwood and von Zahn [1991] described four layers observed at EISCAT. The radar was operated in a four-position mode, which allows for the determination of the electric field overhead, but yields little more information on the spatial extent and horizontal motion of layers than does a fixed beam experiment. On 21 October 1987, 1920-2030 UT, a layer was observed between 100 and 105 km. The electric field was to the SW at 40 mV/m. On 12 November 1988, 2208-2220 UT, a layer formed at 106 km. The electric field had been to the NW for several hours before the layer appeared, but swung momentarily to the SW as the layer appeared over the radar. The third layer was observed on 12 August 1986, 2250-2315 UT at an altitude of approximately 100 km. In this case the electric field was to the SE at 20 mV/m. On 14 February 1985, a very short-lived (1955-2005 UT) layer was observed at approximately 125 km, when the electric field was to the NW at 40-60 mV/m. The authors drew several implications from this data. First, most layers formed when the electric field was to the south, but were thinner than expected from theory. This discrepancy was attributed to the possible existence of an upward vertical wind, which would tend to sharpen the density peak. The February event was offered as a case when NW electric fields led to the convergence of molecular ions. Kirkwood and von Zahn suggested that the lack of layers at other times when NW fields were present (as seen on 12 November 1986) resulted from

fluctuations in the field which, would cause the altitude of convergence to also fluctuate, thus "smearing" the layer out.

Turunen et al. [1993] conducted observations at EISCAT for three nights over the period 9-12 December 1990 for geomagnetically quiet times. They saw many layers, typically with of low density (< $8x10^4$ cm^{-3}), forming at high altitudes (120 to 140 km), and drifting downward to an apparent dumping altitude between 100 and 110 km. The meridional electric field was also measured, and found to be nearly zero on average, with fluctuations of ±10 mV/m. The authors attributed these layers to the wind-shear mechanism (tides or gravity waves). This assertion is strongly bolstered by the striking resemblance of their results to those of Mathews et al. [1993] from radar observations at Arecibo (18.3° N, 293.2° E; 50° dip angle).

Kirkwood and von Zahn [1993] in the course of a month-long campaign (10 September to 4 October 1991) at EISCAT detected six layers with the incoherent-scatter radar. Characteristics of these layers are presented in Table 1.1. They argue that these layers probably formed under the combined action of electric fields and wind shear. The assumption of an upward neutral wind is an important element in their interpretation of this data, since the layers were seen to be thinner, and more symmetric than those predicted to form under the action of a southward electric fields, by itself. Significantly, Kirkwood and von Zahn are silent on whether NW electric fields were observed, so one cannot judge the relative effectiveness of this mode of layer formation.

Bristow and Watkins [1993] conducted a series of observations at Sondrestrom over a one year period (August 1990 through August 1991) in three different radar modes.

Table 1.1 Summary of Layers reported by Kirkwood and von Zahn [1993].

DATE	TIME (UT)	DENSITY (cm^{-3})	ALTITUDE (km)	WIDTH (km)	E-FIELD (mV/m)
10 Sep 91	2120->2320	$>4x10^4$	96 to 93	2.5	20SW to 20S
11 Sep 91	1954-2012	$8x10^5$	102 to 97	1.5	20SW
17 Sep 91	2250->2340	$2x10^4$	93 to 95	2.0	15S to 7SE
18 Sep 91	2224-2320	$2x10^4$	98 to 92	3.0	30W to 40S
20 Sep 91	2130->2400	$1x10^5$	97 to 89	1.5	10S to 180SE
22 Sep 91	2257-2314	$4x10^5$	101 to 98	1.5	5S to 20S

Table 1.2 *Layer and Electric Field Data from Bristow and Watkins [1993].*

DATE	TIME (UT)	ALTITUDE (km)	E-FIELD DIR. (deg W of N)	E-FIELD MAG. (mV/m)
17 Aug 1990	2200	105	70-100	4
	2320-2340	115	80-130	4-6
18 Aug 1990	2200-2230	105	60-140	2
22 Aug 1990	2150-2315	105-115	40-100	14-18
12 Mar 1991	2300-2315	110	80	24-34
	2315-0010	100	100	20
13 Mar 1991	0015-0120	100	100-120	5-15
26 Jul 1991	2105-2120	115	80-100	4-6
3 Aug 1991	2340-0015	100	80-100	24-26

Layers were observed on 12 of 16 nights. One mode was designed to measure ion temperature. It revealed a layer on 27 July 1991, persisting from 2000 to 2200 UT, at an altitude of 110 km. This layer was 2 km thick, and was quite dense (~10^6 cm^{-3}). The second mode, for which the radar scanned along the magnetic meridian, was used for three nights in late July and early August 1991. This unique experiment revealed that layers have limited latitudinal extent, typically about 100 km. The layers observed also appeared to drift from north to south. The electric field was not measured in the above two experiments, but was when the radar was operated in its third mode. Characteristics of the seven layers detected in this mode are described in Table 1.2. Layer thickness ranged from 1.5 to 2.5 km, and the peak density always exceeded 10^5 cm^{-3} (Bristow, 1992). As can be seen, the electric field was in the NW or SW quadrant when layers were observed. However, Bristow and Watkins found that on nights when no layers were observed, the electric field was also often in one of these two quadrants. Contrary to the findings of Kirkwood and von Zahn, Bristow and Watkins' results lend some support to Nygrén's theory of layer formation for NW electric fields. However, the layers formed at altitudes less than that predicted by theory, and once again did not appear whenever favorable electric fields were above the station.

1.4 Scope of this Study

The focus of this study is on the formation of thin metallic ion layers at high latitudes for geophysical conditions when the effects of electric fields dominate those of the neutral winds. For strong enough electric fields, the winds will play a minor role, especially at altitudes above 105 km. At lower altitudes (<100 km) it is difficult to separate the effects of winds and electric fields. As discussed in the previous section, at higher altitudes layers under the influence of the wind-shear mechanism display distinguishing behavior, as seen by Turunen et al. [1993]. This proves useful when evaluating observations of thin layers.

As can be seen in the previous section, much work remains to be done before a clear understanding of thin metallic layers at high latitudes is to be had. The observational base is lacking, but several problem areas are apparent. First, orientation of the electric field in the northwest quadrant does not appear to assure the formation of a layer, and when layers do form for this field orientation they tend to be lower than anticipated. This suggests both a deficiency in the current theory of layer formation, and the possibility of an inadequate population of metallic ions at the requisite altitudes. Second, the contention that southerly fields can contribute to layer formation is better supported, but once again their existence is no guarantee of layer formation. Third, the effect of layer transport cannot be evaluated from previous experiments, due either to modes of operation which did not allow for detection of layer advection, or did not concurrently measure the electric field. Thus, the possibility of layer formation remote from the radar site (where electric fields may be favorably oriented) cannot be assessed. This possibility clearly may impact the validity of tests of the theory based on measurement of the local electric field.

The observations also suggest new lines of inquiry. The horizontal extent of layers at high latitudes seems to be much smaller than for layers formed at temperate latitudes. Does this result from the spatial structure of the convective electric field? The observations also indicate that those layers most likely to be associated with electric fields tend to occur during the summer, but are too few to draw statistically reliable conclusions. Is there a seasonal effect in the occurrence layers, similar to that seen at lower latitudes? If so, what is its cause?

The present investigation seeks to resolve the issues raised above, and to explore aspects of the role of electric fields in the formation of thin metallic ion layers not before examined. Both theoretical and observational initiatives are undertaken. The current theory of vertical ion transport is reevaluated, with emphasis on the significance of the ion-neutral collision frequency in determining the altitude of layer formation. A theoretical analysis of horizontal transport, as it relates to the drift motion of layers, is com-

pleted. The role of direct meteoric input of metals into the upper atmosphere is studied to ascertain its effect on the seasonal and altitudinal distributions metallic ions. A new model of the convection field (Weimer, 1995) is used to examine the impact of spatial and temporal variations in the electric field on layer formation. Supporting this theoretical effort was a year-long observational program, conducted at Sondrestrom, which employed a novel radar experiment. This new radar mode allows for determination of ion density along the magnetic meridian (like a standard scanning experiment), and also for simultaneous calculation of the convective electric field along the meridian. Direct estimation of the velocity of layer drift is also possible.

At the conclusion of this study, answers to the following scientific questions are put forward:

- Why aren't thin layers observed whenever the electric field is "properly" oriented (according to the current theory of layer formation)?
- Why are layers observed at lower altitudes than predicted by the current theory when the electric field is directed to the northwest?
- To what extent do thin ion layers drift horizontally?
- What is the typical horizontal dimension of high-latitude thin ion layers?
- Is there seasonal variation in the occurrence of thin layers, and if so what is its cause?

1.5 Organization

Before delving into the transport of metallic ions, it is necessary to set the stage by examining from where the metals come, and the subsequent chemistry which modifies their populations. Chapter 2 provides an overview of the processes which establish the population of metallic ions in the upper atmosphere. The primacy of ion transport (versus direct meteoric deposition and metallic chemistry) is established.

Chapter 3 is a comprehensive development of the theory of thin ion layer formation. The current theory of (vertical) ion motion is revisited with emphasis on the importance of ion-neutral collision frequency, and the sensitivity of convergence altitude to the specific direction of the electric field. Then new ground is broken by considering horizontal ion motion. Horizontal layer drift is calculated as a function of electric field strength and direction. The basic theory is coupled with a one-dimensional model of layer formation, in order to address a number of the scientific questions identified in the previous section.

Chapter 4 contains a description of incoherent-scatter radar observations made at Sondrestrom in the course of this investigation. The design of the radar experiment allows for the simultaneous determination of the ion density (as a function of time, latitude, and altitude), and of the convective electric field (as a function of time and latitude). Furthermore, the velocity of horizontal drift of a layer as a whole is measured in several cases.

In Chapter 5, a qualitative analysis of the occurrence of thin metallic ion layers is outlined. This effort represents a synthesis of the theoretical and observational results addressed in the earlier chapters. These results, coupled with a realistic model of the convective electric field (Weimer, 1995), allow one to gain useful insights into the spatial and temporal distribution of thin layers.

In Chapter 6, conclusions that can be drawn on the basis of this work are presented along with a description of unresolved issues. In addition, some of the results of this study have implications beyond the scope of the scientific questions explicitly addressed; these will be commented upon here. Finally, directions for further investigation are suggested.

CHAPTER 2
METALS IN THE UPPER ATMOSPHERE

2.1 Introduction

Although the emphasis of this thesis is upon the role of transport in the formation of thin metallic ion layers, it is instructive to first examine the source and chemistry of metals in the upper atmosphere. These processes obviously establish the population of the ions from which layers form. Beyond this, one cannot *a priori* dismiss their potential for a direct role in layer formation. The objective of this chapter is to provide a perspective on the importance of meteoric deposition and metallic chemistry with respect to the formation of thin ion layers.

The primary source of metals in the upper atmosphere is now accepted to be the ablation of meteors. The spectra of meteorite fragments and those of the vapor trails of meteors are in good agreement (Harvey, 1973; Hughes, 1973). The major metallic components of meteoroids have been reported to be Na, Ca, Ni, Al, Fe, and Mg with abundances (by mass) of 0.6%, 1.0%, 1.5%, 1.7%, 11.5%, and 12.5%, respectively (Mason, 1971). In the next section the influx of meteoric metals is discussed with emphasis on temporal variations in that influx and on the range of altitudes at which the ablation occurs.

The understanding of the metallic chemistry of the upper atmosphere remains quite incomplete, although progress continues to be made (e.g., Plane, 1991; Kane and Gardner, 1993a; Plane, 1994). For historical reasons the most studied metal has been sodium, since emissions from that element were discovered in the nightglow spectrum over fifty years ago. Unfortunately, thin ion layers have been observed to consist primarily of iron and magnesium. Although iron and magnesium are thought to have similar chemistries, neutral magnesium atoms cannot be readily observed from the ground owing to absorption of magnesium's spectral emissions by ozone in the stratosphere. On the other hand, neutral iron can be readily measured with ground-based lidars. Thus, in section 2.3 the

discussion of metallic chemistry is limited to that of iron, since it is an important constituent of ion layers that can also be observed in its neutral form.

In section 2.4, this chapter concludes with a discussion of observations of the vertical distribution of metallic (specifically Fe^+) ions in the upper atmosphere, in the context of the foregoing analysis of meteoric deposition and chemistry. This is a critical issue, since the efficiency of the electric field mechanism of layer formation depends upon having sufficient numbers of ions at requisite altitudes.

2.2 Meteoric Influx of Metals

2.2.1 The Origin of Meteoroids. Frictional interaction of meteoroids with atmospheric particles, i.e., meteor ablation, is the primary source of metals in the upper atmosphere. Hence, an understanding of meteoric processes is fundamental to the study of the formation of metallic layers. In this section the magnitude and periodicity of the meteoric influx is examined, along with the physics of ablation, since these factors might reasonably be expected to influence the time and altitude of ion layer formation. Before pursuing these topics it is useful to consider a more fundamental issue... from where do meteors come? The answer to this basic question turns out be of extreme importance for the subsequent development of this subject.

It has been established that the major source of meteoroids is the decay of comets (Hughes, 1978), although a small portion derives from asteroids (Lovell, 1954). Comets are composed of water ice, intermixed with impurities (Greenberg, 1982). As a comet follows its elliptical orbit about the Sun, the water sublimates as it nears perihelion. Fragments break away, entering their own ballistic orbits, also around the Sun. Interparticular collisions will tend to give some of the fragments velocities which are faster than the comet, and some slower than the comet. The former will advance before the comet, the latter will lag behind. Over time this causes the region surrounding the comet's orbital path to become populated with debris. Over even more time, further collisions and perturbation of the particle orbits caused by gravitational interaction with

the planets tend to more or less uniformly spread the particles into what is referred to as the interplanetary (or cosmic) dust cloud; all connection with the parent comet is lost. Thus, the interplanetary dust cloud can be thought of as the product of the extinction of countless comets.

Two distinct populations of meteoroids arise as a result of the collisional evolution of cometary particles. *Sporadic* meteoroids are the result of the motion of the Earth through the interplanetary dust cloud. The Earth essentially sweeps out these meteoroids as it orbits the Sun. The other class of meteoroids is associated with meteor streams. *Stream* meteoroids are those which still can be identified with a comet's orbit (although the comet may be long gone). The visual manifestations of stream meteors are the periodic meteor showers. As might be expected, despite the fact that sporadic and stream meteoroids share a cometary source, their physical characteristics (e.g., size and velocity distributions) and the temporal structure of their influxes are quite different. Stream meteoroids tend to be larger and faster than their sporadic cousins. Figure 2.1 illustrates the difference in the size distribution. The average geocentric velocity of sporadic meteoroids is ~15 km/s (Southworth and Sekanina, 1973). On the other hand the average velocities for the four major streams (Quadrantid, Perseid, Orionid, and Geminid) are 42, 59, 66, and 34 km/s, respectively (Hughes and McBride, 1989). These differences can be understood in the context of the collisional histories of the two species of meteoroids. Sporadic meteoroids, having suffered relatively more collisions, will tend to be more fragmented (smaller), while energy lost in the during the collisions will tend to reduce their velocities.

The fluxes of the two classes of meteoroids will be treated separately below, since each has distinctive spatial and temporal characteristics (which are again the ultimate consequence of the difference in their collisional histories).

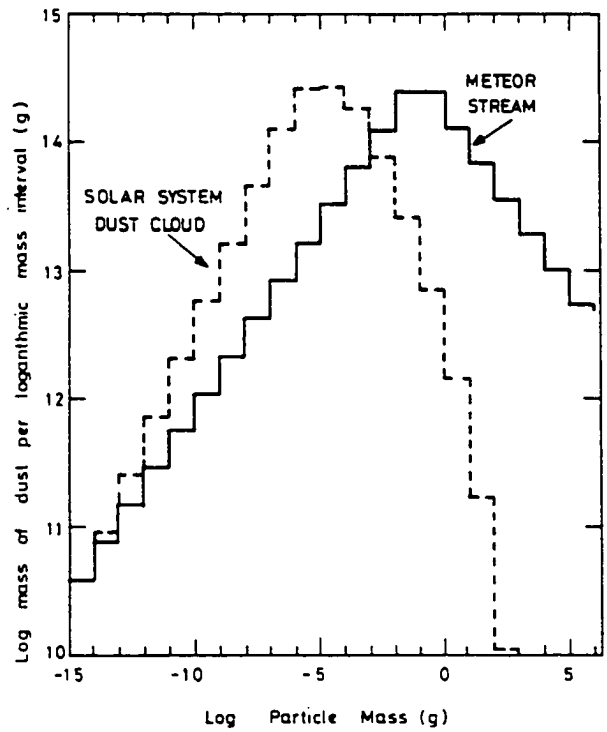

Figure 2.1 Mass distribution by particle mass for sporadic (dust cloud) and typical stream meteoroids (from Hughes, 1978).

2.2.2 Flux of Sporadic Meteoroids. Sporadic meteoroids are examined first, because, despite the fact that they do not responsible for the visually spectacular meteor showers, they contribute much more metal to the upper atmosphere than do stream meteoroids. This section begins with a description of the annual mass influx to the Earth. Then diurnal and seasonal variations in this flux are detailed.

Meteoroids are detected by three means: visual observation of the luminosity produced by de-excitation of atoms and molecules along the ablation path; radar detection of the trail of ions left in the wake of the meteoroid; and examination of impact craters on satellite-borne targets. Hughes [1978] has estimated the annual mass influx, deduced from observations made by these three techniques. Figure 2.2a shows the flux of sporadic meteoroids as a function of particle mass. Note that the apparent discontinuity

between the satellite and radar values, occurring at a meteoroid mass of approximately 10^{-6} g, has been resolved by subsequent observations (Hunten et al., 1980; Love and Brownlee, 1993). The annual mass influx as a function of particle mass is given in Figure 2.2b. Integration of this curve yields the annual mass influx to the Earth, the value of which is 16100 metric tons, with most of the mass is contained in meteoroids with mass 10^{-6} to 10^{-2} grams. Hughes' estimate of the sporadic influx remains widely accepted, but recent satellite observations suggest a higher annual influx of 40000 ± 20000 metric tons (Love and Brownlee, 1993). In this work, Hughes' estimate, 16100 metric tons, has been adopted. This is equivalent to 44 tons per day, which gives an *average* mass flux incident on the atmosphere of 1×10^{-16} g/cm^2/s. The actual flux at any instant at a given location will generally differ from this value. The variation in flux is systematic, with both diurnal and seasonal components.

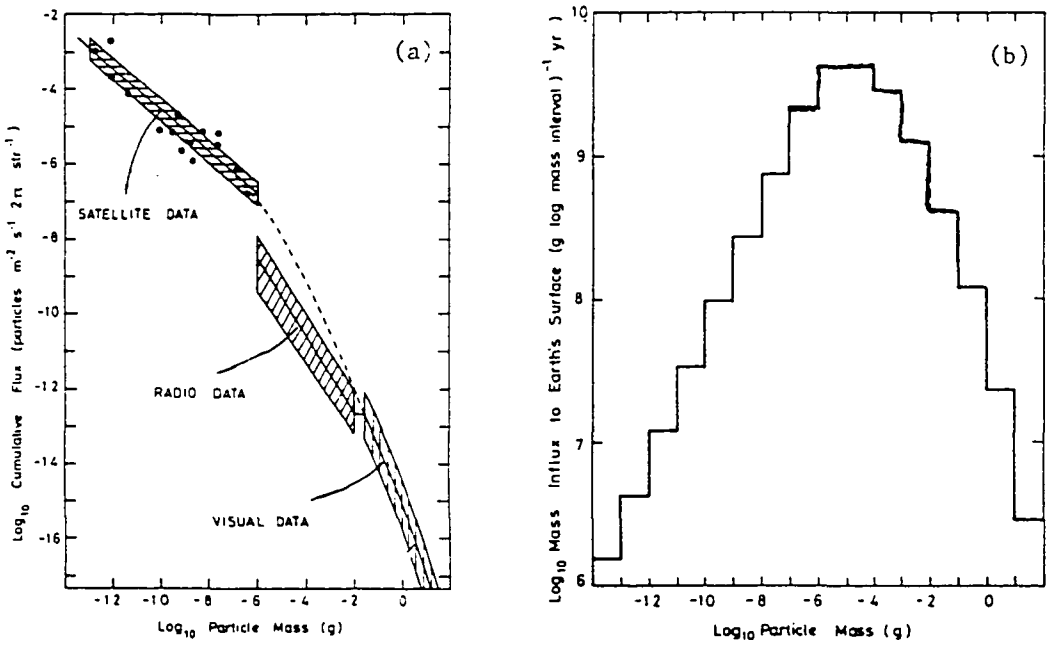

Figure 2.2 Sporadic meteoroid mass influx into the atmosphere: (a) flux as a function of particle mass; (b) annual mass influx over $\log_{10}$ particle mass interval (based on Hughes, 1978).

The temporal variation in flux is due predominantly to the motion of the Earth through the interplanetary dust cloud. As the Earth orbits the Sun, its leading face will intercept more meteoroids. Thus, one would expect the highest flux at dawn, and the lowest at dusk. In addition a seasonal effect is anticipated, since the Earth's rotational axis is not normal to the ecliptic plane (the tilt angle is ~23°). As the Earth revolves about the Sun, the Northern Hemisphere leads in September, and the Southern Hemisphere leads in March... thus producing a flux enhancement in the autumn months. The magnitude of the seasonal and diurnal variation in the flux can be estimated by adopting a simple model for the interplanetary dust cloud in the vicinity of the Earth.

Assume that the sporadic meteoroids are uniformly distributed in space with a Maxwellian heliocentric velocity distribution. If the Earth was nonrotating and at rest within the dust cloud, one can easily show that the flux of meteoroids would be constant everywhere around the Earth; call this flux F_o. Now adopt a coordinate system with origin at the center of the Earth, the x-axis in the direction of orbital motion, and the y-axis directed toward the Sun. Let the orbital velocity of the Earth be given by $\mathbf{v}_o$. In terms of polar spherical coordinates (polar angle θ; azimuthal angle φ), the flux is no longer the same everywhere, but rather becomes

$$F = F_o\left[e^{-\sin^2\theta\cos^2\varphi} + \sqrt{\pi}\,\sin\theta\cos\varphi\left(1+erf\left(\sin\theta\cos\varphi\right)\right)\right], \qquad (2.1)$$

where it has been reasonably assumed that $\frac{1}{2}mv_o^2 \approx kT$, since the average speed of the meteoroids (effectively characterized by a temperature, T) is on the order of the Earth's orbital speed (~30 km/s).

In order to relate the result expressed in equation (2.1) to a specific location on the Earth's surface, one must make a suitable coordinate transformation, accounting for the tilt of the rotational axis and the rotation of the Earth about that axis. Within the original coordinate system, the Earth's axis is tilted from the z-axis by a constant angle α (23°), and precesses clock-wise about the z-axis with a period of one year. The precession can be expressed in terms of the angle β, measured clock-wise from the y-axis (β=0° corre-

sponds to the June solstice, $\beta=90°$ to the September equinox, etc.). The program for transforming from the original coordinates to a system fixed in the rotating Earth proceeds as follows. Form an intermediate coordinate (xyz)′ system by rotating the (xyz) system by α about the x-axis, then rotating by β about the original z-axis. The x′-axis will be in the x-y plane, and the z′-axis coincides with the Earth's axis. From the primed system, rotate by an angle γ to get to a system fixed in the Earth. Note that γ varies uniformly in time with a period of one day. The transformation is illustrated in Figure 2.3. By application of the transformation one can express $\sin\theta\cos\varphi$ in equation (2.1) in terms of trigonometric functions involving α, β, γ, and the geographic latitude (the resulting expression is quite complicated).

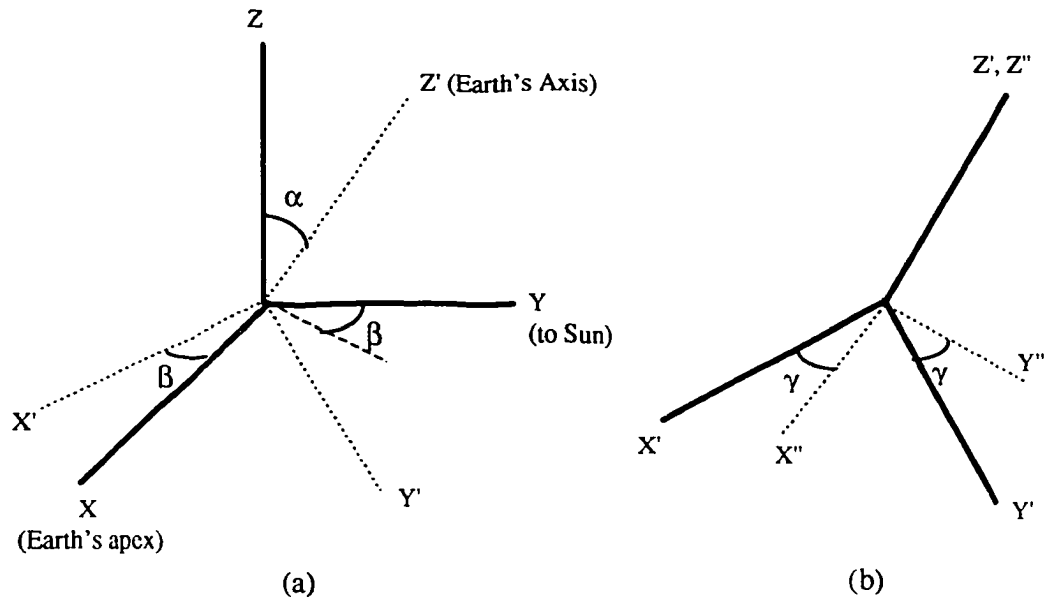

Figure 2.3 Coordinate transformation (described in the text) used in the model for the flux sporadic meteoroids. Step (a) is an intermediate; the double-primed system (b) is fixed in the Earth.

Equation (2.1), coupled with the above described coordinate transformation, was used to generate Figure 2.4, which shows the relative meteoroid flux (F/F_o) as a function of latitude and local time on four selected days. The diurnal variation is evident with a maximum occurring at 0600 LT and a minimum at 1800 LT. The effect is strongest at low latitudes. Another interesting feature is that the variation is not in the form of a perfect sinusoid, but rather is more sharply peaked in the morning than in the afternoon. As can be seen in Figure 2.5, the form of the diurnal variation in flux predicted by the model matches observations quite well. The occurrence of the maximum flux at ~0400 LT, and the minimum at ~1600 LT, rather than 0600 LT and 1800 LT, results from observational selection (Hughes and Stephenson, 1972), not a defect in the model. Also obvious from Figure 2.4 is a strong seasonal dependence in intensity of the meteoric influx.

Integration of equation (2.1) over a day allows one to calculate the average daily flux. Figure 2.6 shows the daily relative flux $\langle F/F_o \rangle$ over the period of a year at selected latitudes. The variation over time clearly is seasonal with the two hemispheres 180° out of phase. Once again the variation is only approximately sinusoidal. Interestingly, the daily influx has a more complicated latitudinal dependence than does the instantaneous flux. During the autumn, daily flux tends to increase with latitude, while during the spring months the daily flux decreases with latitude. Finally, note that the peak daily flux is much less than the value at 0600 LT, as expected by consideration of the averaging process. The observational record generally confirms the seasonal variation in daily meteoroid flux predicted by the model (Hughes, 1978). However, when the seasonal effect is subtracted from the data, the result is not F_o, as expected, but rather maximizes between October and December and minimizes in April and May, in both hemispheres (see Figure 2.7). This has been attributed to an actual difference in the distribution of meteoroids about the Sun. Thus, to apply the results of the model developed above to calculations of flux on a given day, one should apply a multiplicative factor derived from observation to correct for the nonuniformity of the meteoroid distribution. For example,

examination of Figure 2.7 suggests a correction factor of 0.8 for March and 1.2 for September.

Using Hughes' estimate of F_o, $1x10^{-16}$ g/cm^2/s, and noting that 11.5% of this is iron, one can use the model to calculate the iron flux for different latitudes and dates. Table 2.1 shows the average daily iron flux, determined for four different days at a variety of latitudes. Note that a correction for the spatial nonuniformity of the cosmic dust cloud has been applied. Of the influx of iron shown in Table 2.1, most will be liberated in the upper atmosphere as neutral atoms, some will be ionized, while a portion will remain in solid form as a part of incompletely ablated meteoroids. These factors are addressed later in this chapter.

Table 2.1 Model-derived Average Daily Fe Flux ($x10^{-17}$ g/cm^2/s).

LAT/DATE	21 Sep	21 Dec	21 Mar	21 Jun
90N	2.54	1.38	0.42	0.92
75N	2.53	1.42	0.45	0.94
60N	2.49	1.54	0.56	1.03
45N	2.41	1.71	0.71	1.14
30N	2.30	1.85	0.91	1.23
15N	2.14	1.96	1.09	1.31
000	1.91	2.00	1.27	1.34
15S	1.65	1.96	1.42	1.31
30S	1.36	1.85	1.53	1.23
45S	1.07	1.71	1.61	1.14
60S	0.84	1.54	1.65	1.03
75S	0.67	1.42	1.68	0.94
90S	0.64	1.38	1.69	0.92

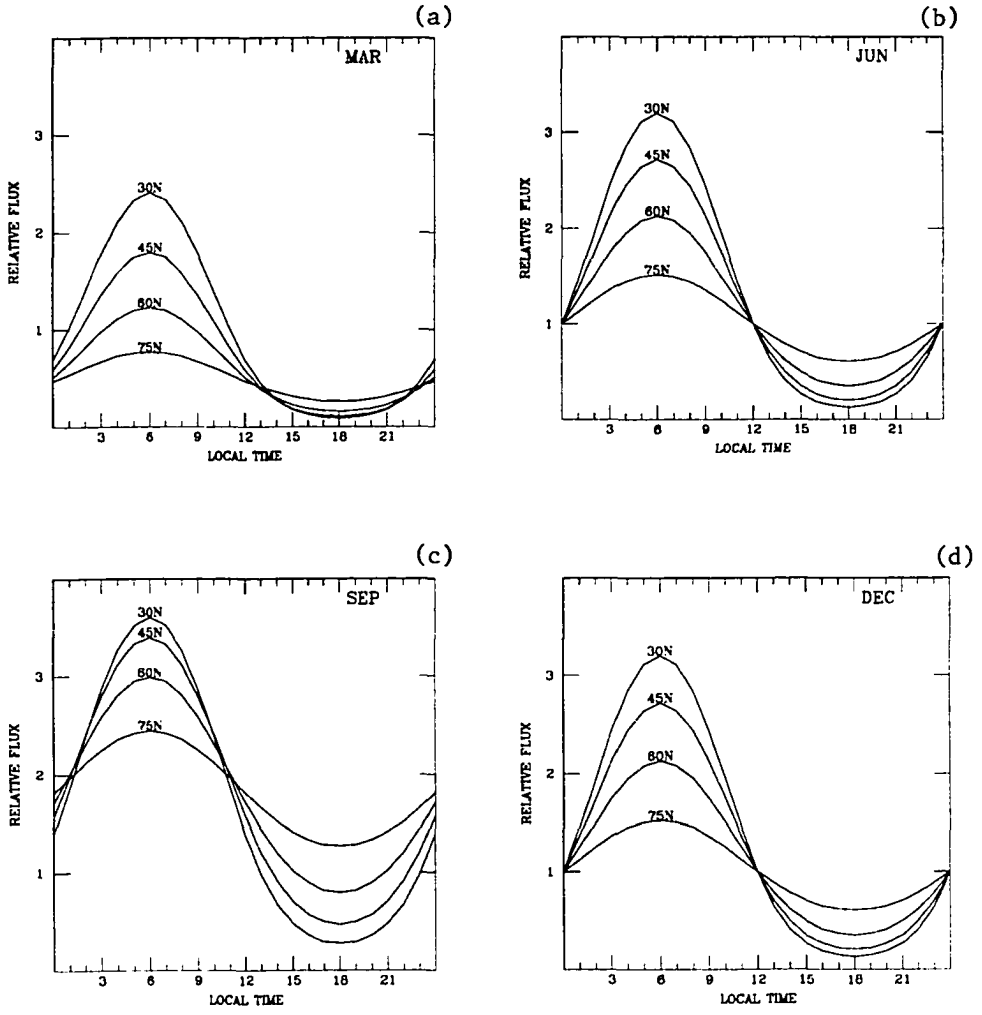

Figure 2.4 Relative instantaneous sporadic meteoroid flux at selected latitudes, based on model calculations for the: (a) March equinox; (b) June solstice; (c) September equinox; and (d) December solstice.

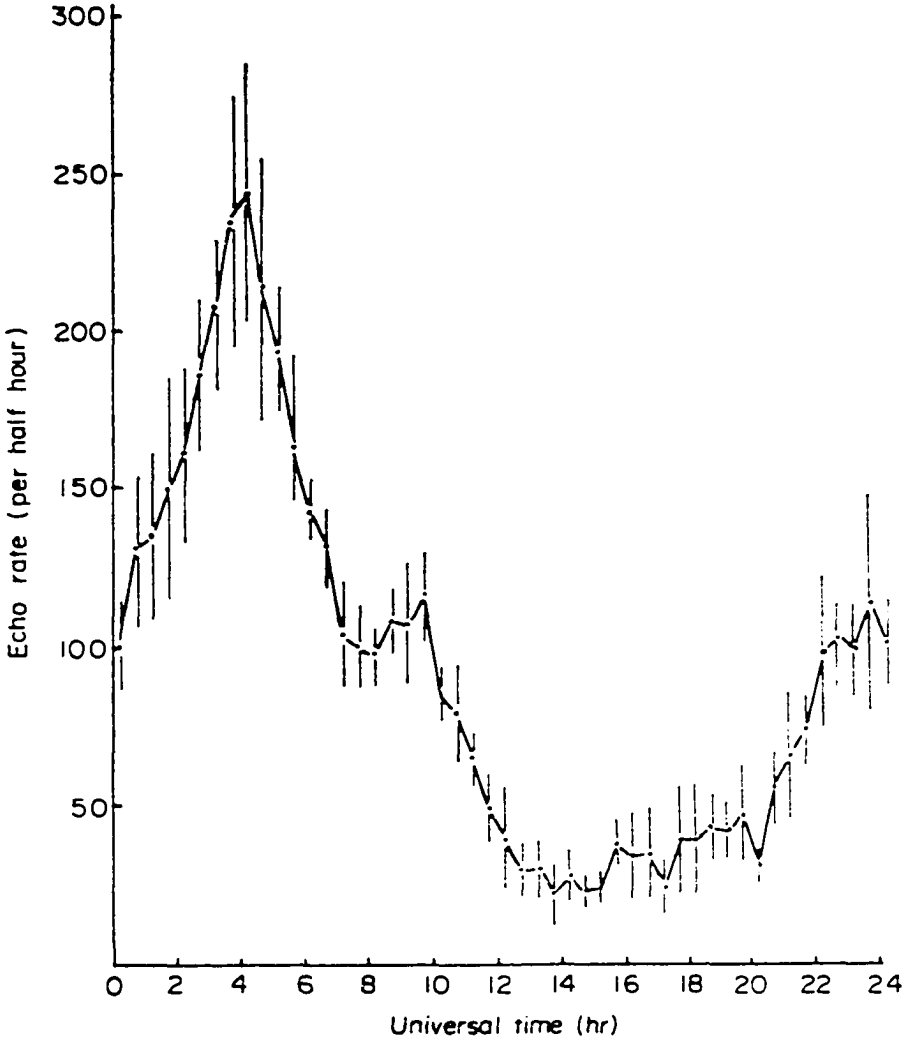

Figure 2.5 Observed sporadic meteor flux (proportional to the "echo rate") measured with a radar near Sheffield, England (lat. 53° 26' N, long. 1° 35' W) from Hughes and Stephenson [1972].

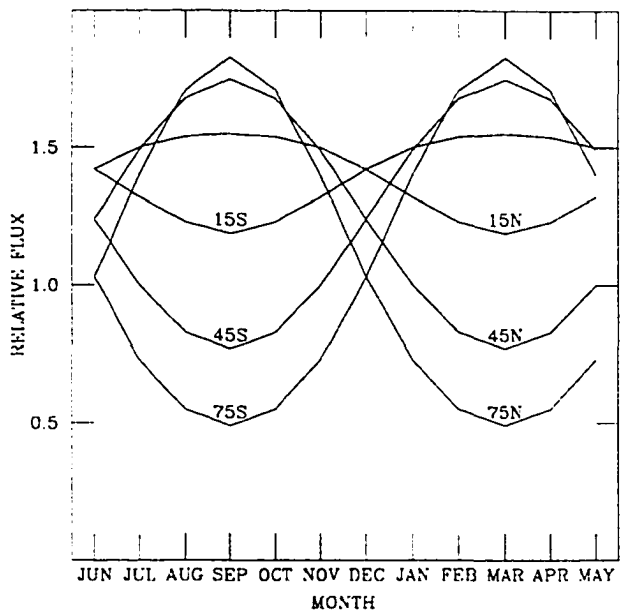

Figure 2.6 Average daily relative flux of sporadic meteoroids, $\langle F/F_o \rangle$, as a function of month-of-the-year for selected latitudes.

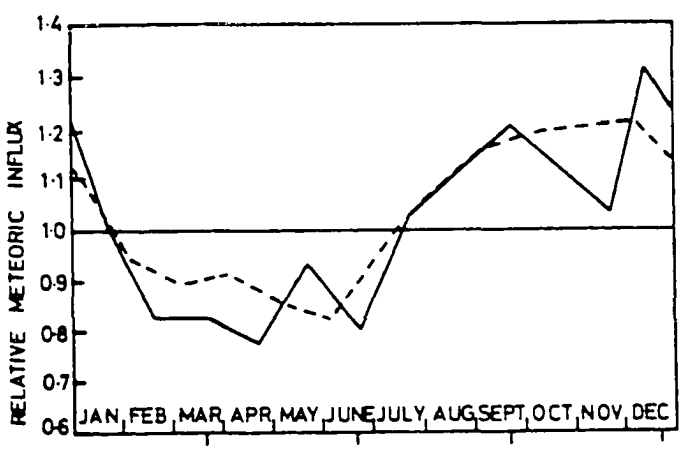

Figure 2.7 Observed annual variation in sporadic meteoroid flux with the seasonal effect removed: solid line - Southern Hemisphere (Weiss, 1957); dashed line - Northern Hemisphere (Kresákova and Kresák, 1955). (taken from Hughes, 1978).

2.2.3 Flux of Stream Meteoroids. The influx of stream meteoroids is extremely periodic in nature. Whenever the Earth's orbit intersects that of a comet (perhaps extinct) an influx of stream meteoroids occurs. The time of passage through the region about the comet's orbit populated by particles determines the dates for which stream meteors are incident upon the Earth. Thus, stream meteoroids associated with a given comet typically appear annually over a definite period of time, on the order of days.

A distinguishing characteristic of stream meteoroids is that their flux has a well-defined direction, closely related to the orbit of the parent comet. Hence, stream meteors appear to emanate from a specific place in the sky, called the *radiant.* The orientation of the radiant is usually specified in GEI (geocentric equatorial inertial) coordinates. In this coordinate system, the angle to the radiant, measured from the equatorial plane, is called the *declination* (positive to the north), while the angle measured from the vernal equinox is called the *right ascension.* Table 2.2 gives characteristics of four major streams. In the table the equivalent duration is the duration the meteor shower would have if all of the influx occurred at the peak flux, and the flux-to-radiant is the peak flux through a plane normal to the radiant. Since the Earth is spherical in shape the flux-to-radiant represents the maximum flux incident on the Earth, and would only occur at one location on the globe at any given instant in time. Figure 2.8 shows the average daily flux relative to the peak flux for the four major streams. The values plotted are all less than one due to the process of averaging the flux over a day. It is clear that the sporadic flux is much larger than even the peak stream fluxes. For example, at a latitude of 60°N the average daily mass flux on the peak day (in $g/cm^2/s$) is $2.5x10^{-18}$, $2.3x10^{-19}$, $6.0x10^{-20}$, and $1.3x10^{-18}$, for the Quadrantid, Perseid, Orionid, and Geminid streams, respectively. The sporadic (mass) fluxes on the peak days are $1.4x10^{-17}$, $2.1x10^{-17}$, $2.4x10^{-17}$, and $1.7x10^{-17}$ $g/cm^2/s$. Clearly, the sporadic mass influx is much greater than that from streams. However, a greater portion of the stream meteoroids ablates, so that the above figures overstate the contribution of the sporadic meteors to the population of metallic atoms and ions in the atmosphere.

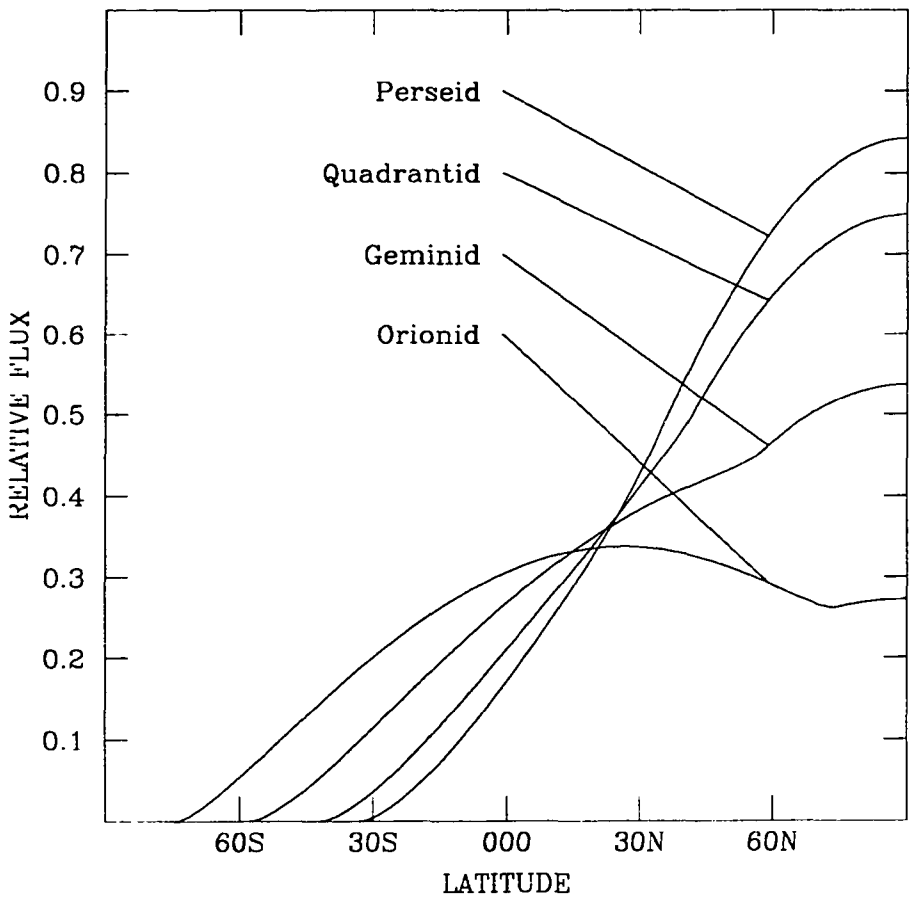

Figure 2.8 Model-derived average daily flux of stream meteoroids relative to peak flux for four major streams. The "humps" in the plots for the Geminid and Orionid streams occur at latitudes above which the Earth is bathed by the shower throughout the entire day.

TABLE 2.2 Characteristics of Major Meteoroid Streams.

	Quadrantid	Perseid	Orionid	Geminid
Date (peak)	3 Jan	12 Aug	21 Oct	14 Dec
Right Ascension (radiant)	230.1°	46.2°	94.5°	112.3°
Declination (radiant)	48.5°	57.4°	15.8°	32.5°
Equiv. Duration (days)	0.7	8.8	8.2	5.6
Geocentric Vel. (km/s)	41.5	59.4	66.4	34.4
Mass Flux-to-Radiant ($gm/cm^2/s$)	$3.3x10^{-17}$	$2.8x10^{-18}$	$1.8x10^{-18}$	$2.4x10^{-17}$

2.2.4 Meteoroid Ablation. To this point, estimates of the influx of meteoric matter into the atmosphere have been developed, but several questions remain, e.g., what portion of the meteoroid mass actually ablates in the atmosphere, at what altitudes is meteoric iron deposited, and how much of it is initially ionized? By considering the theory of meteor ablation, one can see how a meteoroid's initial mass and geocentric velocity determine the answers to the above questions.

Theoretical study of the process of ablation has been well-developed over the past forty years (e.g., Öpik, 1958; Lebedinets et al., 1973; Bronshten, 1983). The basic approach is to simultaneously solve the momentum, the energy, and the ablation equations (the ablation equation relates the rate of mass loss to the heating of the meteoroid). Since the diameter of most meteoroids is much less than the mean free path of the atmospheric molecules in the region where ablation is observed to occur, the physics can be modeled in terms of individual atmospheric particles colliding with the meteoroid. Qualitatively, the main results of the theory are: (1) for meteoroids with the same initial mass, those with higher geocentric velocities ablate higher up; (2) for meteoroids with the same geocentric velocity, those with larger mass burn up lower in the atmosphere.

Hunten et al. [1980] applied the theory to the sporadic component of the meteoric influx. Their analysis indicates that most ablation should occur between 80 and 100 km, with a peak at 84 km. Hunten et al. note that their estimate is subject to uncertainty relating to imprecise knowledge of the velocity and mass distributions of the meteoroid population. Additionally, the theory itself relies upon poorly known physical parameters, e.g., a coefficient relating conversion of kinetic energy to heat. Thus, a comparison of the Hunten model with observations is in order. Representative results of radar and lidar studies of the ablation altitude of sporadic meteoroids are shown Figure 2.9. Both types of observations indicate that ablation occurs about 5-10 km higher than theoretically predicted, nominally peaking at 90-95 km. Recent radar observations suggest that stream meteoroids ablate higher than for the sporadic component with a peak at ~105 km, distributed symmetrically about the peak with a full-width-half-maximum value of 20 km and significant ablation up to at least 140 km (Olsson-Steel and Elford, 1987; Elford and Olsson-Steel, 1988; Steel and Elford, 1991). These results are consistent with ablation theory, since stream meteoroids have much higher geocentric velocities than do the sporadics, and thus are expected to burn up higher in the atmosphere.

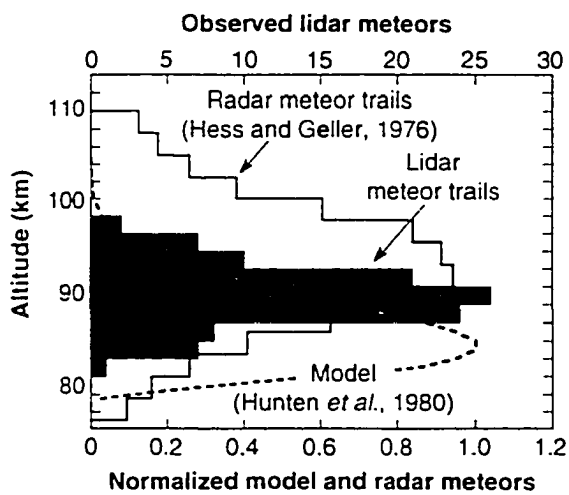

Figure 2.9 Height distribution of meteor ablation: comparison of theoretical model with observations (from Kane and Gardner, 1993).

Ablation theory also can be applied to the problem of the "residual mass" of the meteoroid influx. Residual mass is simply that part of the influx which does not ablate, but rather remains in the solid state (forming meteorites or dust). Nicol et al. [1985] have shown that the degree of ablation is strongly related to the initial velocity of the meteoroid. Their theoretical analysis indicates that for geocentric velocity greater than 24 km/s, there is no appreciable residual mass. Since the stream meteoroids have velocities greater than this value, one expects them to completely burn up in the atmosphere. On the other hand, recall that the velocity of sporadic meteoroids is lower, averaging ~15 km/s. Nicol et al. estimate that at this initial velocity, the final mass of meteoroids, having an initial mass in the range 10^{-6} to 10^{-2} g, is ~10^{-6} g (those smaller than 10^{-6} g don't ablate at all). Using the distribution of sporadic meteoroid sizes given earlier (Figure 2.1), a rough estimate of the portion of the sporadic mass influx that is ablated is ~75%, i.e., only ~12000 of the 16100 metric tons incident upon the atmosphere annually is deposited in the upper atmosphere as neutral atoms or ions.

The degree of ionization of the atoms ablating from a meteoroid is also strongly dependent upon the geocentric velocity of the meteoroid. When an atom ablates it initially retains approximately the same velocity as its parent body, and hence a good deal of kinetic energy. It will typically collide with a number of air molecules before being reduced to thermal energy, losing energy via elastic scattering, excitation, and ionization. The probability, that a given atom is ionized in the process of this series of collisions, is termed the *ionizing probability*, β. Slattery and Friichtenicht [1967] conducted experiments in the laboratory, which replicate the physical conditions prevailing in the upper atmosphere under which ablation occurs. They found that the ionizing probability for iron can be expressed as

$$\beta = 5.96 \times 10^{-6} v_o^{3.12} \tag{2.2}$$

where velocity here is in km/s. A theoretical study by Sida [1969] showed that $\beta \propto v_o^{3.5}$ for iron which is in reasonable agreement with the experimental results. However, Sida's

model predicts an ionizing probability at least an order of magnitude smaller (see Table 2.3). To date the discrepancy between experiment and theory has not been reconciled. In this thesis, the experimentally deduced results of Slattery and Friichtenicht have been adopted.

To appreciate the influence of ablation physics on the flux of iron atoms and ions into the atmosphere, consider Table 2.4 which gives fluxes on the peak shower days from both stream and sporadic meteoroids, calculated at a latitude of 60°N. Both the effect of incomplete ablation, and the ionization probability are incorporated in the calculated fluxes. Stream meteoroids can significantly enhance the flux of Fe^+ (while the shower is ongoing), since the iron ablated from them is predominantly ionized. Whether this increase in the flux can by itself produce enough ions to form a specific thin layer is addressed in the next section. However, it should be noted that the sporadic influx is by far the greater source of iron in the upper atmosphere, when considered on an annual basis.

TABLE 2.3 Ionizing Probability (β) for Fe for Various Geocentric Velocities.

SOURCE / v_0 (km/s)	20	30	40	50	60
Slattery & Friichtenicht (experimental)	0.068	0.242	0.594	~1	~1
Sida (theoretical)	0.001	0.009	0.026	0.057	0.107

TABLE 2.4 Calculated Fe & Fe^+ Flux at 60°N for Sporadic and Stream Meteoroids.

	Fe Flux ($cm^{-2}s^{-1}$)		Fe^+ Flux ($cm^{-2}s^{-1}$)	
	Stream	**Sporadic**	**Stream**	**Sporadic**
3 Jan	$9.0x10^3$	$1.1x10^5$	$1.8x10^4$	$3.1x10^3$
12 Aug	0	$1.6x10^5$	$2.5x10^3$	$4.5x10^3$
21 Oct	0	$1.9x10^5$	$6.4x10^2$	$5.3x10^3$
14 Dec	$9.0x10^3$	$1.3x10^5$	$5.2x10^3$	$3.6x10^3$

2.2.5 Meteoroids and Metallic Layers. Knowing that there is an influx of metal ions into the upper atmosphere, a natural question is how long would it take to accumulate enough ions to form a layer, neglecting transport and chemistry? An estimate can be crafted using the results previously developed in this chapter. For the purposes of this calculation, consider a layer located at 60°N latitude, having a thickness of 2 km with a uniform density of $1x10^5$ cm^{-3}. Assume that the layer consists exclusively of Fe^+ (neglect of the other major meteoric constituent, Mg, is justified, since its ionizing probability is much lower than that of Fe). Neglect chemical sources/sinks and horizontal transport. The maximum instantaneous flux from sporadic meteoroids occurs at 0600 LT on 21 September. At that time the flux of Fe^+ is $9.0x10^3/cm^2/s$, and it would require ~26 days to deposit enough ions to form the layer. Since the instantaneous Fe^+ flux varies widely over the course of a day (down to $2.5x10^3/cm^2/s$, at 1800 LT), a more meaningful estimate can be made using the daily flux. Using the average daily flux for that date ($6.8x10^3$ $/cm^2/s$), the accumulation time is ~34 days. Since layers formed through the action of electric fields arise within tens of minutes (this will be elaborated upon in the next chapter), it appears clear that the influx of sporadic meteoroids cannot produce ions rapidly enough to account for the formation of a specific thin metallic layer.

A similar assessment can be made of the impact of meteoroid streams, by calculating the maximum density attainable in a 2 km thick layer assuming all of the ions deposited by the stream are uniformly distributed within the layer. The estimate is again made at a latitude of 60°N, with horizontal transport neglected. The maximum densities (in cm^{-3}) would be $5.4x10^3$, $9.5x10^3$, $2.3x10^3$, and $1.3x10^4$ for the Quadrantids, Perseids, Orionids, and Geminids, respectively. These densities could only be attained after the entire meteor shower had occurred, typically several days in each case. It is apparent that deposition of ions by the meteoroid streams is not likely to be responsible for the formation of the dense ion layers observed in this study, which have densities exceeding 10^5 cm^{-3} (see Chapter 4).

Several observational studies have aimed to establish the relationship between the meteoroid influx and the occurrence of sporadic E, however their results are unclear and sometimes contradictory (Whitehead, 1989). Some evidence indicates a time-lagged correlation (increase in E_s following an increase in influx): 3-9 hours (Hedberg, 1976) or 1-2 weeks (Sinno, 1980). However, in a comprehensive study, Baggaley and Steel [1984] find no correlation between meteor showers and the observation of sporadic E. This confusing state of affairs is taken to support the conclusion drawn from the simple calculations made earlier, i.e., direct meteoroid influx cannot alone account for the formation of a given thin ion layer, although variations in the flux may account for variations in the rate of occurrence of layers over longer time scales.

2.3 Iron Chemistry

As is true with the other metals in the atmosphere (except perhaps Na), the chemistry of Fe is not well understood. Two challenges hinder advancement in the quest for knowledge in this area. The first is that rate coefficients for many key reactions are only speculative, although laboratory research should ameliorate this problem within a few years (J.M.C. Plane, personal communication, 1994). The second problem is common in atmospheric chemistry, i.e., the very identification of the important reactions. Fortunately, consideration of a simple chemical model is sufficient to determine the relative importance of chemistry in the formation of thin ion layers.

Kane and Gardner [1993a] have proposed a model for Fe chemistry in the upper atmosphere, which is similar to a well-known model developed by Brown [1973]. The chief difference between the two is the inclusion of reactions with CO_2 in the former, which provides for $FeCO_3$ to serve as an Fe "sink" at altitudes less than 80 km. Table 2.5 shows the reactions incorporated into their model (note that photoionization of Fe and neutralization of Fe^+ were not included, since both proceed at an extremely slow rate). Kane and Gardner showed that in chemical equilibrium (neglecting transport) most atmospheric iron is in neutral atomic form between 80 and 90 km, and is Fe^+ above

90 km. This is in agreement with Brown's model, and is consistent with many ion observations (e.g., Narcisi, 1971; Zbinden et al., 1975; Steinweg et al., 1992) which show Fe^+ peaking between 90 and 95 km, while lidar measurements of neutral Fe (e.g., Alpers et al., 1990; Kane and Gardner, 1993a) show the background Fe layer to be peaked at ~85 km. Table 2.6 gives reasonable values for the densities of the background neutral atmospheric constituents and primary ions assumed for the subsequent analysis (based on Rees, 1989), while Table 2.7 presents the associated time constants for the reactions in the model.

TABLE 2.5 Fe Chemistry Model (Kane and Gardner, 1993a).

Reaction #	Reaction	Rate Coefficient
1	$FeO + O \rightarrow Fe + O_2$	10^{-11} cm^3/s
2	$Fe + O_3 \rightarrow FeO + O_2$	10^{-10} cm^3/s
3	$FeO + CO_2 + M \rightarrow FeCO_3 + M$	10^{-27} cm^6/s
4	$FeCO_3 + O \rightarrow Fe + CO_2 + O_2$	10^{-13} cm^3/s
5a	$Fe + NO^+ \rightarrow Fe^+ + NO$	10^{-9} cm^3/s
5b	$Fe + O_2^+ \rightarrow Fe^+ + O_2$	10^{-9} cm^3/s
6	$Fe^+ + O_2 + M \rightarrow FeO_2^+ + M$	10^{-30} cm^6/s
7	$Fe^+ + O_3 \rightarrow FeO^+ + O_2$	1.5×10^{-10} cm^3/s
8	$FeO_2^+ + O \rightarrow FeO^+ + O_2$	10^{-10} cm^3/s
9	$FeO^+ + O \rightarrow Fe^+ + O_2$	10^{-10} cm^3/s
10	$FeO_2^+ + e^- \rightarrow Fe + O_2$	2×10^{-6} cm^3/s
11	$FeO^+ + e^- \rightarrow Fe + O$	4×10^{-7} cm^3/s

Table 2.6 Assumed Background Atmosphere (number density in cm^{-3}).

	80 km	90 km	100 km	110 km	120 km
$[O_3]$	$1x10^9$	$1x10^8$	$4x10^6$	$1x10^5$	$5x10^3$
$[CO_2]$	$3x10^{10}$	$2x10^{10}$	$3x10^9$	$2x10^8$	$2x10^7$
[O]	$1x10^8$	$2x10^{11}$	$2x10^{11}$	$1x10^{11}$	$5x10^{10}$
$[O_2]$	$7x10^{13}$	$1x10^{13}$	$2x10^{12}$	$3x10^{11}$	$4x10^{10}$
$[N_2]$	$3x10^{14}$	$6x10^{13}$	$7x10^{12}$	$1x10^{12}$	$3x10^{11}$
$[NO^+ + O_2^+]$	$1x10^1$	$1x10^3$	$1x10^4$	$1x10^4$	$1x10^4$
n_e	$1x10^2$	$1x10^3$	$1x10^4$	$1x10^4$	$1x10^4$

Table 2.7 Time Constants for Reactions in the Fe Model (seconds).

Reaction #	80 km	90 km	100 km	110 km	120 km
1	1000	0.5	0.5	1	2
2	10	100	3000	$1x10^5$	$2x10^6$
3	90	700	$4x10^4$	$4x10^6$	$1x10^8$
4	$1x10^5$	50	50	100	200
5a&b	$1x10^8$	$1x10^6$	$1x10^5$	$1x10^5$	$1x10^5$
6	40	1000	$5x10^4$	$2x10^6$	$6x10^7$
7	7	70	2000	$7x10^4$	$1x10^6$
8	100	0.05	0.05	0.1	0.2
9	100	0.05	0.05	0.1	0.2
10	5000	500	50	50	50
11	$3x10^4$	3000	300	300	300

The model of Kane and Gardner is used below to investigate several issues of interest in the study of metallic thin layers: the stability of Fe^+ as a function of altitude; the regeneration of a background Fe^+ layer depleted by, e.g., vertical transport; and the influence of auroral precipitation on enhancement the Fe^+ population. A schematic representation of the model is given in Figure 2.10, with calculated portions of total iron residing (in chemical equilibrium) in Fe^+, Fe, FeO, and $FeCO_3$, shown in Table 2..8.

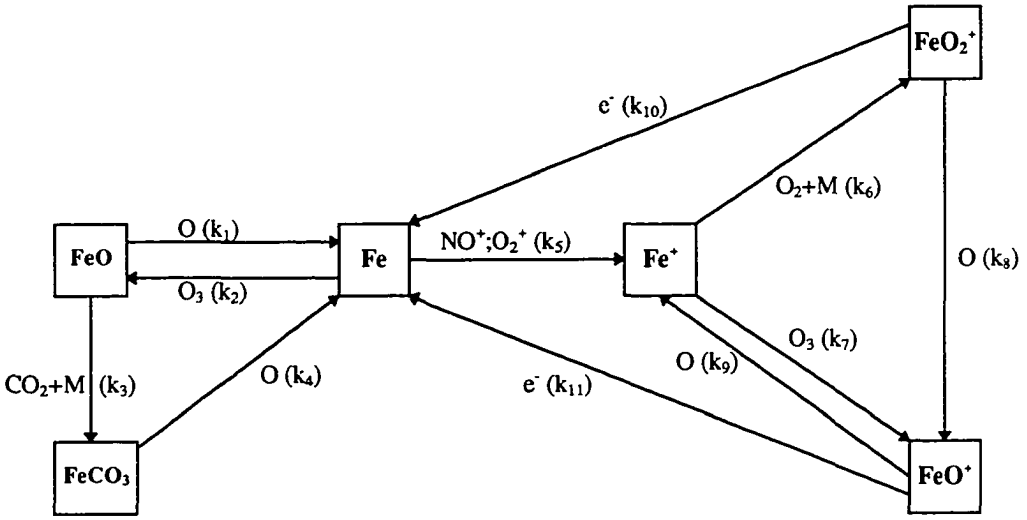

Figure 2.10 Schematic of the Kane-Gardner iron chemistry model.

Table 2.8 Equilibrium Portions of Total Iron in Various Species (model-derived).

	80 km	90 km	100 km	110 km	120 km
Fe^+	~0	0.737	0.989	~1	~1
Fe	~0	0.262	0.011	~0	~0
FeO	0.001	0.001	~0	~0	~0
$FeCO_3$	0.999	~0	~0	~0	~0

How stable is Fe^+ at a given altitude? Without further analysis, it is apparent from Table 2.8 that Fe^+ must be extremely stable at altitudes above 100 km, since the model predicts that in equilibrium virtually all iron is in the ionic form. At the other extreme, suppose that Fe^+ is suddenly introduced into the atmosphere at 80 km, and further assume that the atmosphere had been in chemical equilibrium (i.e., virtually no Fe^+ was initially present). The fraction of the Fe^+ enhancement remaining, as a function of time, is given by

$$\frac{[Fe^+]}{[Fe^+]_o} \cong 0.952e^{-t/6} + 0.049e^{-t/19300} - 0.001e^{-t/86} \qquad (2.3)$$

where time is in seconds. The system will rapidly approach equilibrium; less than 25% of the Fe^+ remains after 10 s, and the fraction falls to less than 5% within a minute. This calculation indicates that Fe^+ is effectively lost from the atmosphere, if it is transported to below ~80 km. The situation is slightly more complicated at altitudes where the Fe^+ concentration at equilibrium is on the same order as another constituent, e.g., at 90 km where the atomic Fe concentration is close to that of the ionic form. Now suppose that the system is initially in chemical equilibrium. Then if the Fe^+ concentration is rapidly increased by a factor of two (up to 84.9% of total iron), the system will adjust to a new equilibrium, with Fe^+ again comprising 73.7% of total iron. As a fraction of Fe^+ concentration prior to the introduction of additional ions, the approach to equilibrium is given by

$$\frac{[Fe^+]}{[Fe^+]_{initial}} \cong 1.735 + 0.265e^{-t/40000} \qquad (2.4)$$

With a time constant greater than 200 hours, it is clear that an enhancement of Fe^+ concentration at 90 km has a long lifetime. Taken together, the above observations indicate that Fe^+ is stable for time-scales on the order of days for altitudes above 90 km, but that between 80 and 90 km, there is an abrupt transition to a situation for which an enhancement of $[Fe^+]$ is chemically removed within a few seconds.

Now suppose that chemical equilibrium exists, when suddenly the Fe^+ layer is removed. How rapidly does the system to return to equilibrium, thus regenerating a portion of the lost Fe^+? To address this question, again consider an altitude of 90 km, and assume no transport or influx of iron. First, note that the equilibrium portion of Fe^+ will remain unchanged at 73.7%. If the original concentration of Fe^+ was 10^4 cm^{-3}, then the new equilibrium concentration will be only ~2600 cm^{-3}, coming from the neutral atom population via reaction #5. As a fraction of the final equilibrium, the approach to equilibrium is given by

$$\frac{[Fe^+]}{[Fe^+]_{final}} \cong 1 - e^{-t/7400} \tag{2.5}$$

Thus, the time constant for regeneration of lost Fe^+ is ~2 hours. Again it must be emphasized that only a part of the original concentration will be obtained, unless more iron enters the system.

It seems plausible that an increase in $[NO^+]$ and $[O_2^+]$, due to intense auroral precipitation down to altitudes at which Fe atoms reside, might cause a significant increase in $[Fe^+]$ via reaction #5. To check this assertion, suppose that $[NO^+]+[O_2^+]$ increases by two orders of magnitude to 10^5 cm^{-3} at an altitude of 90 km. According to the model, the equilibrium fraction of iron in Fe^+ would only increase very slightly, from 0.737 to 0.738. The reason that the increase is so small is that an increase in electron density, which necessarily accompanies enhancement of the ion population, accelerates reactions #10 and #11. This has the effect of converting Fe^+ to Fe , substantially negating the impact of the increase in the rate of reaction #5.

Before leaving this section, a discussion of the impact of photoionization on the population of Fe^+ is in order. Photoionization for metallic gases proceeds very slowly. Swider [1969] analyzed this process for various metals assuming an unattenuated flux of solar radiation, thus establishing upper limits on the rate of photoionization in the E-region. The resulting time constant for Fe is 2×10^6 s (over 23 days). Clearly, photoioni-

zation is much less important source of Fe^+ than is charge transfer, justifying its exclusion from the model.

2.4 Vertical Distribution of Fe^+ in the Upper Atmosphere

Based on the preceding analysis, one can draw several conclusions about the source of Fe^+ in the upper atmosphere. Most of the iron (and other metals) entering the atmosphere does so below 100 km through the ablation of sporadic meteoroids, and is initially in the form of neutral atoms (however, a significant portion of the neutral atoms deposited above 90 km is eventually ionized through charge transfer). Stream meteoroids supply a much smaller quantity of iron to the system, but do so in impulsive surges. This contribution tends to be deposited higher than in the case of the sporadics (perhaps as high as 140 km with a peak at 105 km) and is largely in ionic form. Evaluation of incident fluxes show marked diurnal and seasonal variations in the sporadic component, and inherent periodicity for the stream meteoroids, with strong latitudinal dependencies in both cases. However, the magnitude of both sporadic and stream fluxes is too small to account for the formation of a given layer; ions trickle into the system too slowly to account for the rapid rate at which thin layers are observed to grow.

The chemistry of Fe^+ also has implications for the height distribution of that ion in the atmosphere. Fe^+ should essentially vanish between an altitude of 80 and 90 km. Furthermore, Fe^+ should be the most abundant species containing iron above 95-100 km.

Measurements made using rocket-borne mass spectrometers are consistent with the above picture. For example, the results of four observations made by Steinweg et al. [1992] over northern Scandinavia are shown in Figure 2.11. Flights F1 and F2 were launched from Andøya, Norway (69.17°N, 16.02°E), while F3 and F4 were launched from Kiruna, Sweden (67.88°N, 21.10°E). In each case, Fe^+ is the most abundant metallic ion, and exists primarily in the altitude range in which most meteoroid ablation is

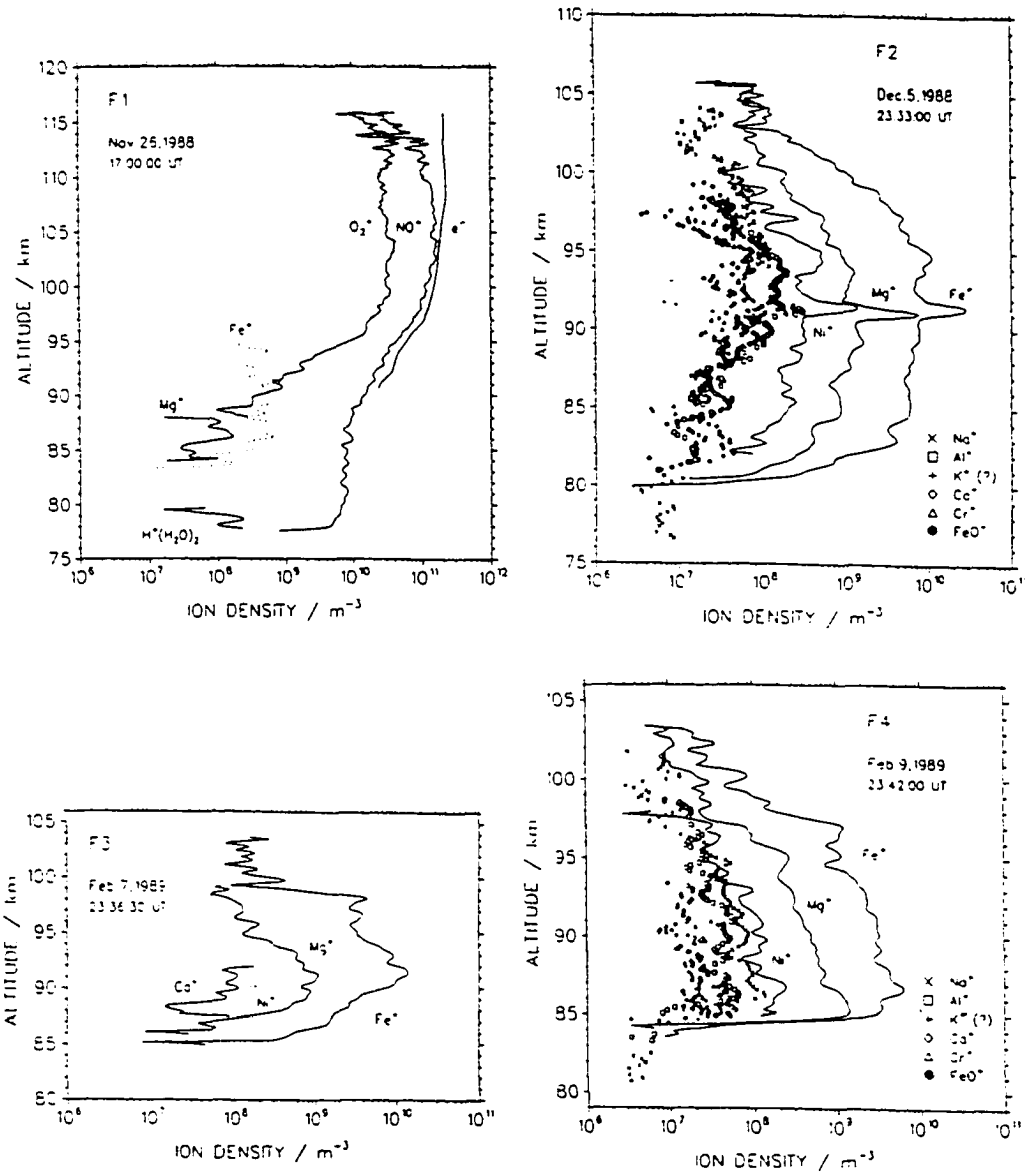

Figure 2.11 Rocket-borne mass spectrometer measurements of metallic ions over northern Scandinavia. Flights F1&2 were made at Andøya, Norway, F3&4 at Kiruna, Sweden. (from Steinweg et al., 1992).

expected. The rapid drop off of Fe^+ between 80 and 90 km is predicted by the chemical model. Also, note that a thin layer (superimposed on the background layer) is present for F4, but has a rather low peak density (~$4x10^4$ cm^{-3}).

However, if these measurements are indicative of the normal state of the background metallic ion layer, a major problem exists for explaining both the dense thin layers observed above 105 km (e.g., Bristow and Watkins, 1993), and the multiple layers seen descending from the upper E-region following nodes in the neutral wind structure (e.g., Turunen et al., 1993). Where do the ions come from for these layers? An obvious possibility is the vertical transport of ions (note that transport was explicitly ignored in the discussion of meteoric deposition and metallic chemistry). A reevaluation of cases F1 and F2 from the observations of Steinweg et al. [1992] provides a clue that transport driven by the convective electric field is at work. Notice that the metallic layer is much weaker on 26 November 1988 (F1), than it is only nine days later for F2. In fact the column density on 5 December 1988 is nearly 20 times greater (an Fe^+ column density of $5.2x10^8$ cm^{-2} for F1 versus $120x10^8$ cm^{-2} for F2). Incoherent-scatter radar measurements of the electric field were made simultaneously with the rocket launches (Rose et al., 1992). They found a field of 38 mV/m directed 351° west of magnetic north (i.e., in the NE quadrant) for F1, and 25 mV/m directed at 155° west of magnetic north (in the SW quadrant) for F2. As will be shown in the next chapter, electric fields oriented in the NE quadrant lead to uplift of ions, while those in the SW quadrant lead to downward motion. Thus, a plausible explanation of the difference in the two ion profiles is that the background layer observed for F1 had been depleted by uplift of the ions. This could be the source of metals that are seen to form layers at higher altitudes. Furthermore, this mechanism has been invoked to explain satellite observations of Fe^+ in the F-region where no significant meteoroid ablation should occur (Grebowsky and Pharo, 1985). In the next chapter, the transport of metallic ions will be studied in considerable detail.

CHAPTER 3
THEORETICAL STUDY OF THIN LAYER FORMATION

3.1 Introduction

The purpose of this chapter is to develop the theory of the formation of thin metallic ion layers, with emphasis on conditions when electric fields dominate the neutral wind, then apply it in a number of situations to better understand the phenomenon.

The fundamental task is to solve the ion momentum equation. Analysis of the resulting velocity field alone yields significant insights into the nature of the ion motion, because at the altitudes of interest the metallic ions have extremely long lifetimes relative to the time-scale of the transport process. However, solution of the momentum equation is only the starting point for this inquiry. To investigate such issues as the influence of the initial ion distribution and the ion-neutral collision frequency on the time required for a layer to form (or dissipate) under various electric field conditions, a one-dimensional simulation is employed. This simulation solves the continuity equation in the vertical direction, using the velocity field derived from the momentum equation to determine the particle flux.

This chapter begins with a discussion of the basic theory of ion motion, followed by a description of the one-dimensional simulation. The basic theory is then employed to gain a better understanding of the effect of electric field direction on layer formation, and to estimate the drift motion of layers already formed. A foundation is established from which the observations (detailed in Chapter 4) can be effectively interpreted. Furthermore, the theoretical developments made here serve as vital role in the synthesis of a heuristic model of layer occurrence, which is introduced in Chapter 5.

3.2 Basic Theoretical Model

3.2.1 Momentum Equation. The starting point for the analysis of the formation of thin metallic ion layers is the familiar ion momentum equation

$$\frac{\partial \mathbf{v}}{\partial t}+(\mathbf{v}\circ\nabla)\mathbf{v}=-\frac{\nabla p}{nm}+\mathbf{g}+\frac{q}{m}(\mathbf{E}+\mathbf{v}\times\mathbf{B})-\nu(\mathbf{v}-\mathbf{u}), \tag{3.1}$$

where v is the ion velocity, p is ion pressure, n is ion number density, m is ion mass, **g** is the acceleration due to gravity, q is the charge on an ion, **E** is the electric field, **B** is the geomagnetic field (taken to be constant), ν is the ion-neutral collision frequency, and **u** is the velocity of the neutral wind.

It will be assumed that electric fields in the ionosphere map downward along geomagnetic field lines without attenuation (since the magnetic dip angle is large at high latitudes, this is approximately equivalent to saying that the electric field is constant with altitude). A number of theoretical studies (e.g., Farley, 1959; Chiu, 1974) have shown this to be the case, so long as the scale length of the electrostatic field is sufficiently large, typically ≥10 km. The theoretical predictions have found support in the balloon observations made by Mozer and Serlin [1969].

The terms on the left-hand side of the equation (3.1) can be dropped (yielding the stationary state equation), but this step requires further justification. If the electric field and collision frequency are treated as constants, then the consequence of neglecting the inertial terms is clear: this merely suppresses the gyromotion leaving the calculated field to only include drift motion. However, the electric field varies with time, and the collision frequency with altitude. The temporal variation in these terms is unimportant so long as the time-scale of the variation is greater than ν^{-1}, the characteristic time-scale for this problem. Meeting this requirement poses no difficulty, since ν^{-1} is typically much less than one second in the E-region (and even in the lower F-region), while the scale of temporal variations in the convective electric field is on the order of minutes to hours. The effect of the vertical variation of the collision frequency (which is proportional to the

neutral particle density) is to create a gradient in the velocity field. If this gradient is large, then the advective term on the left-hand side of equation (3.1) could become significant. The importance of the advective term can be checked by calculating the velocity profile with the term neglected. Then the velocity gradient can be determined, and the advective term compared to those retained on the right-hand side of the equation. Such calculations show that the advective term is on the order of 1 m/s^2 or less, much less than the acceleration due to gravity, indicating that the term is indeed negligible for this problem.

After dropping the inertial terms, equation (3.1) can be solved for the ion velocity, yielding

$$\mathbf{v}=\frac{1}{1+\kappa^2}\left\{\mathbf{u}+\kappa\left[\frac{\mathbf{u}\times\mathbf{B}}{B}+\frac{\mathbf{g}}{\Omega}-\frac{\nabla p}{mn\Omega}+\frac{\mathbf{E}}{B}\right]+\kappa^2\left[\frac{(\mathbf{u}\circ\mathbf{B})\mathbf{B}}{B^2}+\frac{\mathbf{g}\times\mathbf{B}}{B\Omega}-\frac{(\nabla p\times\mathbf{B})}{Bmn\Omega}+\frac{\mathbf{E}\times\mathbf{B}}{B^2}\right]\right.$$
$$\left.+\kappa^3\left[\frac{(\mathbf{g}\circ\mathbf{B})\mathbf{B}}{B^2\Omega}-\frac{(\nabla p\circ\mathbf{B})\mathbf{B}}{B^2mn\Omega}+\frac{(\mathbf{E}\circ\mathbf{B})\mathbf{B}}{B^3}\right]\right\} \tag{3.2}$$

where $\kappa \equiv \Omega/\nu$ (Ω is the ion gyrofrequency, which is equal to 85 s^{-1} for Fe^+). Considerable simplification of this equation is possible, since several of the terms are negligible. Assume the ion to be Fe^+, that the convective electric field strength exceeds 10 mV/m, and that B $\approx$ 5x10^{-5} T, then $\frac{g}{\Omega}\approx 0.1\,m/s$ and $\frac{E}{B}\geq 200\,m/s$. Assuming isothermal conditions and that the ion density varies exponentially with altitude with scale height, H, it can be readily shown that $\frac{|\nabla p|}{mn\Omega}\approx\frac{900}{H}$ (where H is in meters). This term is at its largest in the vicinity of a thin layer, which will have a typical width on the order of a kilometer, so the pressure gradient term will not exceed ~1 m/s, and will likely be much less than this value. Retaining the neutral wind term for now (it will be treated separately in section 3.2.3), it is clear that the gravitational and pressure gradient terms can be neglected in the first two terms in brackets (the terms proportional to κ and κ^2, respectively). The term proportional to κ^3 merits special attention. It can be large at altitudes

above ~ 200 km (as can be appreciated from consideration of Figure 3.1), but is negligible at the altitudes where layers are observed to form. The electric field here is the ambipolar electric field, for which the associated velocity term will have magnitude on the order of the pressure gradient term, which should be quite small, as argued above. Thus, it is assumed that the gravitational component dominates this term. Although neglected for now, the term proportional to κ^3 is of great significance in the development of a conceptual model of large-scale horizontal transport, described in Chapter 5.

Taking the above discussion into account, the expression for ion velocity can be simplified to

$$\mathbf{v} = \frac{1}{1+\kappa^2}\left\{\mathbf{u} + \kappa\left[\frac{\mathbf{E}}{B} + \frac{\mathbf{u}\times\mathbf{B}}{B}\right] + \kappa^2\left[\frac{\mathbf{E}\times\mathbf{B}}{B^2} + \frac{(\mathbf{u}\circ\mathbf{B})\mathbf{B}}{B^2}\right]\right\}, \tag{3.3}$$

E is the *convective* electric field.

Before continuing, a coordinate system is introduced, so that equation (3.3) can be expressed in useful form (see Figure 3.2). The y-axis is to the magnetic north, the z-axis is vertically upward, and the x-axis completes the triad (being to the magnetic east). The angle I is the inclination of the geomagnetic field. A convenient convention is adopted whereby the electric field (assumed to be perpendicular to the geomagnetic field) is expressed in terms of two vector components: E_n is in the y-z plane, positive towards the magnetic north; and E_e is positive along the x-axis. Using this coordinate system, and making the reasonable approximation that the neutral wind's vertical component is usually negligible in comparison to terms involving the horizontal wind or the electric field, one obtains the below components from equation (3.3):

$$\mathrm{v}_x = \frac{1}{1+\kappa^2}\left\{u_x + \kappa\left[\frac{E_e}{B} - u_y \sin I\right] - \kappa^2\left[\frac{E_n}{B}\right]\right\} \tag{3.4a}$$

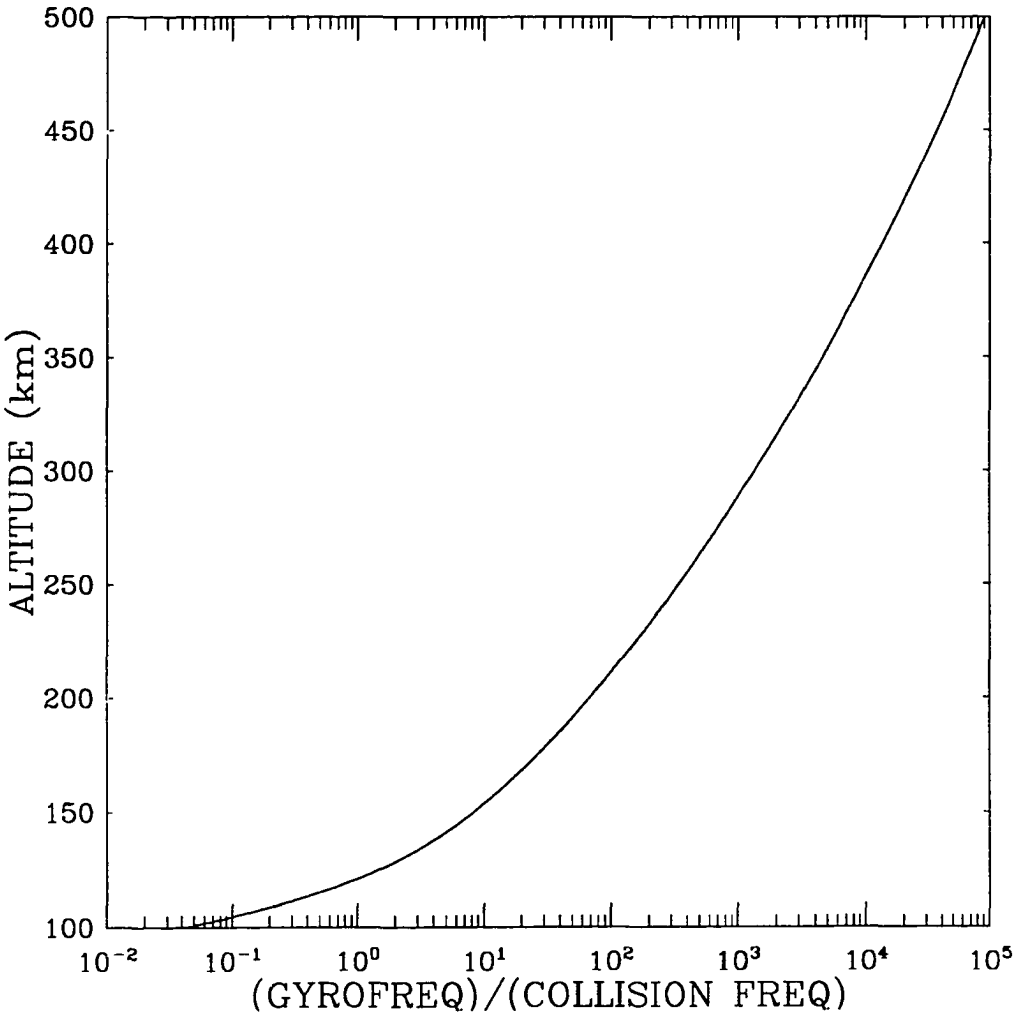

Figure 3.1 Plot of κ, the ratio of gyrofrequency to collision frequency, for Fe^{+}.

$$v_y = \frac{1}{1+\kappa^2}\left\{u_y + \kappa\left[\frac{E_n}{B} + u_x\right]\sin I + \kappa^2\left[\frac{E_e \sin I}{B} + u_y \cos^2 I\right]\right\} \quad (3.4b)$$

$$v_z = \frac{1}{1+\kappa^2}\left\{u_z + \kappa\left[\frac{E_n}{B} + u_x\right]\cos I + \kappa^2\left[\frac{E_e}{B} - u_y \sin I\right]\cos I\right\} \quad (3.4c)$$

Now consider equation (3.4c) with u_z set to zero, to see the conditions under which ions might converge at some altitude, forming a layer. The vertical velocity must go to zero for convergence, thus the required condition is

$$\frac{E_n + \kappa E_e}{B} + \left[u_x - \kappa u_y \sin I\right] = 0. \quad (3.5a)$$

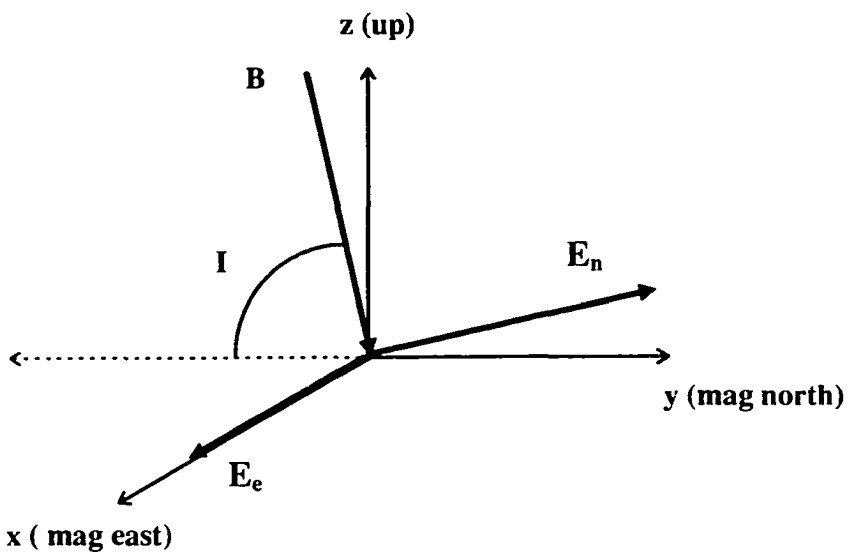

Figure 3.2 Coordinate system adopted to write ion velocity components (described in the text).

As will be shown in section 3.2.3, for an electric field >10 mV/m (not uncommon at polar latitudes) the electric field will dominate the neutral wind at most altitudes, so that the condition for convergence becomes

$$E_n + \kappa E_e = 0. \tag{3.5b}$$

Upon reflection, one can see that the direction of the electric field determines whether and at what altitude convergence will occur. A "null" in the velocity profile is possible (found by solving (3.5b)), if the electric field is directed to the magnetic northwest (NW) or southeast (SE). However, consideration of equation (3.4c) shows that for the SE case, ions move away from the null. Thus, a convergent (vertical) velocity field is established only when the electric field is directed to the NW (Nygrén et al., 1984a). Note the when the electric field is to the northeast (NE), ion motion is everywhere upward; while when it is to the southwest (SW), ion motion is everywhere downward. It has been shown that layer formation is possible in the SW and SE cases (Bristow and Watkins, 1991; Kirkwood and von Zahn, 1991), because the magnitude of the downward velocity decreases with decreasing altitude, leading to a "piling up" of ions into a relatively thick layer. Figure 3.3 summarizes the above discussion.

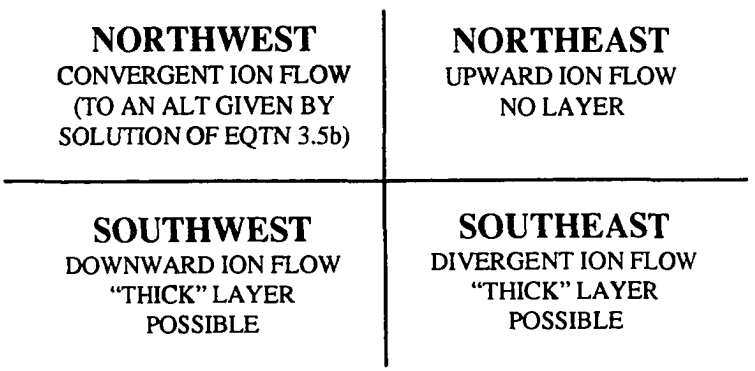

Figure 3.3 Electric field direction and vertical ion motion.

3.2.2 Sensitivity to the Collision Frequency Model. A discussion of the parameter κ is in order, as it strongly influences the overall configuration of the ion velocity field (see equations (3.3) and (3.4)), particularly the height of layer formation (as can be appreciated from equations (3.5a-b)). Recall that κ is defined as Ω/ν. Ω, given by qB/m, can be calculated with a great deal of confidence. On the other hand, the ion-neutral collision frequency, ν, poses a bit more of a challenge.

Banks and Kockarts [1973] provided an expression for the ion-neutral collision frequency which remains widely quoted today (e.g., Kelley, 1989), and is equivalent to the formulations developed in recent texts (e.g., Rees, 1989). Importantly, their model has been adopted in earlier studies of metallic thin layers (e.g., Nygrén et al., 1984a; Bristow and Watkins, 1991; Kirkwood and von Zahn, 1993). The Banks and Kockarts expression for the collision frequency is

$$\nu_{in} = \left(2.6\times10^{-9}\right)\frac{m_n\, n_n}{m_n + m_i}\left(\frac{\alpha_o}{\mu_A}\right)^{1/2} \quad (s^{-1}), \tag{3.6}$$

where ν_{in} is the ion-neutral collision frequency (previously denoted without subscripts), m_n is the mass of a neutral particle, m_i is the mass of an ion, n_n is the number density of the neutral species (cm^{-3}), α_o is the polarizability of a neutral particle (in units of 10^{-24} cm^3), and μ_A is the reduced mass expressed in amu. Banks and Kockarts warn that this expression may be inadequate, especially at temperatures above 300 K. Equation (3.6) was derived based on the assumption that the primary interaction between ions and neutrals is an induced dipolar attraction (which leads to a collision frequency without a dependence on temperature). At temperatures above ~300 K, dipolar attraction is countered by short-ranged quantum mechanical repulsion. At high temperatures, this repulsion would dominate, yielding a collision frequency which varies as $T^{1/2}$. Citing a lack of high temperature experimental data, Banks and Kockarts chose to model collisions over all temperatures using the dipole interaction alone.

Application of the induced dipole model for the collisional frequency, depends upon knowledge of the molecular polarizability and the number density of the neutral constituents of the atmosphere. For the former, the values quoted by Banks and Kockarts have been used here: 1.76, 1.59, and 0.79 for N_2, O_2, and O, respectively. The MSISE-90 thermospheric model (Hedin, 1991) has been used to calculate neutral densities. To appreciate the sensitivity of the ion velocity to the collision frequency, consider Figures 3.4 and 3.5.

In Figure 3.4, the altitude of convergence (z_c) for a northwesterly directed electric field is shown has a function of field direction for several multiples of the collision frequency derived from the model of Banks and Kockarts (henceforth called the B-K model). Notice that reducing the collision frequency tends to reduce the altitude of convergence. This suggests that a systematic error in the collision frequency model may account for a common problem in earlier theoretical analyses, i.e., the prediction of altitudes of convergence higher than expected. This proposition can be tested experimentally by measuring the electric field and layer altitude, then applying equation (3.5b). Although limited in number, observations made as a part of the present research project support the assertion of a systematic error in the collision frequency model (but do not provide information on the source of that error). This issue will be further discussed in Chapter 4.

In Figure 3.5, the vertical velocity profile is plotted for several multiples of the B-K model. For smaller multiples (relatively fewer collisions at a given altitude), the effect of the electric field penetrates deeper into the atmosphere. This would make a larger portion of the background metallic ion layer subject to efficient upward transport for a northerly electric field, thus providing for more ions in upper reaches of the E-region. This subject is revisited in section 3.4.

Since the possibility of a systematic error in the collision frequency has important ramifications for the occurrence of thin ion layers, this factor will be emphasized whenever appropriate in the remainder of this chapter.

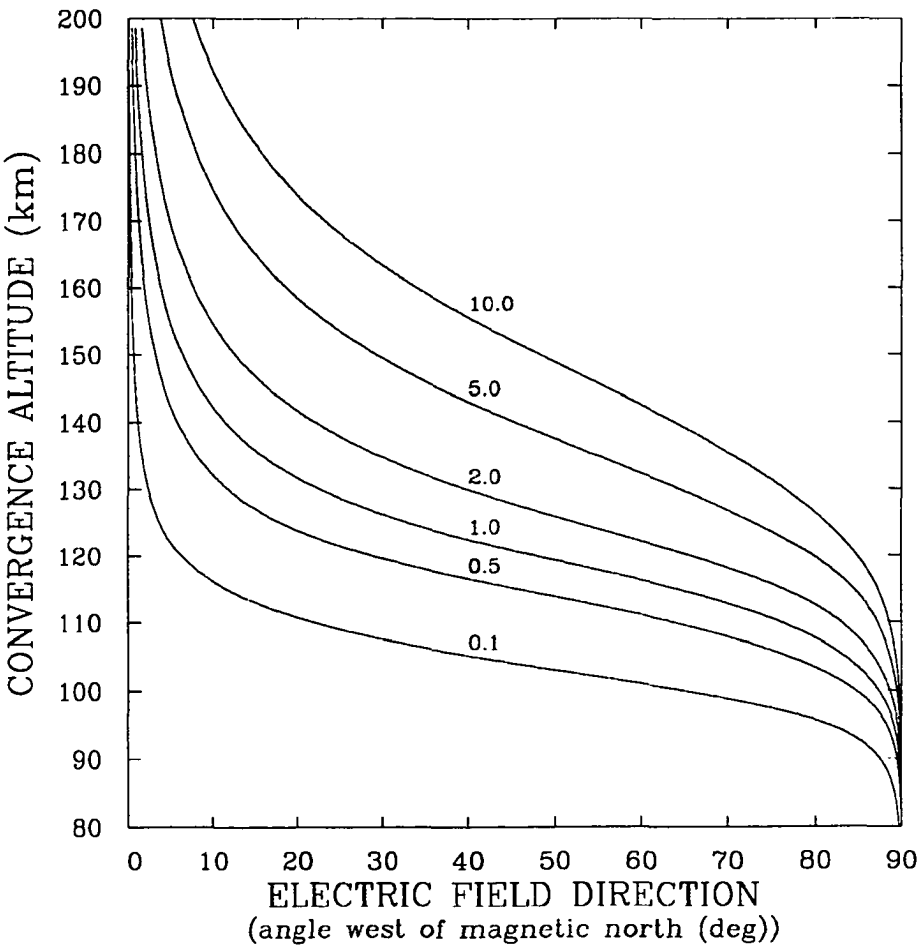

Figure 3.4 Sensitivity of the altitude of convergence to variations in the collision frequency model. Multiples of the B-K model ranging from 0.1 to 10 are shown here.

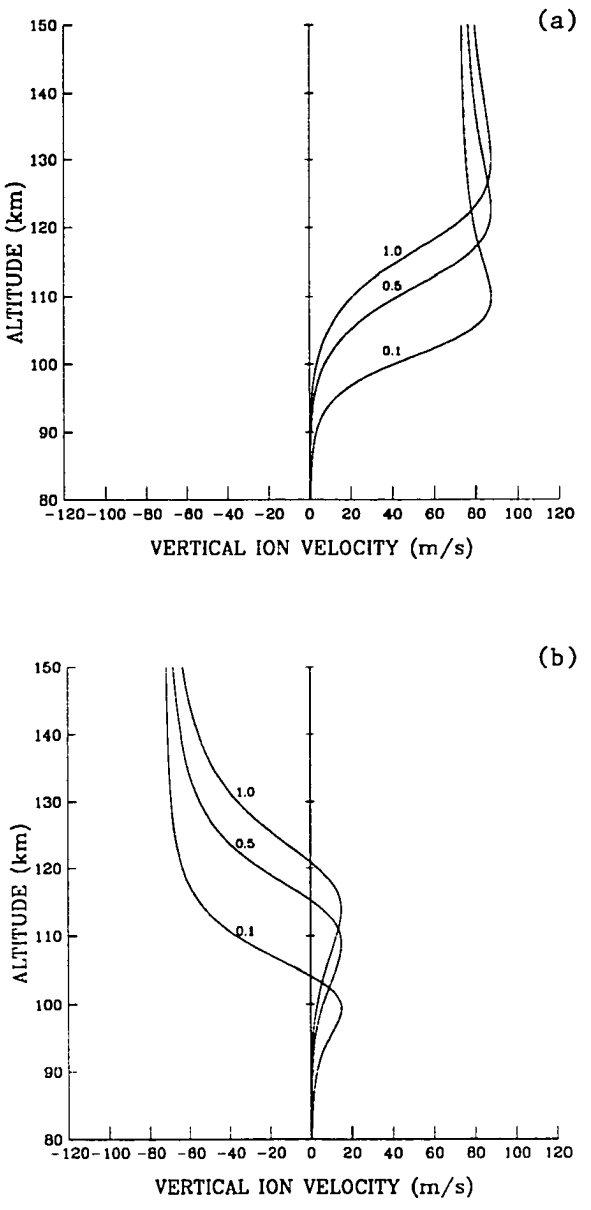

Figure 3.5 Sensitivity of the vertical velocity of Fe^+ ions to the model for collision frequency. Three multiples of the B-K model are shown. The electric field magnitude is 30 V/m. In (a) the field is directed 315° west of magnetic north. In (b) the angle is 45°.

3.2.3 Relative Effect of the Neutral Wind. Equations (3.3) and (3.4) can be evaluated to define conditions under which the electric field should dominate the effect of the neutral wind on ion motion. Notice that the ion velocity is expressed as the sum of three terms which are powers of κ (proportional to κ^0, κ^1, and κ^2, respectively). Since κ increases with altitude, each of the terms dominates at a different range of altitudes: κ^0 at very low altitudes, κ^1 at intermediate altitudes, and κ^2 at high altitudes. Physically, this reflects the decreasing influence of the neutral atmosphere on ion motion as altitude increases, on account of a reduction in the collisional coupling between neutral particles and ions.

Inspection of the second and third terms invites a direct comparison between the electric field and the neutral wind. In cases when κ is large enough that the first term can be ignored, the neutral wind is negligible if

$$\frac{E}{uB} >> 1. \tag{3.7}$$

The magnitude of the geomagnetic field at high latitudes is ~5×10^4 nT, and the magnitude of the neutral wind in the thermosphere is usually much less than 200 m/s (Hedin et al., 1991). Thus, an electric field with strength greater than 10 mV/m will, to a good approximation, determine the ion motion.

At lower altitudes, one cannot *a priori* ignore the term in κ^0. The threshold altitude, below which the first term should be given consideration, is found by setting κ equal to 1. As can be seen in Figure 3.6, the altitude corresponding to this condition is from 105 to 120 km, depending on the selection of a model for collision frequency. Now suppose one wishes to determine the altitude above which a given electric field dominates a wind of a given magnitude. This can be accomplished by requiring $\kappa = uB/E$, then solving for the altitude. In the lower thermosphere, the neutral wind velocity is generally less than 100 m/s in the horizontal plane, and less than 10 m/s in the vertical direction. Thus, for an electric field strength of 10 mV/m, $\kappa = 0.5$ for a wind of 100 m/s, and $\kappa = 0.05$ for a

wind of 10 m/s. The corresponding altitudes are shown in Figure 3.6. The horizontal components of the ion velocity become wind-dominated at higher altitudes than does the vertical component, since the magnitude of the horizontal wind is usually greater than the vertical component of the neutral wind.

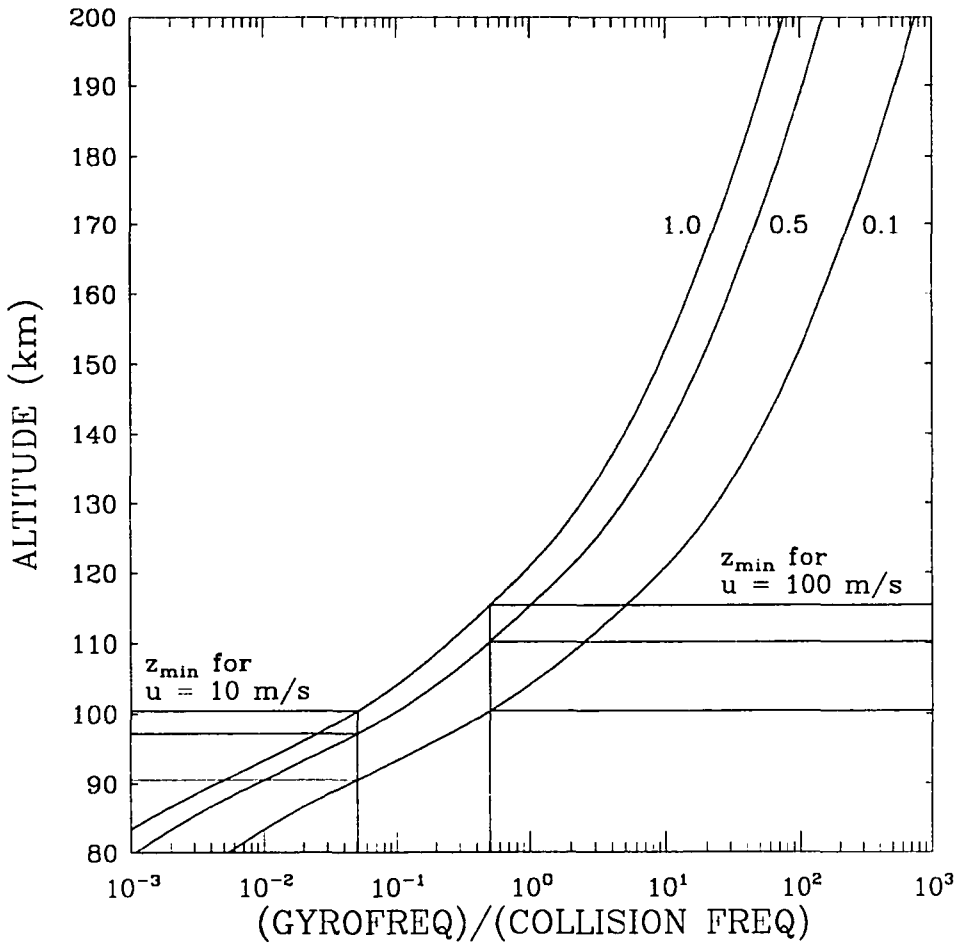

Figure 3.6 Minimum altitude (z_{min}) of domination of a 10 mV/m electric field over the neutral winds of specified magnitude. The situation for three multiples (0.1, 0.5, and 1.0) of the B-K collision frequency model are depicted

In summary, an electric field with magnitude greater than ~10 mV/m will tend to dominate the effect of the neutral wind on ion motion (e.g., see Figures 3.7 and 3.8). As can be seen in Figure 3.7, the assumption of a collision frequency less than the B-K model accentuates the effect of the electric field. This allows one to simplify the equations for the ion velocity field by dropping the wind terms. However, at low enough altitudes the neutral wind becomes dominant due to the exponential increase in collision frequency, which accompanies decreasing altitude. This serves to establish a lower bound on the range of altitudes for which an electric field can effectively cause ions to move. Thus, metallic ions in the lower portion of the background metal layer cannot be transported upward into the upper E-region, unless a sufficiently strong northerly electric field persists for a substantial duration of time. This topic will be taken up again in section 3.4.

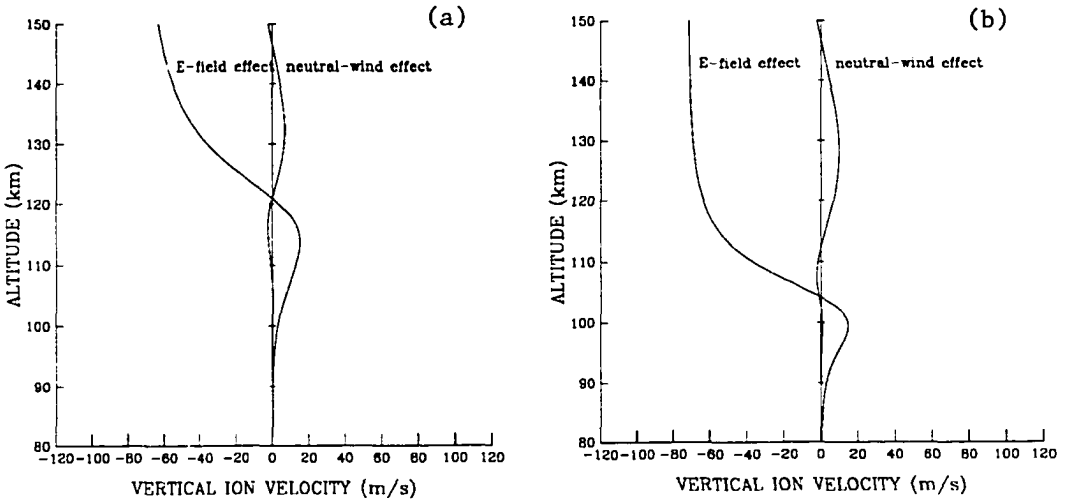

Figure 3.7 Comparison of the effect of an electric field versus the neutral wind on the vertical component of ion motion. Cases (a) and (b) are for the B-K collision frequency multiplied by 1.0 and 0.1, respectively. For this example the electric field is set at 30 mV/m, directed 45° west of magnetic north. The wind used is from HWM90 (Hedin et al., 1991) for 2300 UT, 20 July 1995, A_p = 9, f107 = 72, and f107a = 76, at Sondrestrom.

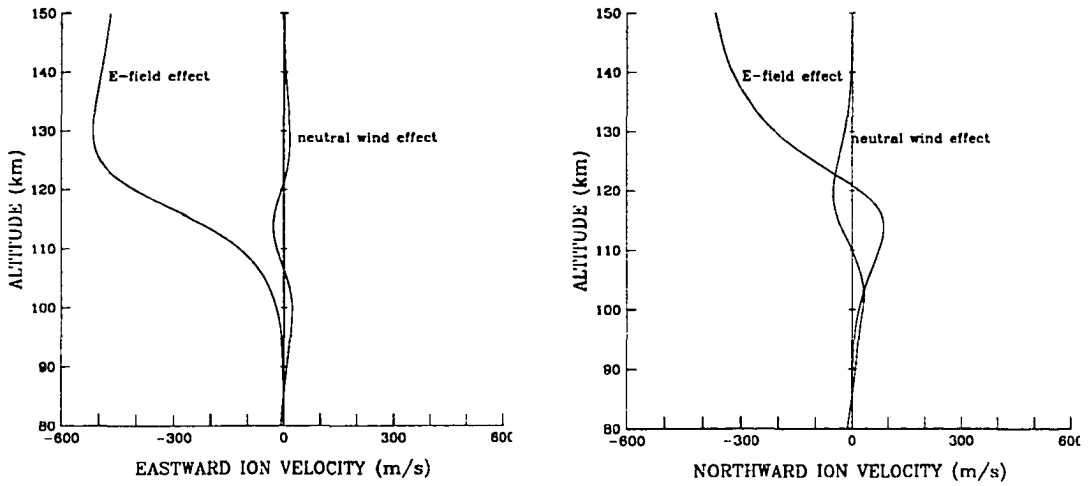

Figure 3.8 Comparison of the effect of an electric field versus the neutral wind on the horizontal components of ion motion. The B-K model for collision frequency is used without modification. For this example the electric field is 30 mV/m, directed 45° west of magnetic north. The wind used is from HWM90 (Hedin et al., 1991) for 2300 UT, 20 July 1995, $A_p = 9$, f107 = 72.0, and f107a = 76.9, at Sondrestrom.

3.3 One-dimensional Simulation

To study the time evolution of thin metallic ion layers, a one-dimensional model is employed. The continuity equation is solved in the vertical direction. In Chapter 2, it was shown that meteoric and chemical processes proceed slowly. This allows one to neglect source and loss terms in the continuity equation, a significant simplification, yielding

$$\frac{\partial n}{\partial t} + \nabla \circ n\mathbf{v} = 0, \tag{3.8}$$

where n is the ion number density, and $\mathbf{v}$ is the ion velocity. Further assuming no horizontal variation in either n or $\mathbf{v}$, equation (3.8) can be rewritten as

$$\frac{\partial n}{\partial t}+\frac{\partial n v_z}{\partial z}=0. \tag{3.9}$$

The vertical component of the ion velocity, v_z, is given by equation (3.4c) with the following modification: a term representing the pressure-gradient force is included. Although the pressure-gradient force is negligible almost everywhere, it must be considered in the immediate vicinity of a layer where the density gradient is large. Physically, the pressure-gradient force establishes a minimum attainable layer thickness for a given electric field. From a computational standpoint, the failure to include the pressure-gradient term invariably results in numerical instability. Therefore, assuming an isothermal ion population (and that the neutral wind is negligible), the z-component of the ion velocity used in this simulation is

$$v_z=\frac{\kappa}{B(1+\kappa^2)}\left\{\left[E_n+\kappa E_e\right]\cos I-\frac{kT}{nq}\left[1+\kappa^2\sin^2 I\right]\frac{\partial n}{\partial z}\right\}, \tag{3.10}$$

where T is the ion temperature and q is the charge on an ion.

The continuity equation is solved explicitly, utilizing the well-known two-step Lax-Wendroff scheme (detailed in several sources, e.g., see Potter, 1973). The algorithm is implemented by first calculating the density at intermediate time and space points:

$$n_{i+\frac{1}{2}}^{j+\frac{1}{2}}=\frac{1}{2}\left(n_i^j+n_{i+1}^j\right)-\frac{\Delta t}{2\Delta z}\left(F_{i+1}^j-F_i^j\right) \tag{3.11a}$$

$$n_{i-\frac{1}{2}}^{j+\frac{1}{2}}=\frac{1}{2}\left(n_i^j+n_{i-1}^j\right)-\frac{\Delta t}{2\Delta z}\left(F_i^j-F_{i-1}^j\right) \tag{3.11b}$$

where F is the particle flux, and the standard convention has been adopted wherein superscripts are associated with time steps, and subscripts with spatial steps. The results of the auxiliary calculation are used to find the fluxes at the intermediate points, i.e.,

$$F_{i\pm\frac{1}{2}}^{j+\frac{1}{2}}=n_{i\pm\frac{1}{2}}^{j+\frac{1}{2}}\left(v_z\right)_{i\pm\frac{1}{2}}^{j+\frac{1}{2}}. \tag{3.12}$$

Finally, the density at the full time step is calculated using the intermediate fluxes via

$$n_i^{j+1}=n_i^j-\frac{\Delta t}{\Delta z}\left(F_{i+\frac{1}{2}}^{j+\frac{1}{2}}-F_{i-\frac{1}{2}}^{j+\frac{1}{2}}\right). \tag{3.13}$$

The two-step Lax-Wendroff scheme is stable providing that the Courant-Friedrichs-Lewy condition is satisfied, i.e.,

$$\Delta t \leq \frac{\Delta z}{|v_z|}. \tag{3.14}$$

In practice, this condition was satisfied by adopting a spatial grid spacing of 0.1 km, and a time step of 0.1 s.

The upper and lower limits in altitude for the simulation are 200 km and 80 km, respectively. Dirichlet boundary conditions are adopted with the density values at the boundaries fixed at their initial values. At the lower boundary this posed absolutely no problem, since the ion velocity there is so small that the density changes little. At the upper boundary, instabilities occasionally occurred, depending on the form of the initial condition assumed. However, the upper boundary is far enough removed from the altitudes of layer formation, that instabilities generated there did not propagate into the region of interest within the time of layer formation.

3.4 Vertical Transport of Metallic Ions

3.4.1 Objective. Earlier theoretical studies (e.g., Nygrén et al., 1984a-b; Bristow and Watkins, 1991; Kirkwood and von Zahn, 1991) have treated vertical transport to identify electric field configurations that should give rise to layers, to gain insight on layer thickness, and to demonstrate that layers should form in tens of minutes when an appropriate field is present. These analyses assumed constant electric fields, the Banks-Kockarts collision frequency, and initial metallic ion distributions well above the background ion layer described in Chapter 2. As outlined in Chapter 1, observations have often been inconsistent with theory, suggesting the need for a revaluation of the theory.

The objective in this section is to revisit the role of vertical ion transport in the formation of thin layers with the intention of better defining the conditions under which layers should form. It must be emphasized that the fundamental theory, based on solution of the ion momentum equation is not questioned. Nor are the earlier conclusions, that

layer formation requires electric fields in the magnetic NW, SW, or SE quadrants, challenged. What distinguishes this effort from those accomplished previously is the degree of scrutiny applied to the study of layer formation. The influences of the initial metallic ion distribution, of the specific direction of the electric field within a given quadrant, and of temporal fluctuations in the electric field are investigated.

This section is organized as follows. First, layer formation for electric fields in the NW, SW, and SE quadrants is examined . Then the upward flux of ions, which should occur for an electric field directed to the NE, is studied as this process is likely to be important in supplying ions to altitudes from which they may be subsequently forced into thin layers. The Banks-Kockarts form of the collision frequency is utilized, since this facilitates the comparison of this analysis to those completed previously. However, since the predictions of the theory can be quite sensitive to the collision frequency, the effect of adopting a different collision frequency model, is discussed where appropriate. Furthermore, the neutral wind is taken to be negligible. Unless otherwise stated an ion temperature of 300 K is assumed. In all cases the following "model day" is adopted to derive characteristics of the neutral atmosphere from MSIS model: date - 20 July 1995; time - 2300 UT; A_p - 9; F10.7 - 72.0; F10.7a - 76.9; location - Sondrestrom, Greenland. Running the simulation for a single set of conditions does not diminish the generality of the results, since the influence of variations in neutral atmosphere due to such factors as time-of-day, season, geomagnetic activity, or solar activity do not have much effect on the calculated ion velocity (Kirkwood and von Zahn, 1991).

3.4.2 Electric Field in the Northwest Quadrant. Whenever the electric field is directed to the magnetic NW, layers should form as ions flow down from above and upward from below toward the null in the velocity profile, defined by equation (3.5b), and illustrated in Figure 3.9. Several generalizations derive from consideration of Figure 3.9.

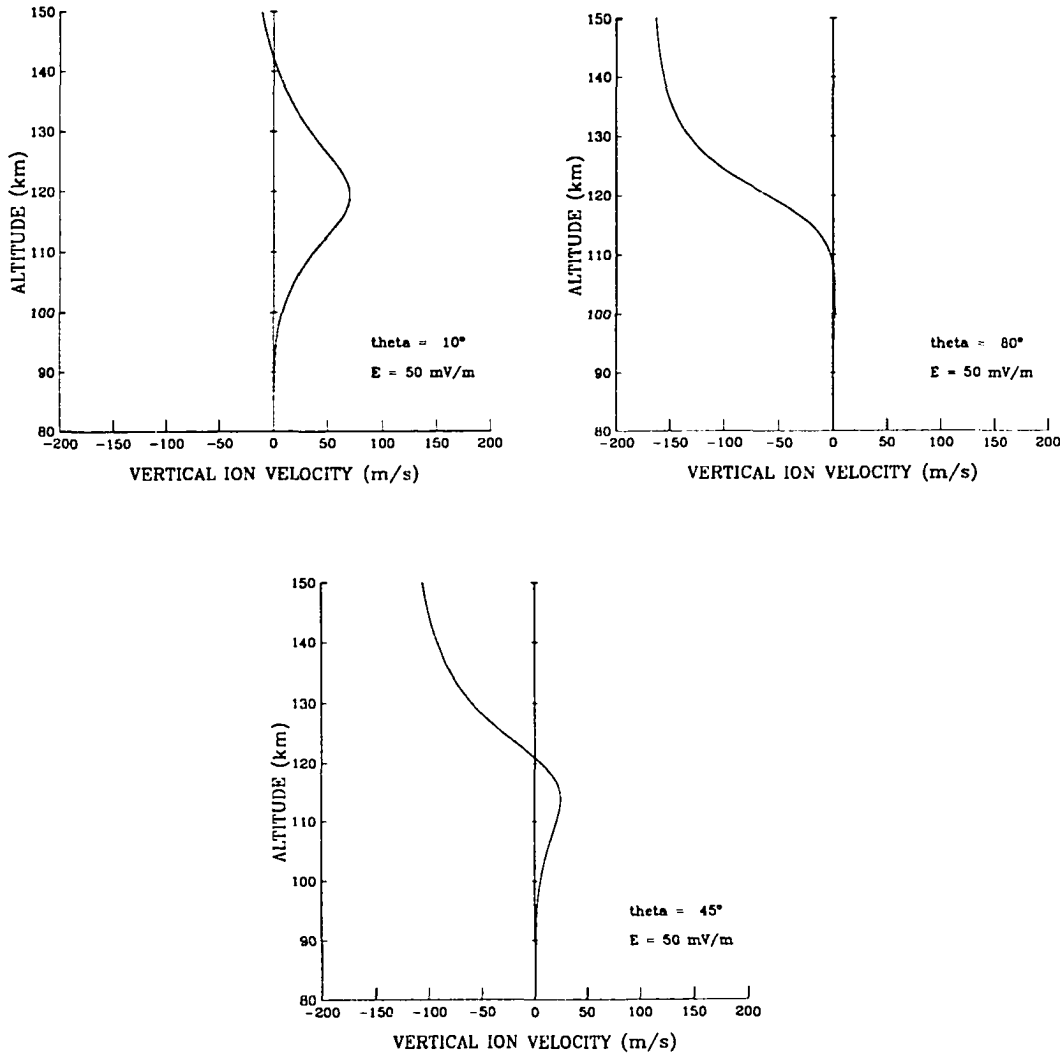

Figure 3.9 Representative metallic ion (Fe^+) vertical velocity profiles when the electric field is directed in the magnetic northwest (NW) quadrant. Electric field strength is 50 mV/m for these examples.

As the field becomes more northerly directed ($\theta \rightarrow 0°$), layers form higher and upward transport becomes increasingly important. On the other hand, as $\theta \rightarrow 90°$ the altitude of the null decreases and downward ion transport becomes dominant. Since the ion velocity is directly proportional to the magnitude of the electric field (see equation (3.4) with $\mathbf{u} = 0$), increasing the magnitude of the electric field will reduce the time required for layer formation, but does not change the altitude at which the null in ion velocity occurs.

A fine point, not noted in previous studies, is that as $\theta \rightarrow 0°$ layers initially form below the null then intensify as they drift toward the altitude of the null. Similarly, as $\theta \rightarrow 90°$ layers initially form above the null. This effect becomes progressively more pronounced as θ approaches magnetic north and west, as illustrated in Figure 3.10. In

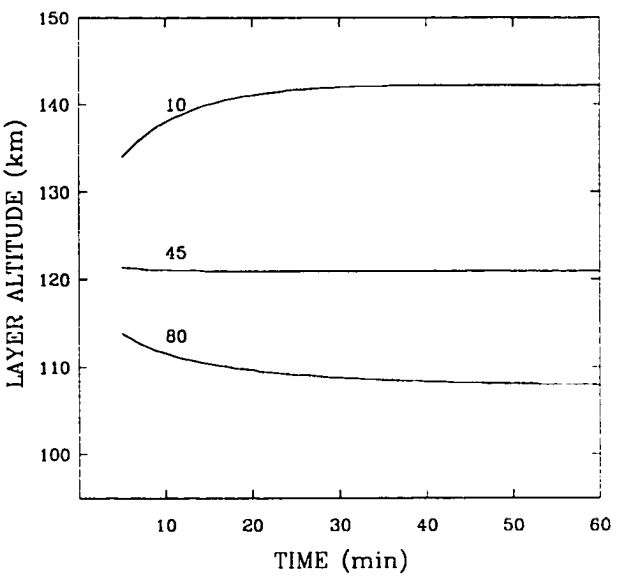

Figure 3.10 Difference between the altitude of peak layer density and the altitude of the convergent null (z_c) for three values of θ in the NW quadrant. For this example, the electric field magnitude is 50 mV/m, and a uniform initial ion distribution is assumed.

the latter case this behavior can be explained using the same argument as earlier proposed to account for layer formation in the SW quadrant (e.g., Bristow and Watkins, 1991), i.e., increasing neutral density impedes the downward flow of ions. In the former case, a similar mechanism is at work, with the negative gradient in the upward ion velocity below the null causing the ions to build into a layer below the null. However, in this case the velocity gradient is a consequence of *decreasing* atmospheric density with increasing altitude; **ExB** drift becomes more important with increasing altitude, which for northerly fields implies a decreasing vertical component of the ion velocity. This vertical drift only exists early in the evolution of a layer, while the layer is of relatively low density. Thus, this effect is likely to be difficult to observe.

Two cases are considered to study the effect of the initial ion distribution on layer formation. The first, depicted in Figure 3.11a, is modeled after observation F2 shown in Figure 2.11. It corresponds to the "background" Fe^+ layer expected from meteoroid ablation. The second case (see Figure 3.11b) has the same column density as the first, but the ions are distributed uniformly between 90 and 170 km, with the density dropping off rapidly above and below these altitudes. Such a distribution is somewhat artificial, but is of the general form one might expect if ions have been redistributed upward from the background metallic layer (a mechanism for this to occur is discussed in section 3.4.4). The column density is 1.3×10^{10} cm^{-2}, which corresponds to a density of 1.3×10^5 cm^{-3} for a layer 1-km thick (the actual thickness and density of a layer will depend upon the electric field magnitude and the ion temperature).

Figure 3.12 depicts the density build up of a layer as a function of field direction and time, when the low-lying background distribution is assumed as the initial condition. A fairly high electric field strength was assumed, 50 mV/m, so that this might be considered

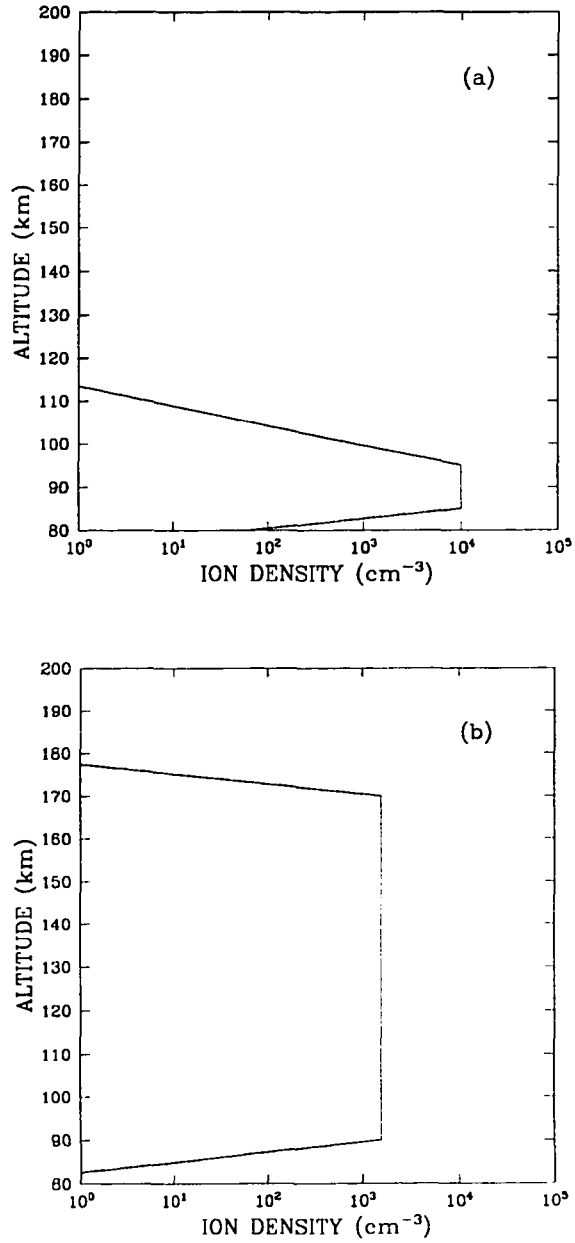

Figure 3.11 Initial Fe^+ profiles adopted in this study: (a) background ion layer associated with meteor ablation; (b) equivalent column density, distributed uniformly over higher altitudes.

a best case for layer formation. For $\theta > 60°$, the altitude of convergence is within the initial distribution of ions, but the velocity is relatively low, so that layer development proceeds very slowly. The strongest layers occur for $10° < \theta < 60°$, but it requires well over 30 minutes for the density to exceed 10^4 cm^{-3}. The unmodified Banks-Kockarts collision frequency was employed for this simulation, which predicts layers above 120 km for most field directions; this contributes to the slow build up of density. However, even adopting a fraction of the B-K collision frequency does not alter the general implication of this analysis: formation of layers when the ions are initially at low altitudes is quite inefficient.

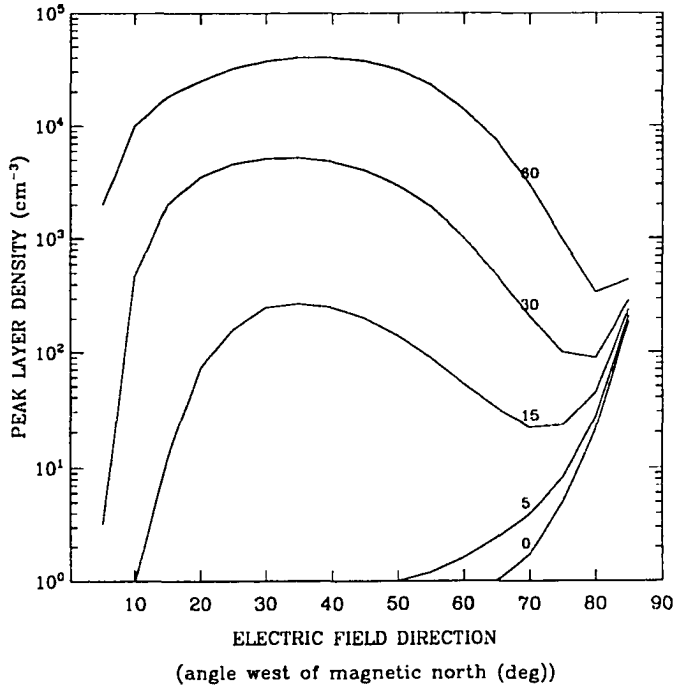

Figure 3.12 Evolution of the density of thin layers as a function electric field direction, θ, when the electric field is in the NW quadrant. The initial ion profile corresponds to the background metallic layer as shown in Figure 3.11a. E = 50 mV/m. The curves correspond to density after 0, 5, 15, 30, and 60 minutes.

If, on the other hand, the metallic ions are initially distributed across higher altitudes, layer formation is much enhanced, since at higher altitudes the ion velocity is typically greater. Figure 3.13 illustrates this point. Densities of over 10^5 cm^{-3} are attainable over a wide range of angles. Rate of build up is greatest for $35° < \theta < 70°$, where strong layers form in less than 15 minutes (even assuming an electric field of only 25 mV/m would yield dense layers in less than 30 minutes). For $\theta < 20°$, layer formation is relatively inefficient. The general conclusions one can draw from this simulation are that layers form more readily when ions are located above the ablation region, and that the rate of formation is quite dependent on specific direction within the NW quadrant.

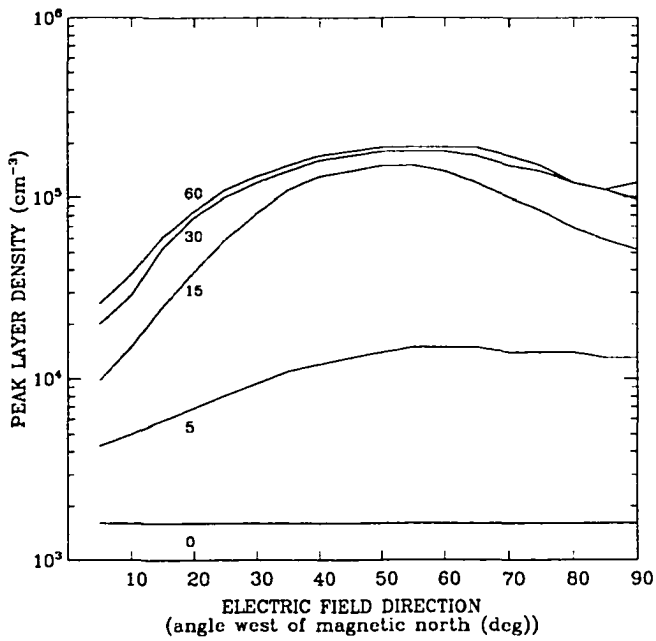

Figure 3.13 Evolution of the density of thin layers as a function of time and angle, θ, when the electric field is in the NW quadrant and the initial ion profile corresponds to the broad distribution of metallic ions shown in Figure 3.11b. E = 50 mV/m. The curves correspond to density after 0, 5, 15, 30, and 60 minutes.

Kirkwood and von Zahn [1991] have pointed out that fluctuations in the direction of the electric field within the NW quadrant will cause the altitude of the convergent null to also fluctuate. They assert that this would lead to broader, less intense layers than expected for a steady field, and thus reduce the chance of observing layers formed for fields directed in this quadrant. This intuitively appealing idea has been tested via simulation, the results of which indicate that it is not applicable.

Assume that the magnitude of the electric field remains constant, while the direction varies as

$$\theta = \theta_o + \Delta\theta \sin(2\pi f t), \tag{3.15}$$

with $\Delta\theta = 5°$. A relatively large electric field strength, 50 mV/m, was adopted, since high field magnitude should enhance the responsiveness of the ions to changes in field direction. The initial ion distribution of Figure 3.11b was employed, so that ions would be initially present near the null in the velocity profile (this serves to diminish lags in layer formation which occur if, for example, the density profile in Figure 3.11a is used). The formation of layers was simulated for values of the frequency, f, ranging from 10^{-4} to 1 Hz. Representative results are shown in Figure 3.14, which gives the layer altitude relative to the convergence altitude and full-width-half-maximum (FWHM) thickness as a function of time, for three values of θ_o. The peak layer density as a function of time (not shown) is very close to that predicted for the DC case (f = 0), and can deduced from Figure 3.13. Note that at very low frequencies, the layer will drift with the fluctuating null in the velocity profile. As the frequency increases, the ions become less responsive to fluctuations in the location of the null, and the layer tends to form at the altitude of convergence for the average value of θ. Another implication of this simulation is that layer thickness is relatively unaffected by fluctuating field direction. This admittedly simple analysis suggests that temporal variation in the direction of the convective electric field does not significantly impact the effectiveness of layer formation for fields in the NW quadrant.

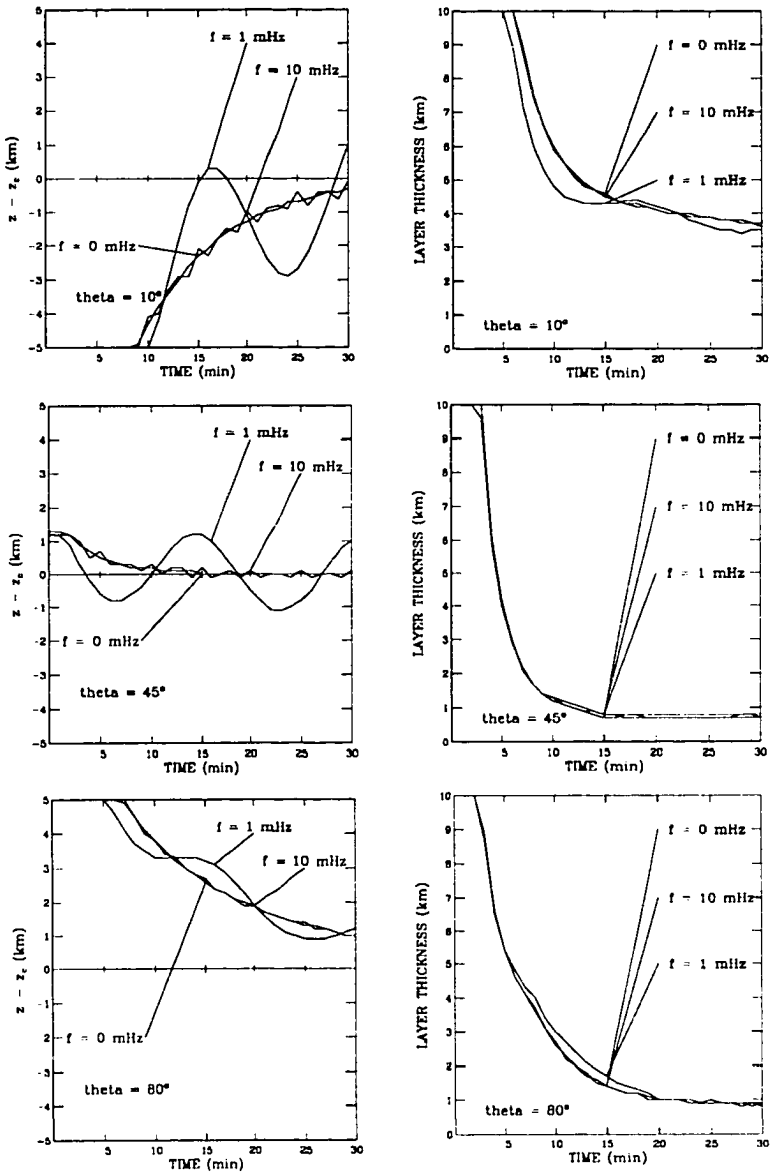

Figure 3.14 Effect of fluctuating electric field direction on the formation of thin layers. Three values of θ_o are depicted, and the frequency of fluctuation set at 0, 10^{-3}, and 10^{-2} Hz. E = 50 mV/m.

3.4.3 Southerly Electric Fields. As illustrated in Figure 3.15, the ion velocity is downward at all altitudes for an electric field in the SW quadrant, and is downward below a null in the velocity profile for fields to the SE. Layer formation results from the same mechanism for fields in both quadrants. The magnitude of the vertical velocity decreases with altitude, causing a layer to form at ~105 km when the Banks-Kockarts collision frequency is adopted. Layers formed by this process will drift downward with ever decreasing velocity, intensifying in the process. By inspection of the initial ion distributions given in Figure 3.11, in comparison to the velocity profiles, it is obvious that southerly electric fields can only cause layers to form slowly, when the metallic ions are initially in the low-lying background layer. Simulation of layer formation under this condition indicates that the background layer is virtually unperturbed after even an hour with fields of 50 mV/m (adoption of a collision frequency lower than given the B-K model, shows the formation of a layers below an altitude of 100 km, superimposed on the background layer). Therefore, without further discussion, it is asserted that for southerly electric fields to be effective in the formation of intense thin ion layers, ions must be initially distributed at higher altitudes. Accordingly, the ion distribution shown in Figure 3.11b with be adopted for subsequent analysis. Results of the one-dimensional simulation of layer formation for southerly fields are given in Figure 3.16.

As can be seen in Figure 3.16a, dense layers can form for $\theta < 170°$, but the rate of formation is relatively slow, even for the strong electric field (50 mV/m) assumed here. For $\theta > 170°$, layer formation is inefficient, primarily because the range of altitudes at which ion flow is downward diminishes as $\theta \rightarrow 270°$, making less ions available for the layer. Furthermore, after 30-40 minutes layers formed for fields in the SW quadrant have thickness comparable to that of layers formed for electric fields directed to the NW (contrast Figure 3.13c with 3.16c). This appears to contradict the results of previous investigations (Kirkwood and von Zahn, 1991; Bristow and Watkins, 1991), which suggest that layers formed by southerly fields should be weaker and thicker than those formed by NW-directed fields. However, these conclusions were based on simulations

running for 18 to ~30 minutes. Therefore, a more precise comparison of the characteristics of layers formed by southerly electric fields, versus fields directed to the NW, is: both orientations can produce layers of comparable thickness and density, the difference is that it generally takes longer for a southerly field to do so.

Notice in Figure 3.16b, that the characteristic downward drift of the layer proceeds at a decreasing rate as the altitude decreases, approaching a quasi-stationary altitude between 90 and 95 km. As might be expected, for weaker electric fields the layers form more slowly and at higher altitudes (e.g., 5 km higher, for E = 30 mV/m).

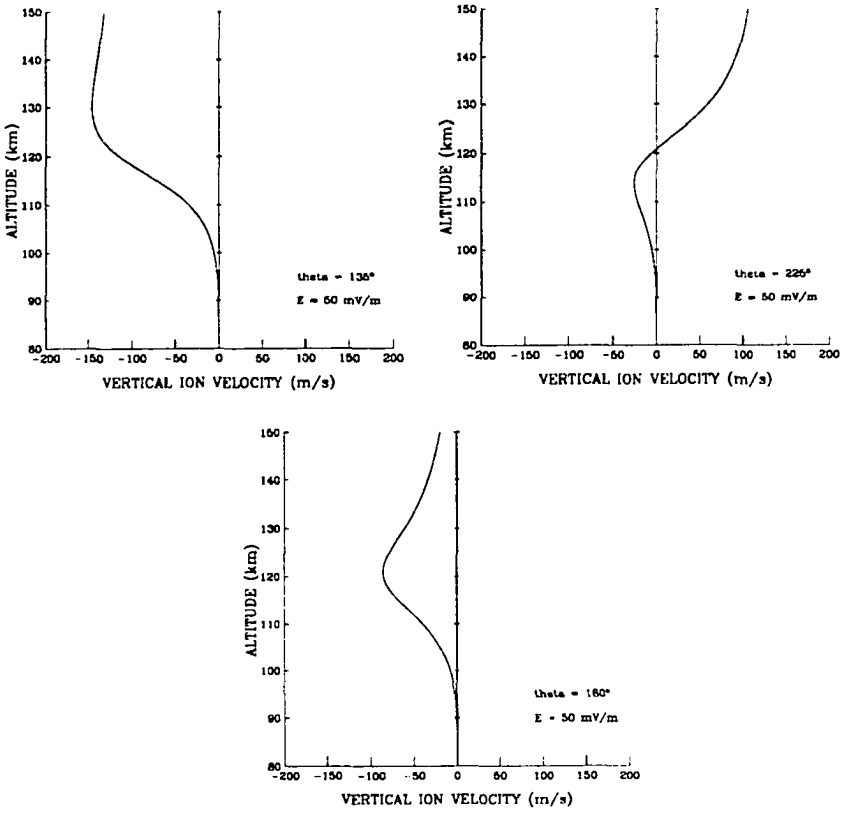

Figure 3.15 Representative metallic ion (Fe^+) vertical velocity profiles for (magnetically) southerly electric fields. E = 50 mV/m.

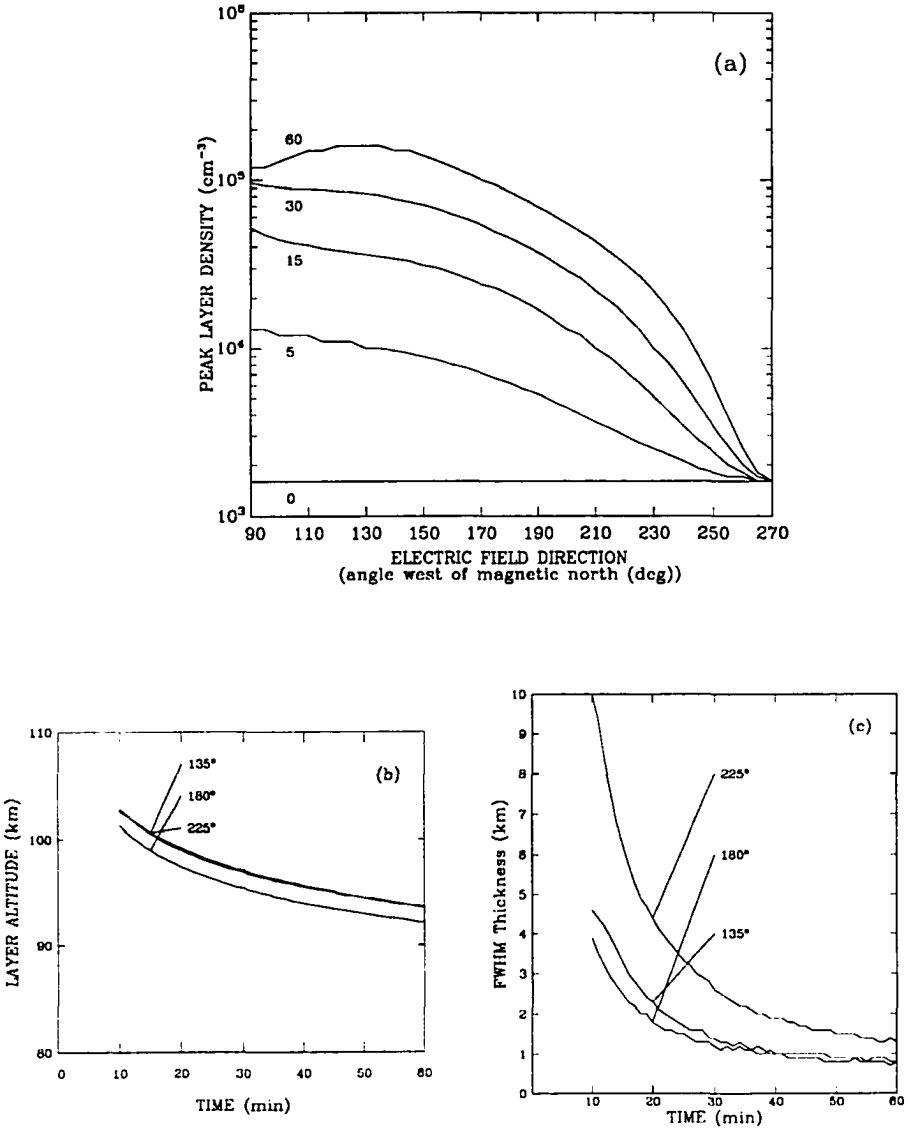

Figure 3.16 Evolution of thin layers for southerly electric fields when the initial ion profile corresponds to the broad distribution of metallic ions shown in Figure 3.11b: (a) peak density as a function of time and field direction; (b) layer altitude as a function of time; (c) layer thickness as a function of time. E = 50 mV/m.

3.4.4 Upward Ion Flux. Electric fields directed to the magnetic NE have been generally excluded from the discussion of the formation of thin ion layers, because such fields give rise to upward ion flow at all altitudes, as illustrated in Figure 3.17. This is not conducive to the formation of thin layers.

However, as was shown above, the rapid formation of dense layers requires ions to be initially located above the normal background metallic ion layer. One earlier study proposed direct meteoric deposition at high altitudes as the ion source (Kirkwood and von Zahn, 1991), but this was shown in Chapter 2 to be unlikely. Another study arbitrarily assumed a layer peaking at 120 km (Bristow and Watkins, 1991). To resolve this issue, it is suggested here that the mechanism by which ions come to populate the higher altitudes is vertical transport driven by a NE electric field.

This assertion was tested by running the simulation with an initial ion background centered below 100 km (see Figure 3.11b). The fraction of ions above specified altitudes (100, 120, and 150 km) was calculated as a function of time, and has been plotted in Figures 3.18 and 3.19. Calculations using both the B-K collision frequency and a tenth of that value are shown, to illustrate the sensitivity of the results to changes in the model of collision frequency. Using the B-K model over 25% of the ions are lifted above 150 km in an hour, if a strong electric field is present. If the collision frequency is less than the B-K value, the upward flux is more significant. It is also apparent that electric fields in the middle of the quadrant are more effective than those to the north or east.

The conclusion here is that upward transport of ions via a moderately strong NE electric field can draw ions out of the background layer (recall the discussion found in section 2.4, which also supports this inference). This provides a source of ions for layer formation without having to rely upon *ad hoc* assumptions. Additionally, ions lifted to higher altitudes can also be transported horizontally over great distances, suggesting a means by which large-scale horizontal redistribution of ions might occur. This matter is revisited in Chapter 5.

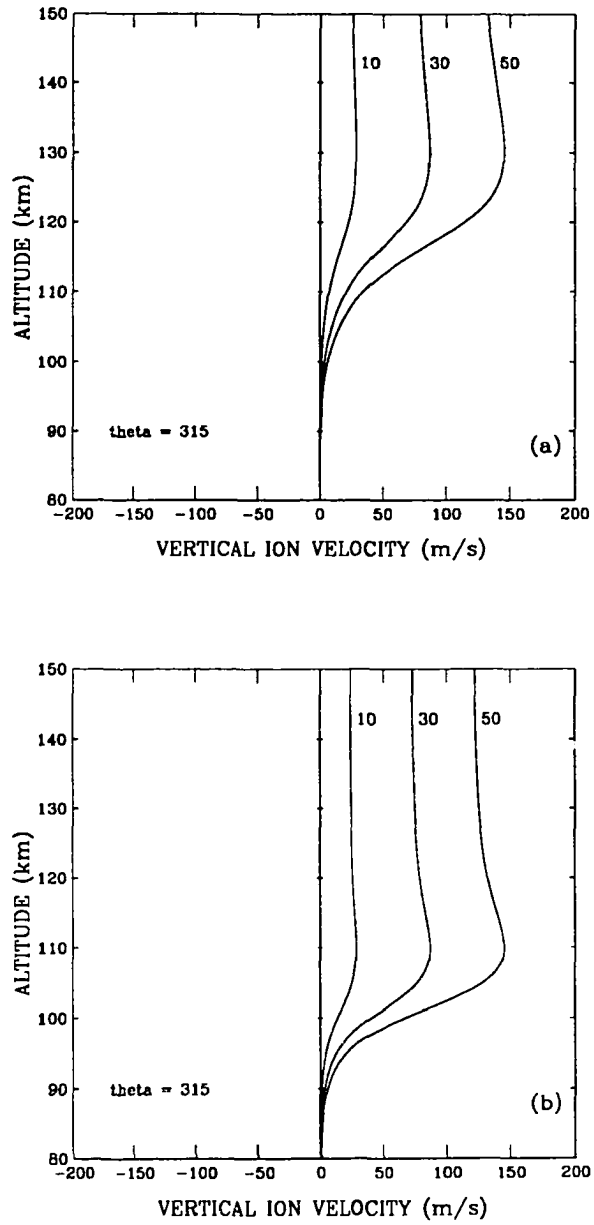

Figure 3.17 Vertical ion velocity for a NE-directed electric field (θ = 315°), with E = 10, 30, and 50 mV/m. Case (a) is for the B-K collision frequency; case (b) for one tenth of that value.

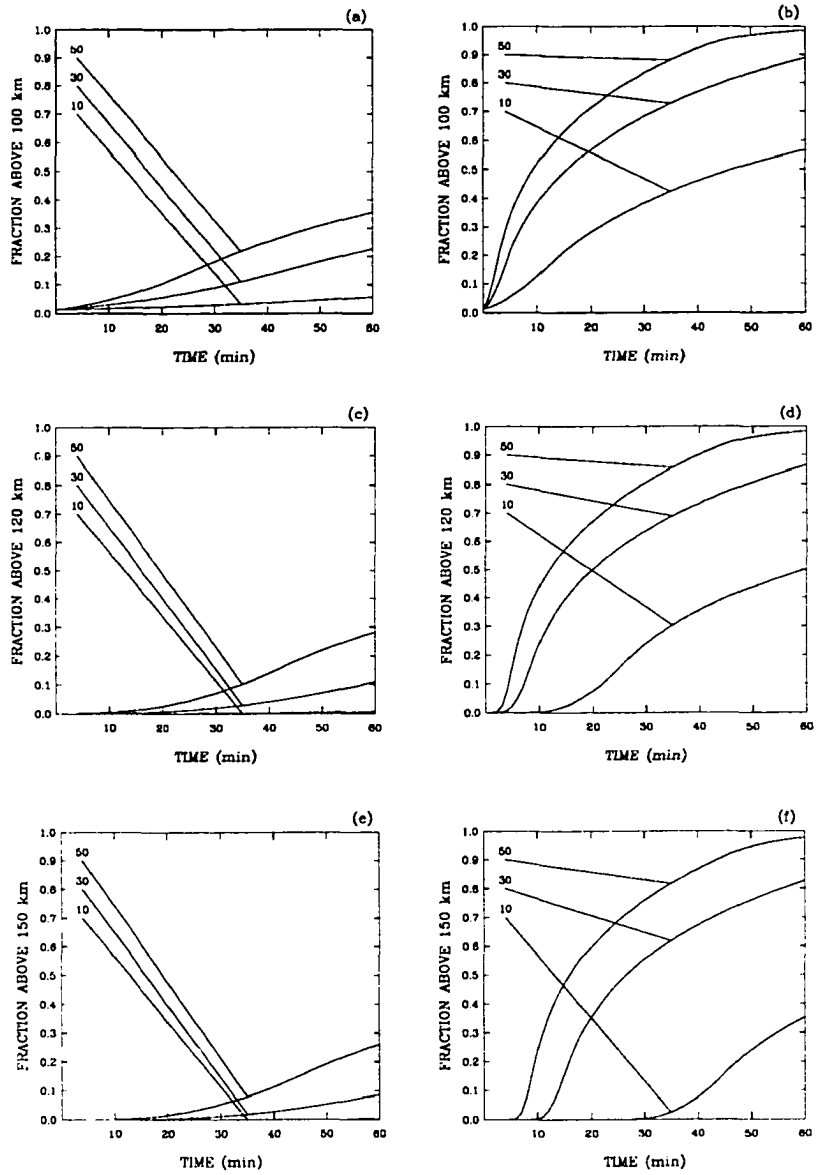

Figure 3.18 Fraction of ions above set altitudes (100, 120, 150 km) as a function of time, for a NE electric field ($\theta = 315°$) and initial ion distribution given in Figure 3.11a. Three field strengths (10, 30, 50 mV/m) are depicted for each case. (a), (c), & (e) assume the B-K collision model; (b), (d), & (f) use one tenth of that value.

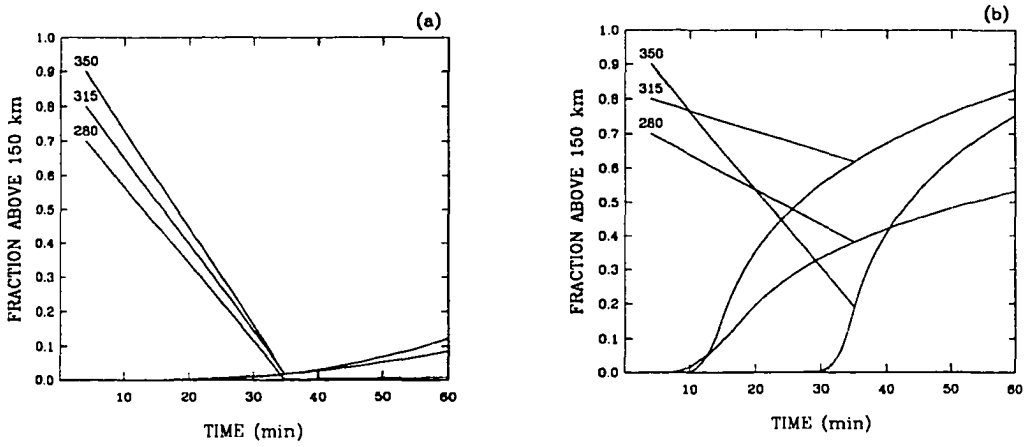

Figure 3.19 Fraction of ions above 150 km as a function of time, for an electric field magnitude of 30 mV/m, and initial ion distribution given in Figure 3.11a. Three values of θ are shown (280°, 315°, 350°). (a) assumes the B-K collision model; (b) uses one tenth of that value.

3.4.5 Closure. The foregoing analysis of the vertical transport of metallic ions has provided several refinements to the current theory of the formation of thin layers; these are recapitulated here.

It is well known that electric fields directed to the NW, SW, or SE are capable of causing thin ion layers to form. However, the rate of layer formation is quite dependent on the specific direction (θ, measured west of magnetic north) of the field, as is reviewed in Figure 3.20a. For $\theta < 20°$ and $\theta > 170°$, layer formation proceeds so slowly that fields so directed are not likely to contribute much to the overall rate of occurrence of very dense layers. Layers form most rapidly for $35° < \theta < 70°$. Quite dense layers can form for southwesterly electric fields, but the rate of formation is slower than in the case of fields to the NW. However, if sufficient time is available, fields to the SW can lead to layers of comparable thickness and density to those originating when the field is to the

NW. Thus, layer thickness and density cannot be used as a reliable indicator of field direction present at the formation of the layer. The preceding results were based upon simulations assuming the standard Banks-Kockarts collision frequency model. As can be seen in Figure 3.20b, adopting a reduced collision frequency does not substantially affect the conclusions cited above.

The proposition, that fluctuation of the direction of electric fields in the NW quadrant might inhibit layer formation, was tested at frequencies below 1 Hz. Simulations indicate no appreciable effect on either the thickness or density of layers formed.

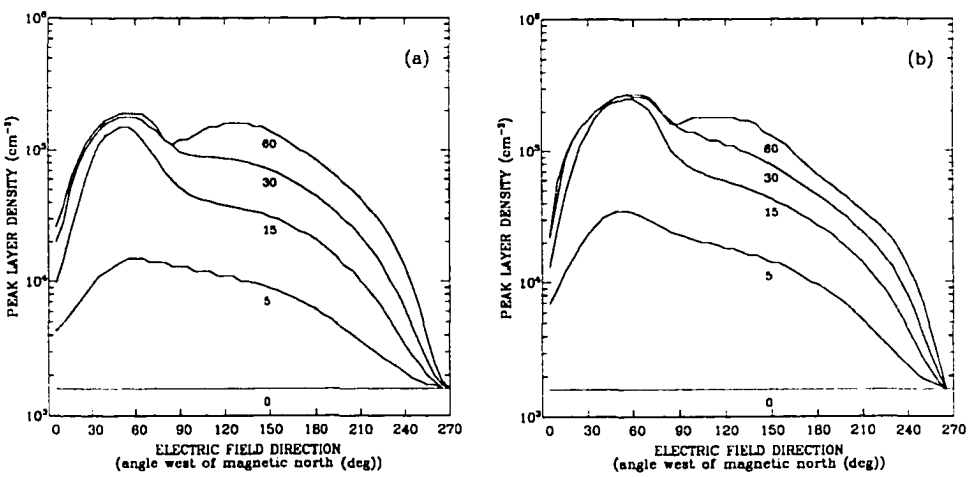

Figure 3.20 Evolution of the density of thin layers as a function of time and angle, $0° < \theta < 270°$, when the initial ion profile corresponds to the broad distribution of metallic ions shown in Figure 3.11b. E = 50 mV/m. The curves correspond to density after 0, 5, 15, 30, and 60 minutes. Assumed collision frequency model: (a) ν_{BK}; (b) $0.1\nu_{BK}$.

Layers form much more readily, if the metallic ions are initially distributed above the background ion layer which typically is located primarily between altitudes of 90 and 100 km. Simulations indicate that electric fields directed to the NE can provide an efficient mechanism for transport of ions upward out of the background layer. This effect is enhanced, if a collision frequency less than the Banks-Kockarts value is assumed.

3.5 Layer Advection

3.5.1 Objective. The interpretations of most earlier observations of thin metallic layers have tacitly assumed that the layers do not advect across the field of view. The formation and duration of layers can then be discussed in terms of the local electric field. In this section the following general questions are examined. Might thin layers form at one location, then horizontally drift to another where the electric field configuration is different? If this is so, then the explication of thin layer observations is much more difficult. A related question is: suppose a layer is stationary over the observer, how long does it persist after the electric field vanishes? Comparing the dissipation time with the time expected for a layer to advect across the field of view, could provide a means for interpreting the results of observations in which advection cannot be simultaneously measured.

The objective here is to determine the nature of the layer drift to be expected under various conditions. For numerical examples given below, the Banks-Kockarts collision frequency has been assumed (the effect of using a reduced collision frequency will be commented upon at the conclusion of this section).

3.5.2 Layer Motion with a Uniform Electric Field. Suppose that the electric field has been either to the NW or southerly directed long enough for a thin layer to form. Consideration of the horizontal components of the ion velocity (equations 3.4a-b), allows one to immediately predict the expected layer drift given the field configuration.

For fields to the NW, the northerly component of the ion velocity vanishes, and the easterly component is negative, *if the layer forms at the convergent altitude.* This implies a horizontal drift velocity for the layer of

$$v_x = -\frac{E}{B}\cos\theta. \tag{3.16}$$

Care is necessary in the application of equation (3.16). In section 3.4 it was demonstrated that layers don't readily form for $\theta < 20°$. Furthermore, as $\theta \to 90°$, which corresponds to the altitude of convergence approaching zero, layers form at ~100 km as increasing atmospheric density retards downward ion flow; this implies a drift velocity becoming small, but non-zero. The predicted magnitude of the layer drift can be quite high, with an upper limit of *E/B* (e.g., ~1000 m/s, for an electric field of 50 mV/m).

Southerly electric fields tend to cause layers to drift in the same direction as the electric field (Pederson motion) with a relatively low speed, since such layers form at low altitudes (~100 km). Recalling the analysis presented in section 3.2.3, it is clear that the effect of the neutral wind on horizontal ion motion is likely to be non-negligible at the altitudes that these layers form. Thus, one would expect to encounter difficulty in ascribing observed layer drift to the convective electric field , unless that field was quite large.

Figure 3.21 illustrates the magnitude of the velocity of layer drift, as a function of electric field direction for a field strength of 50 mV/m. The altitude of the layer is taken to be 100 km for $\theta \geq 90°$, and for $20° < \theta < 90°$ is set at either the convergent altitude, or 100 km, whichever is greater.

3.5.3 Layer Dissipation. Above, the expected horizontal motion of a thin ion layer due to the electric field which caused the layer to initially form was described. Here it is assumed that after a layer has formed, the electric field suddenly vanishes (this is equivalent to the case of a spatially varying electric field in which a layer drifts into a region where the field strength is negligible). The question is: how much time elapses before the layer diffuses away? For the sake of this discussion, the layer is assumed to be

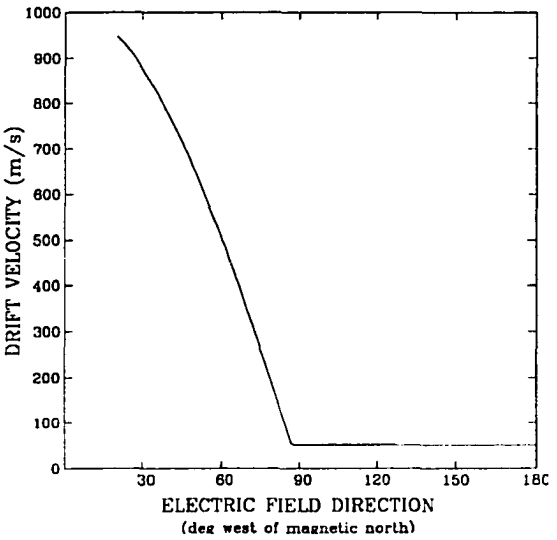

Figure 3.21 Magnitude of the horizontal component of layer drift as a function of electric field direction. E = 50 mV/m.

Gaussian in shape with peak density of $5x10^5$ cm^{-3}, and FWHM thickness of 1 km. Disappearance of the layer is defined as when its density drops below $1x10^5$ cm^{-3}. This seemingly arbitrary set of conditions was selected, since it is consistent with the characteristics and density resolution of layer observations discussed in Chapter 4. As an additional simplification the neutral wind is also assumed to be negligible.

To simulate the diffusion of a layer the one-dimensional algorithm described in section 3.3 is again utilized. However, the expression for the ion velocity requires modification. The stationary-state ion and electron momentum equations are solved simultaneously retaining the pressure-gradient, gravitational, and Lorentz (including the ambipolar electric field) terms. Assuming isothermal conditions with $T_i \approx T_e \equiv T$, and that the density varies only in the vertical direction, the vertical component of the ion velocity is

$$v_z \approx -\frac{2kT}{nmv}\frac{dn}{dz} - \frac{g}{v}. \qquad (3.17)$$

Figure 3.22 gives the results of simulated layer dissipation, assuming two different layer altitudes and a variety of plasma temperatures. As expected, diffusion progresses more slowly at lower altitudes (owing to the higher collision frequency), and proceeds more rapidly with increasing temperature.

These results have implications important to the understanding of observations of thin layers. If one observes a layer at low altitudes to vanish within a few minutes, then the layer is likely to be moving across the field of view, rather than dissipating in place. This argument holds for layers formed at higher altitudes, but is not as strong.

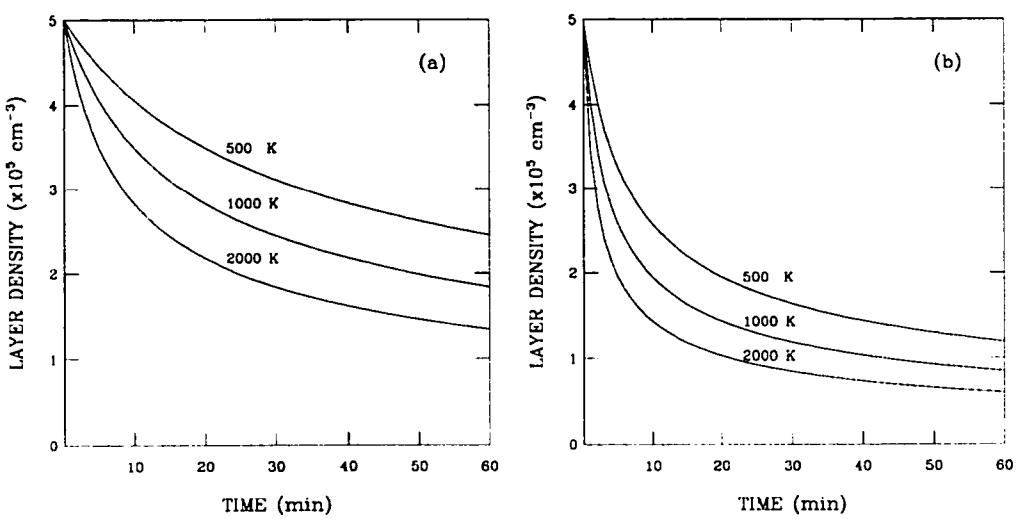

Figure 3.22 Layer dissipation when the electric field strength is zero, for three plasma temperatures: 500, 1000, and 2000 K. The layer altitude is set at (a) 100 km, or (b) 110 km.

3.5.4 Layer Drift with Spatially Varying Fields. To treat this topic rigorously, one would have to refine the approach used in section 3.5.2 for studying layer drift in a uniform field. In that case, it was implicitly assumed that all of the ions in a layer drifted together; an acceptable simplification. But with horizontally varying electric fields, the resultant gradient in the horizontal ion velocity demands that the continuity equation be solved in three dimensions, if one wishes to carefully analyze the resulting behavior of the layer. However, several qualitative insights can be had , even without resorting to a complete three-dimensional analysis. These are discussed below.

As a layer drifts into a region where the direction of electric field changes (or analogously, the electric field changes in time), its horizontal velocity will adjust to the new conditions. This should lead to a change in the direction of layer drift. Changes in field magnitude have a proportional effect the ion velocity, so that rate of drift can be in general expected to vary.

Horizontal variation in the electric field should induce vertical drift, leading to either raising or lowering of the layer, depending upon the initial altitude of the layer, and the direction of the new electric field. For example, if the layer has formed in conjunction with a field in the NW quadrant, then enters a region where the field is to the SW, it should drift downward. On the other hand, if that layer drifts into a region of NE-directed fields, it should rise.

Closely related to the subject of layer drift is that of horizontal structure in layers. For example, suppose the field is to the SW, with constant direction, but with a linearly increasing magnitude. One would then expect to see the layer inclined downward in the direction of increasing field strength. A similar effect would be expected for a NW field, constant in magnitude, but with the direction turning to the north (the layer in this case would be inclined upward in the direction of decreasing θ).

3.5.5 Closure. In this section, it has been demonstrated that thin layers in the presence of a uniform electric field will drift horizontally. The effect is greatest for fields di-

rected to the NW, where velocities >100 m/s can be expected for E > 10 mV/m. Layers formed under southerly electric fields occur at lower altitudes, where collisional interaction with the neutral atmosphere limits the velocities attained to on the order of 10 m/s. These results are not significantly impacted by adopting a different model for the collision frequency; reducing the collision frequency has the effect of shifting the velocity profile downward. Layer drift of the same magnitude is predicted for NW and southerly electric fields; the layers just form at lower altitudes.

Analysis of layer dissipation indicated that in the absence of an electric field, and with negligible neutral winds, layers diffuse rather slowly. The implication is that a layer which vanishes quickly during a single-position observation most likely has advected across the field of view.

Only a qualitative treatment of the effects of spatial variation in the electric field has been presented. However, it is clear that interesting features, both in the drift and in the horizontal structure of layers, can be expected to occur. Qualitative analysis suffices for the general interpretation of observations, but a better understanding of the phenomena will require a detailed theoretical analysis of the problem, that is beyond the scope of this thesis.

CHAPTER 4
OBSERVATIONS

4.1 Background

The incoherent-scatter radar (ISR) technique has proven to be an invaluable tool for studying the ionosphere (for a comprehensive review of this subject, see Evans [1969]). Electron density and the line-of-sight velocity of ions can be measured directly. Additionally, when making suitable assumptions, one can deduce the electron temperature, ion temperature, and ion composition of the plasma. In the context of this study, only the electron density and ion line-of-sight velocity are of importance. How these measurements are used to determine the number density of metallic ions, the convective electric field, and layer drift is addressed in the next section. In the balance of this section, the physics underlying measurements made with incoherent-scatter radars is outlined.

Electromagnetic waves incident upon charged particles will accelerate the particles, which in turn radiate waves, a process referred to as *scattering* of the incident wave. In a plasma, scattering by electrons will dominate that of ions, because of the relatively large mass of the ions. The frequencies of the scattered waves will be equal to the incident frequency plus a randomly varying Doppler shift, due to the thermal motion of the electrons. At the radar, the power of the returned signal will be non-zero, because the phases of the waves scattered along the path of the beam are not correlated. This is the physical basis for the phenomenon known as *incoherent scatter*.

When design of an incoherent-scatter radar was first contemplated (Gordon, 1958), it was assumed that the plasma could be treated as an electron gas, since (as noted above) the contribution to scattering due to ions is negligible. This leads to the conclusion that the returned signal should have a Gaussian spectrum with a relatively broad width, characterized by the mean thermal speed of the electrons. However, Bowles [1958] conducted an experiment which indicated a much narrower bandwidth than had been theoretically predicted. Bowles suggested that the ions in the plasma are responsi-

ble for this observation. Subsequent theoretical analyses (e.g., Fejer, 1960; Dougherty and Farley, 1960) demonstrated that the shape of the power spectrum of the returned signal is significantly modified by the presence of ions whenever the wavelength of the transmitted radiation is much larger than the Debye length (it should be noted that superimposed on this relatively narrow spectrum is a faint, usually undetectable, spectrum with a bandwidth characterized by the thermal motion of the electrons alone; this feature, referred to as the *plasma line*, intensifies as the transmitted wavelength of the radar becomes smaller).

Why this is so can be appreciated by visualizing the plasma as consisting of quasi-particles each comprised of an ion and a nominal cloud of electrons which are participating in the Debye shielding process (or more accurately, think of enhancements of the electron density in the vicinity of the ions). The scattering (i.e., total power returned to the receiver) of a radar beam incident upon such a gas would still be primarily due to the electrons, but the Doppler shift in the received spectrum would be determined by the thermal speed of the ions. This picture is obviously a gross simplification of the process, but captures the essence of the physics. The important results are that the total power of the returned signal is determined by scattering by electrons (and is indeed proportional to the electron density), while the Doppler shift in the spectrum is indicative of the component of the ion velocity along the direction of the radar beam.

4.2 The Scanning Experiment

4.2.1 Description. Observations for this study were made using the ISR located at Sondrestrom in Greenland (66.99° N, 309.05° E; magnetic latitude, 73.9°; dip angle, 80.5°) during the period August 1994 through August 1995. The radar is operated by SRI International, under contract with the National Science Foundation. It transmits at a nominal frequency of 1290 Mhz with an output power of ~3 MW. For the experiments discussed in this thesis, it was operated in two modes simultaneously, one with a frequency of 1290.0 Mhz, and the other at 1290.6 Mhz. A 320-μs single-pulse pattern was

used on the first channel (henceforth referred to as the *long-pulse* mode), while for the second a Barker-coded multi-pulse scheme was employed (referred to as the *short-pulse* mode). Barker-coding refers to introducing 180° phase changes within each transmitted pulse a number of times designated by the baud, which in effect creates a series of sub-pulses (specifically, a 26-μs pulse-length, 13-baud pattern was used for experiments conducted through November 1994, and a 28-μs, 7-baud pattern thereafter); a multi-pulse scheme refers to a particular irregular transmission sequence for the individual pulses designed to optimize the construction of the power spectrum from the returned signal (Farley, 1972; Gray and Farley, 1973). Integration time for both modes was 5 s. The long-pulse mode was selected to determine F-region line-of-sight (LOS) ion velocities (used to calculate the convective electric field), while the short-pulse mode was used to make high-resolution measurements of the electron density in the E-region. The long-pulse mode can generate well-defined power spectra in regions where the electron density is relatively low, which is essential to measuring the LOS ion velocity via determination of the Doppler shift. However, to do so requires that the signal be integrated over a long (21 km) interval in range (in order to consistently achieve a high signal-to-noise ratio, a requirement for well-defined spectra). Hence, the long-pulse mode is not suited for high-resolution E-region electron density measurements. The short-pulse mode delivers a range resolution of 300-600 m, but can only produce well-defined power spectra if the electron density is quite high (in this case $>1 \times 10^5$ cm^{-3}), otherwise the signal is lost in the noise. For detailed information on the operation and internal data processing of the Sondrestrom ISR, see Kelley [1990].

To observe horizontal structure and drift of thin layers, and to facilitate the determination of the convective electric field along the magnetic meridian, a novel scanning technique was employed. This mode combines a standard elevation scan (the radar moves along a fixed azimuth) and an azimuth scan (the radar scans with a fixed elevation). For this experiment, the radar was first scanned west of the station in a plane in-

clined at 69.7° from the horizontal and with an edge aligned with the magnetic meridian. Then it scanned in a similar plane to the east of the station. This sequence of scans was repeated continuously throughout the duration of an experiment. Figure 4.1 illustrates the geometry of this program. Each of the scans required five minutes to complete. The integration time for both the long- and short-pulse modes was five seconds, so that for a given altitude, 60 measurements of electron density (and LOS ion velocity) were made during each scan (but note that the horizontal separation between these measurements increases with increasing altitude). Why this seemingly peculiar scanning mode was adopted will be made clear in sections 4.2.3 and 4.2.4.

The remainder of section 4.2 is devoted to explaining how quantities of interest (metallic ion density, convective electric field, and layer drift velocity) are deduced from measurements of the electron density and the LOS ion velocity when the scanning experiment described above is conducted.

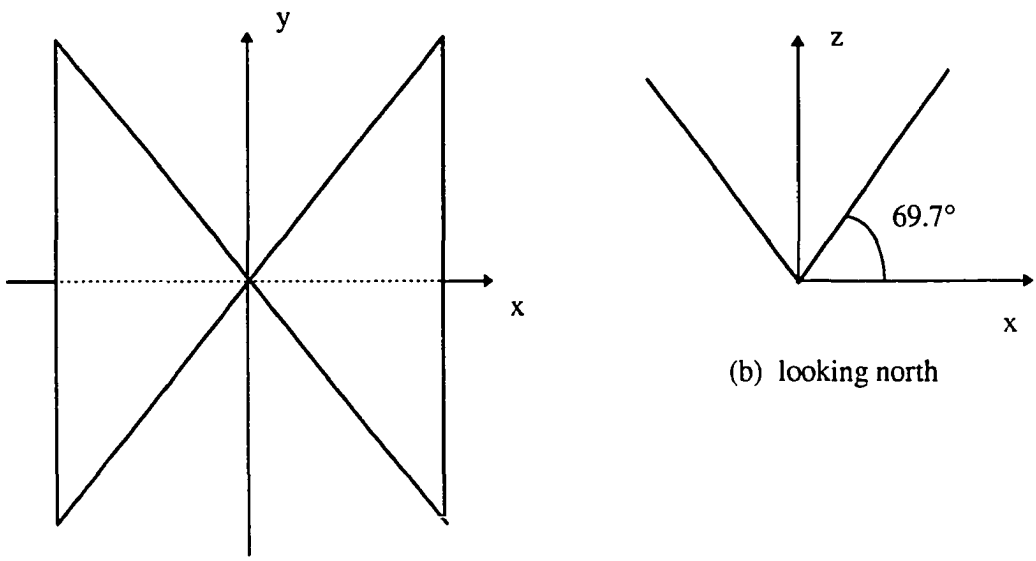

(a) top view

(b) looking north

Figure 4.1 Geometry for the scanning experiment. Note that x is to magnetic east, y is to magnetic north, and z is up. The radar is located at the origin.

4.2.2 Determination of the Number Density of Metallic Ions. The ion density can be directly deduced from the measured electron density by invoking the requirement for charge neutrality within a plasma, i.e., the ion density is simply equal to the electron density. However for this study, the number density of *metallic* ions residing in thin layers is of interest. This immediately suggests three questions: can one be reasonably sure that the ions in a layer are metallics (versus NO^+, O_2^+, or O^+); what is the minimum resolvable density of a layer; and what is the uncertainty in the estimate for the density of a layer? Each of these issues is addressed in turn.

In principle, one can determine the ion composition by analyzing power spectra from ISR experiments, provided that the spectra are well-defined (this generally requires a high signal-to-noise ratio (*SNR*)). This was not practicable for the scanning experiment employed in this study (the integration time was too short for analysis of ion composition, reflecting a trade-off implicit in the adoption of a scanning mode). However, the results of earlier investigations, for which the radar mode was optimized for the analysis of ion composition, indicate that thin ion layers are indeed composed primarily of metallic ions. For example, Behnke and Vickrey [1975] found Fe^+ abundances of 70-80% for layers over Arecibo, Huuskonen et al. [1988] measured 30-80% at EISCAT, and Bristow and Watkins [1993] found 63% at Sondrestrom. These results constitute compelling evidence that dense thin layers are primarily composed of metallic ions (esp., Fe^+). Therefore, thin structures observed in this study are assumed to be comprised of metallic ions.

To detect a thin layer in the data, one must be able to distinguish the layer from the background ionization, measurements of which tend to be quite noisy. If the measured background electron density is n_o, and the uncertainty in that measurement is Δn, then a reasonable definition for the minimum resolvable (or threshold) density for a thin layer is

$$n_{th} = n_o + \Delta n. \tag{4.1}$$

The uncertainty in the electron density measurement is a function of the *SNR*, and also depends upon the operating mode of the radar. In general, it is given by (de la Beaujardière et al., 1984)

$$\Delta n = \frac{n_o}{\sqrt{N}}\left(1+\frac{1}{SNR}\right), \tag{4.2}$$

where N is the number of pulses transmitted during the integration time (219 for the short-pulse mode with 5-s integration time). Typical values observed for n_o and *SNR* for the background ionization were $5\text{x}10^4$ cm^{-3} and 0.06, respectively. From equations (4.1) and (4.2) this yields a minimum discernible layer density of $1.1\text{x}10^5$ cm^{-3}. When analyzing the data for all of the observations, it was found that the threshold density for detection of a layer varied between $0.8\text{x}10^5$ and $1.6\text{x}10^5$ cm^{-3}, a rather narrow range. Thus, as a generalization, the minimum detectable density for a thin layer for the scanning experiment utilized here is ~$1\text{x}10^5$ cm^{-3}; layers with peak density lower than this value could not be distinguished from noise.

Precise determination of the metallic ion density was not an objective of this investigation; all that was needed was to be able to determine where and when a layer occurred. In fact the electron densities reported in this thesis are the "raw" densities (i.e., temperature corrections have not been applied), derived directly from the power of the returned signal. To see how the "raw" density differs from the "true" density, consider the radar equation (Evans, 1969)

$$P_s = A\frac{n\sigma}{R^2}, \tag{4.3}$$

where P_s is the signal power at the receiver, n is the electron density at range R, σ is the total cross section for scattering from a single electron, and A is a constant determined by the operating mode of the radar. Based on measurement of the signal power and range, the electron density is determined by solving equation (4.3), i.e.,

$$n = \frac{P_s R^2}{\sigma A}. \tag{4.4}$$

Calculation of the true, versus the raw, electron density differs in the form of the cross section used in equation (4.4). True densities are based upon (Evans, 1969)

$$\sigma = \frac{\sigma_e}{\left(1+\alpha^2\right)\left(1+\alpha^2+\frac{T_e}{T_i}\right)}, \tag{4.5}$$

where σ_e is the Thomson cross section for an electron, T_i and T_e are the ion and electron temperatures, and $\alpha \equiv \frac{4\pi\lambda_D}{\lambda}$ (λ_D and λ are the Debye length and the transmitted wavelength, respectively). The raw density is calculated assuming $\alpha = 0$, and that the temperature ratio is one. In the lower E-region these assumptions are valid; Horowitz [1976] has shown that adopting the raw density introduces an error of more than 25%. The measured raw density itself is subject to uncertainty, as given by equation (4.2). The *SNR* typically exceeded 0.3 within a layer, implying $\frac{\Delta n}{n} \approx 0.29$. Again it must be emphasized that the precise determination of density was not required for this investigation; the preceding discussion was offered simply to allow for the interpretation of the density values reported later on.

4.2.3 Determination of the Convective Electric Field. The electric field cannot be measured directly with an ISR. However, it can be deduced from LOS ion velocity measurements made in the F-region, so long as the electric field is strong enough to dominate the effects of the neutral wind (recalling the discussion of section 3.2.3, this requires an electric field strength greater than ~10 mV/m). Then, ion motion is governed by **ExB** drift, and the electric field is given by

$$\mathbf{E} = -\mathbf{v} \times \mathbf{B}. \tag{4.6}$$

The challenge is to obtain the ion velocity from the LOS velocity measurements.

Since the ion velocity vector has three components, it follows that three independent LOS measurements are needed to find v at a specific location and time. This is clearly impossible to accomplish with a monostatic radar system (i.e., a radar with collocated

transmitter and receiver), such as the Sondrestrom ISR. One must use three measurements (a *triad*) separated both in space and time in order to make an estimate of the velocity vector. The resultant velocity vector (and electric field) thus represents a sort of average over space and time.

For this experiment, the electric field was calculated at points along the magnetic meridian (the y-axis in Figure 4.1) at 25-km intervals. LOS measurements at a nominal altitude of 250 km were used to form the triads. The scheme for forming triads is illustrated in Figure 4.2. The electric field assigned to a given point along the meridian is the average of that calculated by two different triads. One is formed by using two LOS measurements from a westward scan, and one from an eastward scan. The other is formed using two from the eastward scan, and one from the westward scan. The calculated electric field is an average over 130 km in the y-direction, 186 km in the x-direction, and ~5 minutes in time.

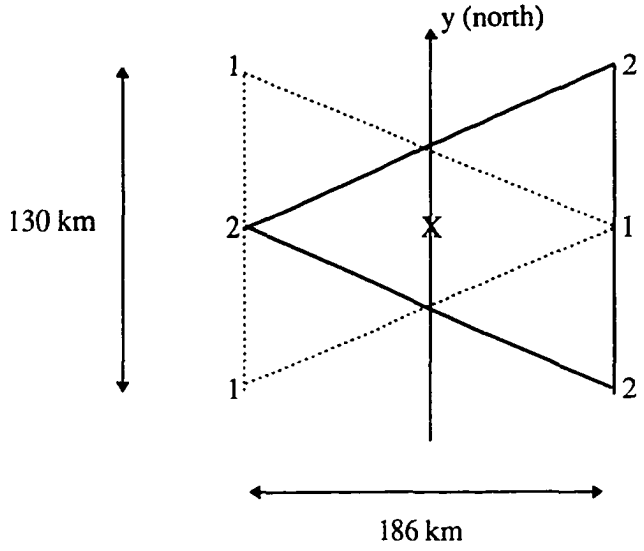

Figure 4.2 Scheme for selecting LOS velocity triads used to calculate the electric field along the magnetic meridian at point X. The electric field is calculated using the two triads labeled "1" and "2", respectively. The electric field at X is taken to be the average of the two.

Even if the ion velocity had been found using three LOS observations made simultaneously at the same point in the F-region, there would be two sources of error in the calculated velocity vector (and hence in the electric field determination). The first is the uncertainty in the LOS velocity measurement itself. The second is related to the relative angles of the LOS velocities in a given triad, and in this thesis is referred to as the *geometric effect*. Each of the above errors is discussed below.

The LOS velocity is determined through analysis of the power spectrum. The Doppler shift in the frequency is found through calculation of the first moment of the spectrum. Knowing the Doppler shift, the LOS velocity is given by

$$v_{LOS} = -\frac{c\Delta f}{2f_o}, \tag{4.7}$$

where c is the speed of light, Δf is the Doppler shift, and f_o is the transmitted frequency. The negative sign in equation (4.7) is introduced so that v_{LOS} is positive looking away from the radar. The uncertainty in the calculated LOS velocity (Δv_{LOS}) is proportional to the error in the determination of the Doppler shift, which in a qualitative sense must be related to how well-defined the power spectrum is. Although one would expect the "goodness" of the power spectrum to be related to he *SNR*, there is no straightforward way to establish this association. Rather, Δv_{LOS} is determined by means of a computer simulation which incorporates specific attributes of the radar mode (personal communication, M. McCready, SRI International, 1995). Such estimates were provided by SRI. It was found that if the *SNR* for a given measurement of v_{LOS} exceeded 0.1, then the average Δv_{LOS} was less than 50 m/s. Therefore, for this investigation the electric field was calculated using v_{LOS} measurements with $SNR \geq 0.1$, and Δv_{LOS} was set at 50 m/s.

To see how the geometric effect arises, it is helpful to review how the ion velocity is determined from the LOS measurements. Each LOS velocity is fully defined by its magnitude (with a sign to indicate whether it is direct towards or away from the radar, as given in equation (4.7)), and two angles, the elevation and the azimuth. Figure 4.3 illus-

trates how the elevation and azimuth (η and μ, respectively) are defined. Given three LOS measurements, the ion velocity is found by solving a system of three equations:

$$\begin{bmatrix} \cos\eta_1 \sin\mu_1 & \cos\eta_1 \cos\mu_1 & \sin\eta_1 \\ \cos\eta_2 \sin\mu_2 & \cos\eta_2 \cos\mu_2 & \sin\eta_2 \\ \cos\eta_3 \sin\mu_3 & \cos\eta_3 \cos\mu_3 & \sin\eta_3 \end{bmatrix} \begin{bmatrix} v_x \\ v_y \\ v_z \end{bmatrix} = \begin{bmatrix} v_{LOS1} \\ v_{LOS2} \\ v_{LOS3} \end{bmatrix}. \quad (4.8)$$

The solution for each component of the ion velocity will be of the form

$$v_x = c_{x1} v_{LOS1} + c_{x2} v_{LOS2} + c_{x3} v_{LOS3}, \quad (4.9)$$

where the coefficients on the LOS velocities are functions of the η's and μ's. If the uncertainty in each v_{LOS} is equal, the uncertainty in the x-component of the velocity is

$$\Delta v_x = C_x \Delta v_{LOS}, \quad (4.10)$$

where $C_x \equiv \sqrt{c_{x1}^2 + c_{x2}^2 + c_{x3}^2}$, with similar expressions for the other two components. Thus, if the uncertainty in the measured LOS velocity is nonzero, the geometry of the triad used to calculate the ion velocity serves to magnify the effective uncertainty in the estimate. The magnification factor will always be greater than or equal to one. It is unity if the three LOS velocities are mutually orthogonal, and gets progressively larger as the lines-of-action of the vectors become more closely aligned. This factor drove the spacing of the triad measurements shown in Figure 4.2.

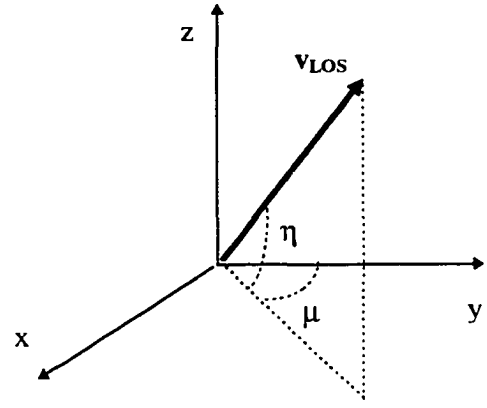

Figure 4.3 Convention adopted for specifying the elevation (η) and azimuth (μ) of a LOS velocity measurement.

Estimates of the uncertainty in the calculated electric field can now be made. Recall equation (4.6), and adopt the convention for specifying components of the electric field defined in Chapter 3, i.e., E_e is the component to the magnetic east, and E_n is perpendicular to the magnetic field, and oriented towards the magnetic north. Uncertainties in the estimates of the two components of the electric field are then given by

$$\Delta E_n = B C_x \Delta v_{LOS}, \tag{4.11a}$$

$$\Delta E_e = B \sqrt{C_y^2 \sin^2 I + C_z^2 \cos^2 I}\ \Delta v_{LOS}, \tag{4.11b}$$

where I is the inclination of the geomagnetic field. For the geometry adopted for this experiment, and with the uncertainty of the LOS velocity equal to 50 m/s, application of equations (4.11a-b) indicate that $\Delta E_n \approx 4$ mV/m, and $\Delta E_e \approx 7$ mV/m. Be aware that this calculation is only strictly valid if the three LOS velocity measurements are taken simultaneously at the same point in space. Hence, it does not capture unquantifiable geophysical variations necessarily associated with the actual scheme for composing the triads, for which the LOS measurements are made a different times and places in the F-region (as was discussed earlier).

4.2.4 Determination of Layer Drift. The horizontal drift of a thin ion layer can be estimated in two ways. By examining consecutive latitudinal plots of the ion density, one can track the apparent motion of the layer in the (magnetic) north-south direction. A more sophisticated technique involves analysis of the power spectra from the short-pulse mode. The LOS velocity is found at various positions within the layer. Ion velocity calculations are then made based on the formation of LOS triads. This approach is based on that taken in section 4.2.3. There are, however, significant differences in the way in which the layer drift problem is posed, versus the calculation of the electric field. Below, an algorithm for the determination of layer drift is outlined, drawing on the results of the previous section, where appropriate.

Assume that the layer drifts at a constant velocity everywhere along its extent. From two consecutive scans (one to the east and one to the west of the magnetic meridian)

select all LOS measurements within the layer that have an uncertainty less than a set value, say Δv_{LOS}, and assume that there are N such measurements. From these N measurements, form all possible triads for which the geometric magnification factor is less than some threshold value, C_{th}; suppose that there are M such triads. For each triad calculate the ion velocity. The layer velocity can be estimated by taking the average of these M velocities. For example, the x-component of the layer drift could be written as

$$\bar{v}_x = \frac{1}{M}\sum_{i=1}^{M}\left[c_{1i}(v_{LOS})_{1i} + c_{2i}(v_{LOS})_{2i} + c_{3i}(v_{LOS})_{3i}\right], \tag{4.12}$$

where the coefficient c_{ji} is a function of the elevation and azimuth of the j^{th} member of the i^{th} triad, and $(v_{LOS})_{ji}$ is the LOS velocity of the j^{th} member of the i^{th} triad. Upon reflection, it can be seen that the summation in equation (4.1) could be rearranged as a sum over the N independent LOS measurements, e.g.,

$$\bar{v}_x = \frac{1}{M}\sum_{n=1}^{N} A_n (v_{LOS})_n, \tag{4.13}$$

where A_n is a function of the elevation and the azimuth of the n^{th} LOS measurement. The uncertainty in the x-component of the layer drift is

$$\Delta\bar{v}_x \le \frac{1}{M}\sqrt{\sum_{n=1}^{N} A_n^2}\,\Delta v_{LOS}. \tag{4.14}$$

Similar expressions hold for the y- and z-components, but in general the A_n's will be different.

Implementing this algorithm for the estimation of layer drift poses several interesting problems. From equation (4.14), it appears that the larger the value of M (the number of triads), the lower the uncertainty. However, in order to increase M, the threshold on the multiplication factor, C_{th}, must be lowered. This has the effect of increasing the term under the square root, although not proportionally. The establishment of a value for Δv_{LOS} also has perhaps unexpected consequences: lowering its value will reduce N, and

thus reduce M, since fewer LOS measurements are available to form triads. The optimal values of C_{th} and Δv_{LOS} to achieve a desired limit on the uncertainty in the calculated drift velocity will depend on the specific scans being analyzed. Numerical experiments, varying the two parameters, can be conducted to make the best selection.

The central assumption in the above derivation is that the drift velocity is the same everywhere in the layer. This is likely to be true, if the electric field varies on a spatial scale much larger than the size of the layer. This condition was checked before attempting to calculate drift velocities.

This procedure can only be effectively utilized when the power spectra from the short-pulse mode are well enough defined to allow Doppler analysis. Unfortunately, this was seldom the case during the course of this investigation. Also, Δv_{LOS} estimates are not presently available for the short-pulse mode (personal communication, J. Kelly, SRI International, 1996). Thus, to demonstrate the technique a *SNR* requirement was set in lieu of establishing a minimum value of Δv_{LOS}, in order to generate the triads. Then a value of the uncertainty in the LOS measurements was assumed (50 m/s) to enable computation of the uncertainty in the derived layer drift in those cases that "good" power spectra existed.

4.3 Results

4.3.1 Observational Summary. The radar experiment, as described above, was conducted at Sondrestrom on 34 nights throughout the period August 1994 through August 1995, constituting over 200 hours of observations. Most observations were made from 2200 UT to 0300 UT, although a few runs were made over more extended periods, including a 24-hour experiment on 16-17 Aug 94. Layers were detected on 10 nights, all during the months of May through August. The cumulative time that layers were present was ~7 hours (recall that the density threshold for detection of a layer for this experiment is $\sim 1 \times 10^5$ cm^{-3}, so that relatively low density layers may have been pres-

ent without being discovered). Tables 4.1-3 provide a summary of all of the observations.

Figure 4.4 shows a typical plot of the electron density (equivalent to the ion density, as discussed above) with a thin layer present. It was constructed by projecting the densities measured in a single scan, which is inclined at 69.7°, into the vertical plane. The result is a meridional cross section of the layer. Notice that the layer shown here is very nearly horizontal; this was found to be true of most of the layers seen during this investigation.

Electric fields could not be calculated for runs made in November through March, owing to weak return signals from the F-region. Similarly, electric fields often could not be calculated later in the night, typically after 0100 UT. This is attributable to relatively low F-region plasma densities which occur during the winter (and at night) due to reduced photoionization, and chemical recombination. However, note that determination of the electric field was possible on all of the nights when layers were observed.

4.3.2 Absence of Layers. A part of understanding the occurrence and formation thin ion layers is to understand the conditions under which they are not observed. From the data, two generalizations can be drawn concerning days when layers did not appear.

First, there appears to be a seasonal effect in the occurrence of thin layers, since no layers are seen from September through March. This is consistent with known seasonal dependence in mid-latitude sporadic-E. An explanation of this effect is offered in Chapter 5, which is based on an argument that seasonal variability in the convective electric field will significantly alter conditions over Sondrestrom.

Second, on those nights without layers for which electric fields could be calculated (13 of the 24 "layerless" nights), the electric field was often in directed to the NW or SW

Table 4.1 Observational Summary (Aug 94 - Mar 95).

RUN DATE (TIME (UT))	LAYER TIME (UT)	REMARKS
16-17 Aug 94 (1600-1600)	2345-0037	see Table 4.4
8-9 Sep 94 (2200-0300)	none	E < 10 mV/m
11-12 Sep 94 (2200-0300)	none	before 0000, E≈20 mV/m NW after 0000 UT, E≈35 mV/m SW
20-21 Oct 94 (2200-0300)	none	E≈10-35 mV/m SW
21-22 Oct 94 (2200-0300)	none	E not calculated
17-18 Nov 94 (2200-0300)	none	E not calculated
12-13 Dec 94 (2200-0300)	none	E not calculated
13-14 Dec 94 (2200-0300)	none	E not calculated
14-15 Dec 94 (2200-0300)	none	E not calculated
4-5 Jan 95 (2200-0300)	none	E not calculated
7-8 Feb 95 (2200-0300)	none	E not calculated
8-9 Feb 95 (2200-0300)	none	E not calculated
9-10 Feb 95 (2200-0300)	none	E not calculated
22-23 Mar 95 (2200-1000)	none	E not calculated
23-24 Mar 95 (2200-1000)	none	E not calculated

Table 4.2 Observational Summary (May 95 - Jul 95).

RUN DATE (TIME (UT))	LAYER TIME (UT)	REMARKS
8-9 May 95 (2200-0300)	none	2230-0030, E≈20 mV/m NW signal too weak at other times
9-10 May 95 (2200-0300)	none	E≈20 mV/m, near due W
10-11 May 95 (2200-0300)	0048-0111	see Table 4.4
22-23 May 95 (2130-0300)	2220-2242	see Table 4.4
23-24 May 95 (2200-0300)	none	E≈25-40 mV/m NW: 2200-30, 2245-2345, 0000-0100 SW: 2230-45, 2345-0000 signal too weak after 0100
24-25 May 95 (2200-0300)	none	E≈10-20 mV/m, NW and SW
17-18 Jul 95 (2330-0300)	none	E≈20-35 mV/m NW: 2200-0000, 0020-0045 UT SW: 0000-0020 UT signal too weak after 0045
18-19 Jul 95 (2200-0300)	2236-2304 2321-2350	see Table 4.4
19-20 Jul 95 (2200-0300)	2350-0058	see Table 4.4
20-21 Jul 95 (2200-0300)	0006-0136	see Table 4.4

Table 4.3 Observational Summary (Aug 95).

RUN DATE (TIME (UT))	LAYER TIME (UT)	REMARKS
31 Jul- 1 Aug 95 (2130-0600)	none	2130-2310: E≈15 mV/m NE 2310-0020: E≈25 mV/m NW 0020-0120: E≈55 mV/m N signal too weak after 0120
1-2 Aug 95 (2145-0500)	none	2145-0100: E<10 mV/m 0100-0300: E≈35 mV/m NE (near N) signal too weak after 0300
2-3 Aug 95 (2200-0230)	none	E≈15-25 mV/m, NW-NE, near due N
3-4 Aug 95 (2200-0400)	2311-0001	see Table 4.4
4-5 Aug 95 (2200-0500)	2223-2235 2248-2259	see Table 4.4
14-15 Aug 95 (2145-0300)	2158-2226	see Table 4.4
15-16 Aug 95 (2200-0300)	2330-2346	see Table 4.4
16-17 Aug 95 (2200-0300)	none	E≈25-40 mV/m, NW-NE, near due N
18-19 Aug 95 (2200-0300)	none	E≈25-40 mV/m, NW-NE, near due N

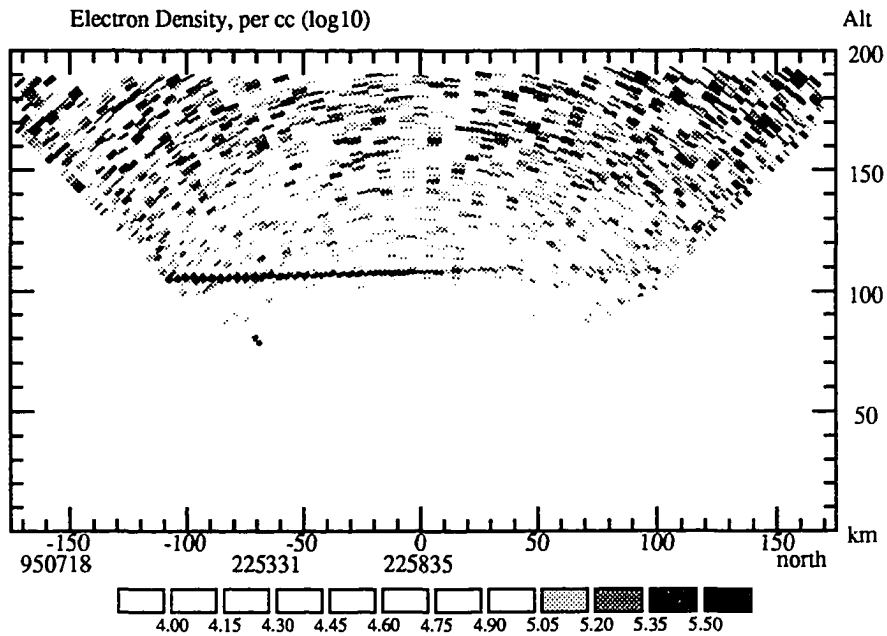

Figure 4.4 A typical plot of electron density for one scan. The vertical axis is the altitude, and the horizontal axis is distance along the magnetic meridian (positive to the north). A thin layer is present at an altitude of ~110 km.

for several hours at a time, suggesting that if metallic ions were present, layers should have been observed. This was true in nine of the 13 cases. On only one night (8-9 Sep 94) was the electric field strength so low that neutral winds might have been expected to dominate the E-field. On only two nights (16-17 and 18-19 Aug 95) was the electric field consistently to the NE or very near to due N in the NW quadrant, conditions which theory indicates as unfavorable for layer formation. On the night of 1-2 Aug 95, the field was very weak for several hours, then intensified, but was directed primarily in the NE quadrant (but near due magnetic north). These observations are consistent with the theoretical expectation that an electric field to the NE (or to the NW, but near due north) prohibits the formation of layers. They also strongly suggest that appropriate (i.e., NW or SW) electric field direction is insufficient to guarantee the formation of a layer. Unless the theory of layer formation is defective (a possibility that seems unlikely), this implies a deficiency in the population of metallic ions on the nights in question. This topic will be discussed further in Chapter 5.

4.3.3 Observed Layers. Some characteristics of the layers observed in the course of this investigation on shown in Table 4.4, which gives the general character of the electric field at the time the layer was observed, the average altitude of the layer (along with an indication of vertical motion or whether it was tilted), and an estimate of its (magnetic) north-south extent. By construction, Table 4.4 provides a snapshot of the layer, but cannot capture such features as layer drift, horizontal variation of the electric field, or the condition of the electric field prior to the appearance of the layer. Therefore, a more complete description of each event is given below. Interpretation of the observations is provided in section 4.4.

Table 4.4 Summary of Layer Characteristics.

DATE (UT)	ELECTRIC FIELD (at layer time)	LAYER ALTITUDE (km)	N-S EXTENT (km)
16-17 Aug 94			
(2345-0008)	20-30 mV/m NW	110	50-100
(0002-0037)	20-30 mV/m SW	100	50-100
11 May 95			
(0048-0111)	<15 mV/m NW	109	150
22 May 95			
(2220-2242)	<25 mV/m SW	drifted from 115 to 110	50-75
18 Jul 95			
(2236-2304)	25 mV/m SW	drifted from 113 to 105	>100
(2321-2350)	<10 mV/m variable	109	>150
19-20 Jul 95			
(2350-0058)	35-50 mV/m NW	tilted up to S, 105-110	>150
21 Jul 95			
(0006-0136)	<10 mV/m variable	105	<75
3-4 Aug 95			
(2311-0001)	15-20 mV/m NW	108	100 to >150
4 Aug 95			
(2223-2235)	15-25 mV/m N	120	75
(2248-2259)	25-40 mV/m N	120	75
14 Aug 95			
(2158-2226)	<10 mV/m variable	tilted up to S, 100-110	100 to >200
15 Aug 95			
(2330-2346)	<10 mV/m NW	105	>100

On 16-17 Aug 94, two layers were observed at times (2345-0008 UT; 0002-0037 UT) when the electric field was in the NW or SW quadrant. However, there was a period of about 75 minutes when the "proper" field was present without layers being seen. Prior to 2230 UT, the electric field was very weak. At 2230 UT it intensified to approximately 30 mV/m NW, then swung to the west at 2320 UT. After 0045 UT the signal strength was too low to allow estimation of the electric field. As indicated in Figure 4.5, the two layers

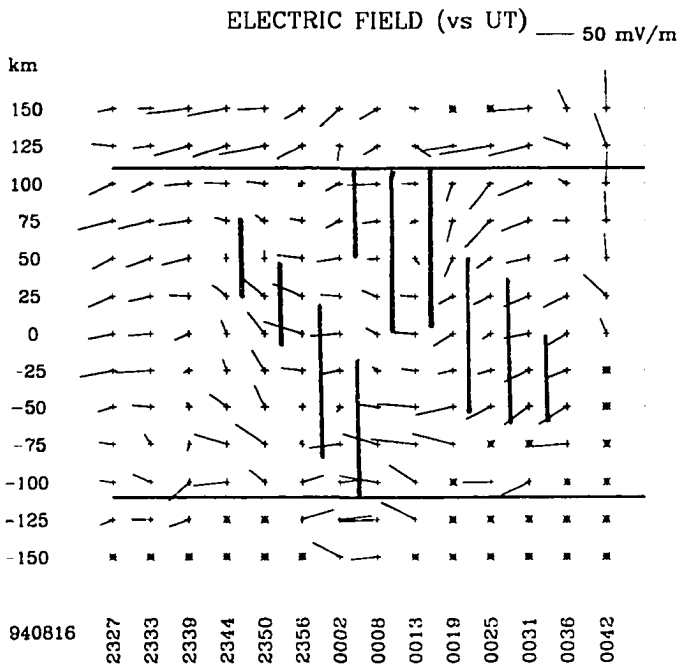

Figure 4.5 Relationship of the layers observed on 16-17 Aug 94 to the electric field. The vertical axis is distance from the station along the magnetic meridian (radar is at zero). The horizontal axis is time in UT. The lines at ±110 indicates the limit-of-view at an altitude of ~110 km. Layers are indicated with vertical lines. The convention for electric field direction is outward from the "+"s. Locations where low signal strength precluded estimation of the electric field have been asterisked.

observed both appeared to drift from the north to the south, the first at ~100 m/s, the second at ~70 m/s (drift estimation was made by inspection of ionization plots, the power spectra were not well enough defined to allow the more sophisticated approach described earlier). Auroral precipitation was present from 2200 UT to 0030 UT, with a bottom-side at ~120 km. The layers were evident at altitudes below the auroral ionization. The horizontal extent of the aurora was broader than that of the layers.

On 10-11 May 95, the geophysical situation was much less complicated; no aurora was observed during the experiment. A layer was observed during 0048-0111 UT. The electric field was weak or to the NE before 0100 UT. As the layer appeared, the field intensified to 20-30 mV/m to the NW. It continued to intensify, and turned progressively more northward, becoming NE at around 0218 UT. The layer had a region of relatively

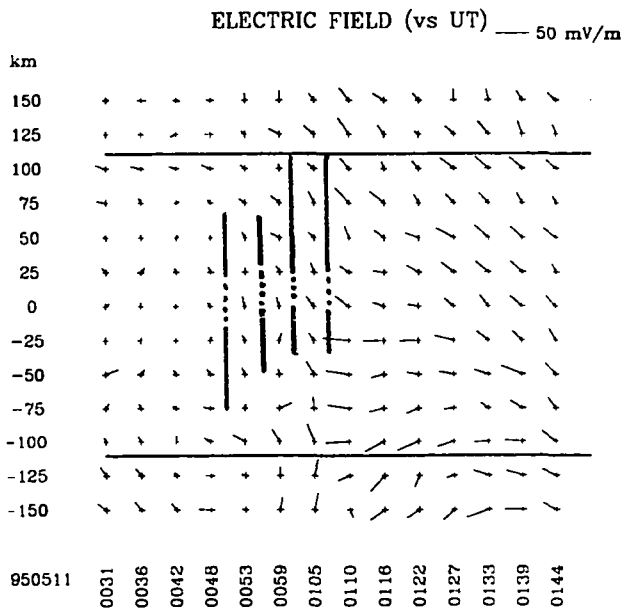

Figure 4.6 Relationship of the layer observed on 11 May 95 to the electric field (see Figure 4.5 for a description of the plot).

low density at its middle, indicated by dashed lines in Figure 4.6. Apparent drift of the layer is to the north. Calculated layer drift was: south at 1±25 m/s; west at 58±35 m/s.

On 22 May 95, no aurora was observed prior to the event, although some auroral ionization was detected later, between 2340 and 0045 UT. A layer was observed from 2220-2242 UT. The electric field was very weak up to the time that the layer was seen. Coincident with observation of the layer, the field intensified, and became generally directed to the SW. It retained this configuration until approximately 0100 UT after which the electric field direction moved into the NW quadrant. As shown in Figure 4.7, the layer was only observed in three scans, and in fact "skipped" a scan, which suggests the existence of two layers and/or rapid horizontal drift. Layer drift velocity was calculated from the power spectra of the first two layer-containing scans, yielding 125 m/s directed to the SW (130° west of north), with an uncertainty in the magnitude of the velocity on the order of Δv_{LOS} (which is assumed to be 50 m/s).

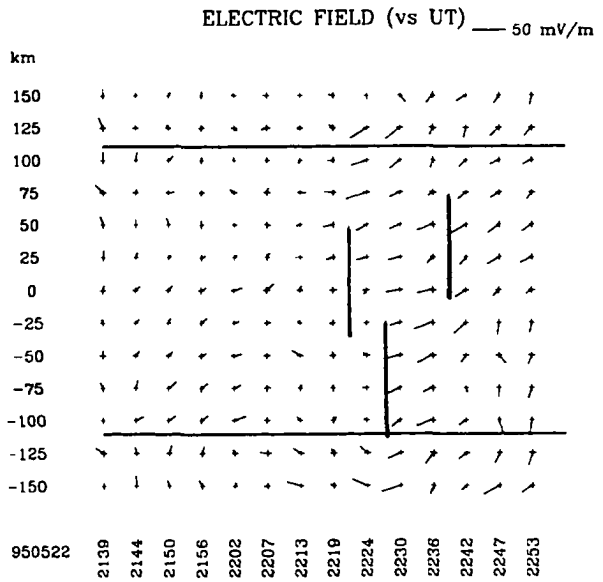

Figure 4.7 Relationship of the layer observed on 22 May 95 to the electric field (see Figure 4.5 for a description of the plot).

For the experiment conducted on the night of 18-19 Jul 95, aurora was not detected until well after the layers were observed, commencing at 0115 UT. Two layers were observed, one at 2236-2304 UT, and the other at 2321-2350 UT. The electric field was initially directed to the NE, turned to the NW at 2230 UT, and passed into the SW quadrant as the first layer formed. The field weakened after the first layer had disappeared, and remained that way while the second layer was observed. At approximately 0030 UT the electric field intensified to ~25 mV/m, and fluctuated in direction from NW to NE for the remainder of the experimental period. Apparent drift velocity for the first layer was 130 m/s to the south which is in rough agreement with analysis of the power spectra, which yielded value ~100±30 m/s to the south and 5±20 m/s to the west. The second layer exhibited similar apparent drift (signal strength was too weak to make an estimate using the power spectra). Figure 4.8 shows the structure of the electric field when the first layer was present.

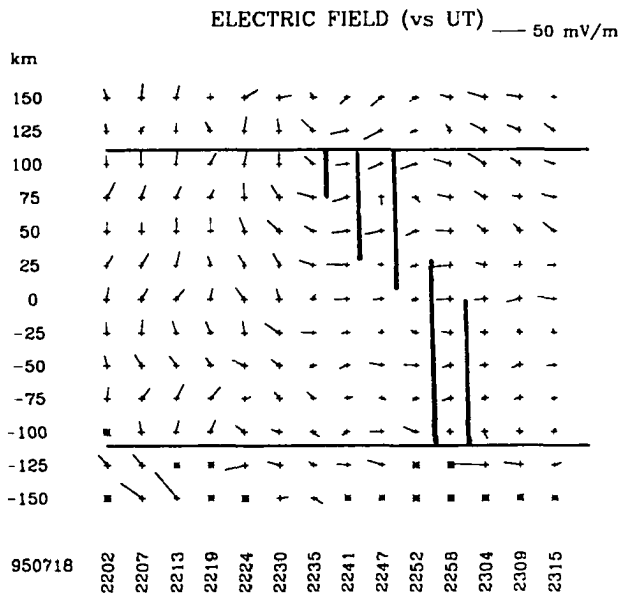

Figure 4.8 Relationship of the first layer observed on 18 Jul 95 to the electric field (see Figure 4.5 for a description of the plot).

The event seen at 2350-0058 UT on the night of 19-20 Jul 95 was the most interesting of all of those observed during this investigation. Other layers tended to be horizontal with no detectable tilt, but here this was not the case. The layer bent upward to the south, as illustrated in Figure 4.9(a-d). The location at which it turned upward coincided with an abrupt change in the latitudinal structure of electric field from NW in the north, to NE in the south, as shown in Figure 4.10. Field strength during the time the layer was present was quite high, 35-50 mV/m. Prior to observation of the layer, the electric field had been directed to the NE at ~25 mV/m for over an hour. As the layer disappeared from view, the strength of the electric field dropped to under 20 mV/m to the NW, where it remained until 0120 UT. At that time the field intensified slightly, and turned to approximately due north. Apparent layer drift was to the south at ~70 m/s, but the spectra derived from the short-pulse experiment were not adequate for a Doppler analysis.

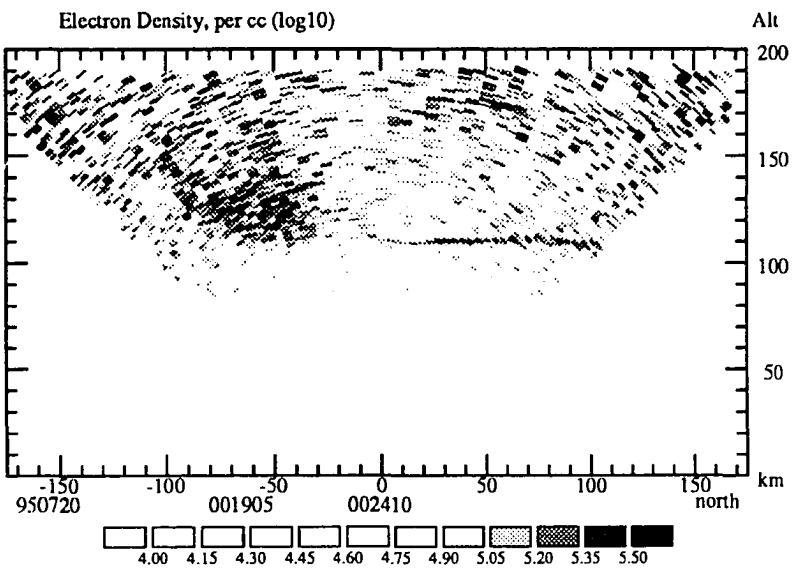

Figure 4.9(a) Density plot for 20 Jul 95, 0019-0024 UT. Auroral ionization can be seen south of the station. The layer extends northward from over the radar.

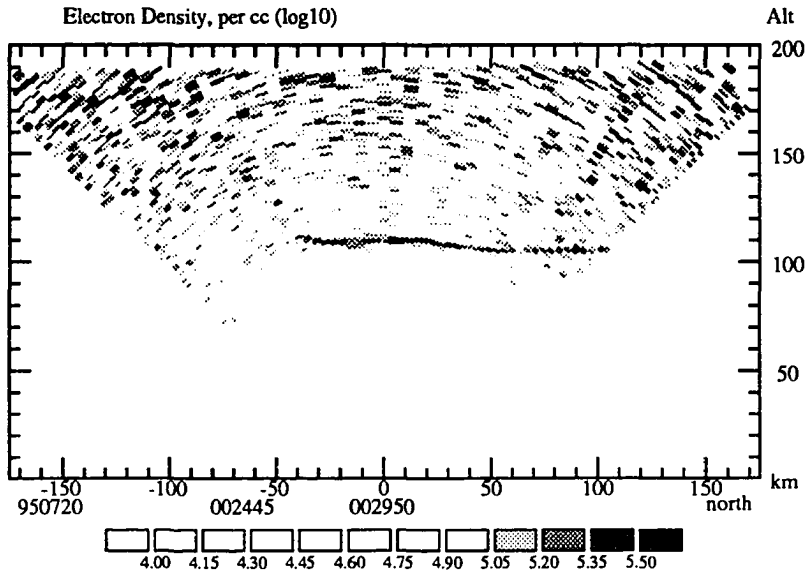

Figure 4.9(b) Density plot for 20 Jul 95, 0024-0029 UT. The layer extends northward from ~50 km south of the station.

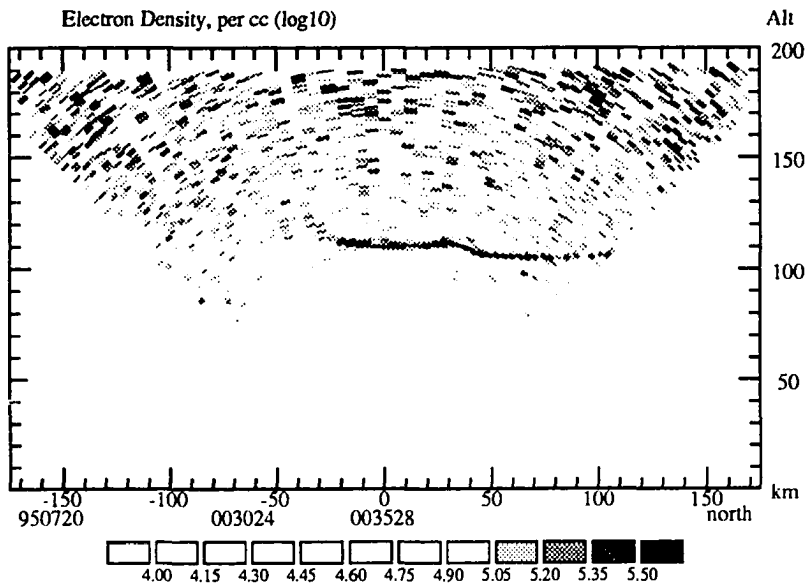

Figure 4.9(c) Density plot for 20 Jul 95, 0030-0035 UT. The layer extends northward from ~25 km south of the station.

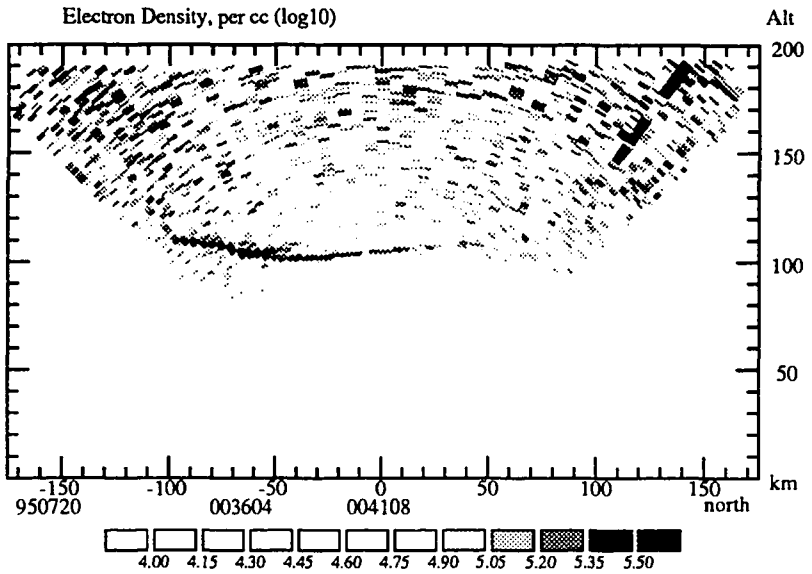

Figure 4.9(d) Density plot for 20 Jul 95, 0036-0041 UT. The layer extends southward from ~50 km north of the station.

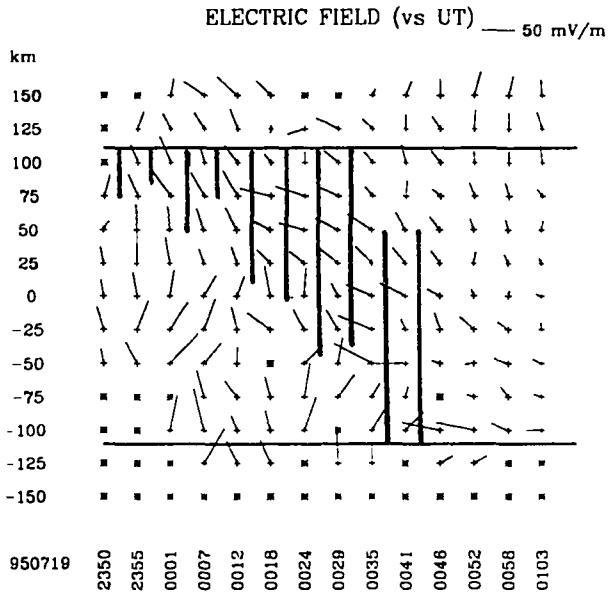

Figure 4.10 Relationship of the layer observed on 19-20 Jul 95 to the electric field (see Figure 4.5 for a description of the plot).

The layer appearing on the night of 20-21 Jul 95, was first detected at 0006 UT, and persisted for approximately 90 minutes. Its density tended to be just at the threshold of detection, weaker than layers seen on other nights. The layer exhibited no apparent drift, but signal strengths were too low to confirm this by calculation of the drift velocity. From 2200 UT, the start time for the experiment, until 2230 UT the electric field was directed to the NE at 20 mV/m. For the remainder of the night (including the time that the layer was observed), it was weak and variable in direction.

Auroral precipitation was prevalent on the night of 3-4 Aug 95, including the time that the layer was observed (2311-0001 UT), e.g., see Figure 4.11(a-d). Interestingly, thin layers sometimes appeared to be superimposed on auroral patterns, as can be seen in Figure 4.11(c). The electric field was usually directed to the NW before, during, and after the event (Figure 4.12). Low signal strength precluded calculation of layer drift. Apparent drift in the north-south direction is difficult to interpret. It is possible that two layers are observed here: the first from 2311-2333 UT with a fainter layer seen from 2333 to 0001 UT.

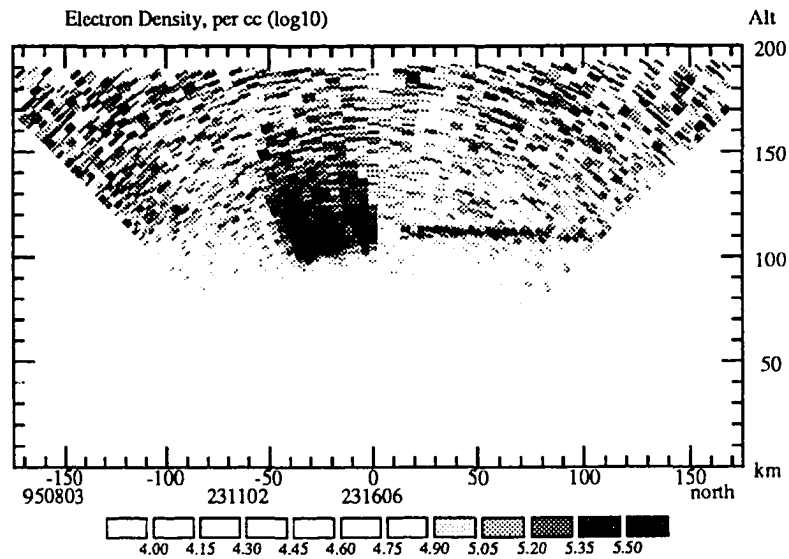

Figure 4.11(a) Density plot for 3 Aug 95, 2311-2316 UT. Notice the intense aurora south of the layer.

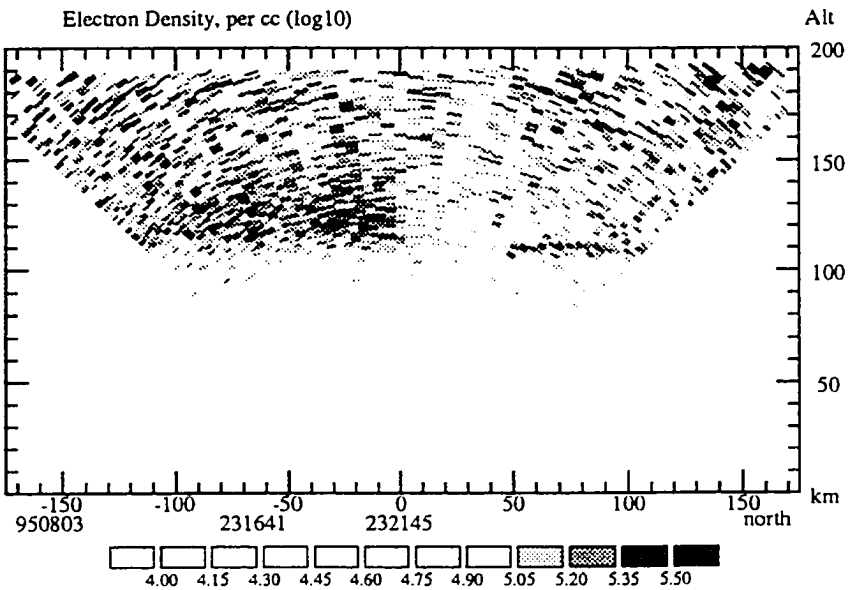

Figure 4.11(b) Density plot for 3 Aug 95, 2316-2321 UT. Relatively faint auroral ionization is present south of the layer.

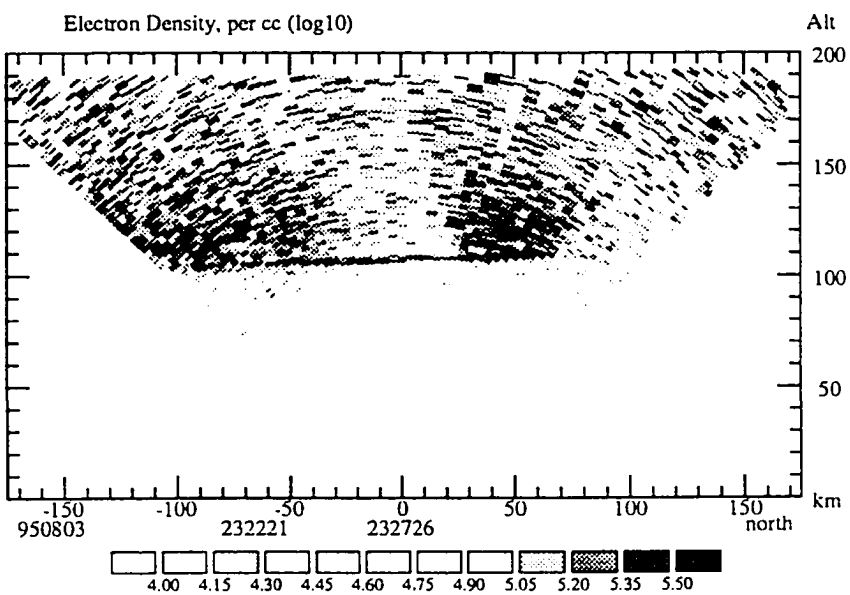

Figure 4.11(c) Density plot for 3 Aug 95, 2322-2327 UT. Here the layer spans two auroral arcs.

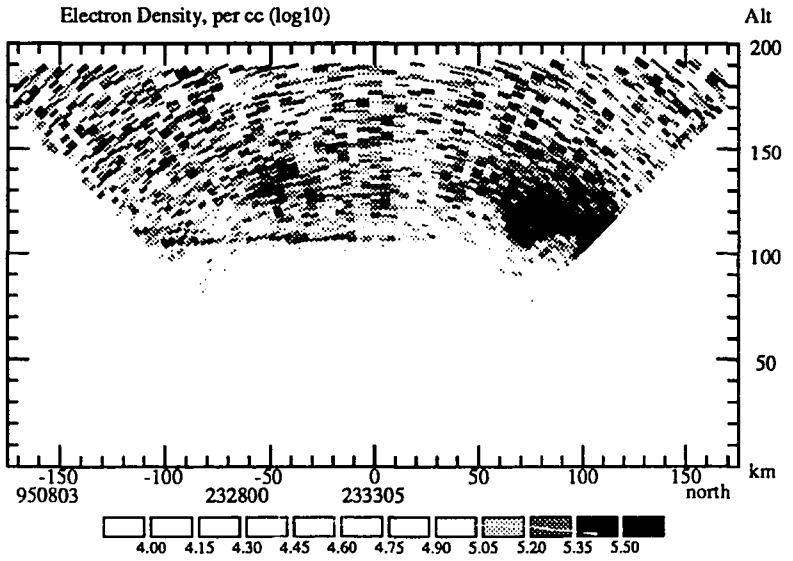

Figure 4.11(d) Density plot for 3 Aug 95, 2328-2333 UT. Notice the intense aurora north of the layer, and less intense precipitation over the layer.

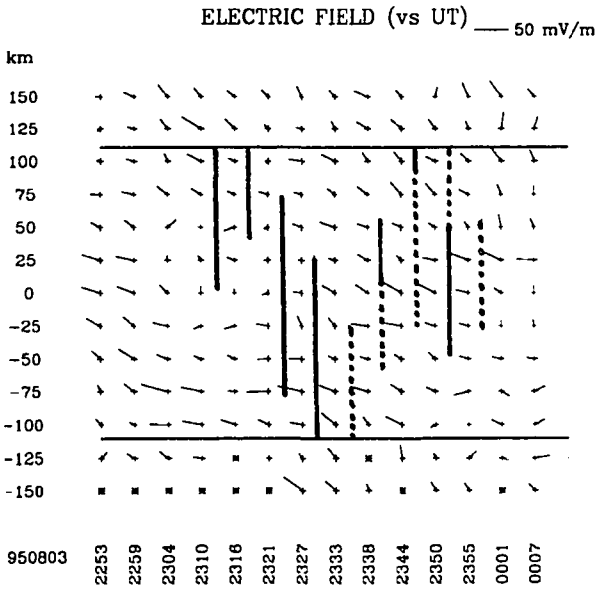

Figure 4.12 Relationship of the layer observed on 3 Aug 95 to the electric field (see Figure 4.5 for a description of the plot).

The two layers seen on 4 Aug 95 (2223-2235 UT; 2248-2259 UT) were both observed for only two scans. They were located at an altitude of 120 km, the highest of any seen during the course of this investigation. The electric field at the time the layers were observed was quite strong, and directed almost due north (see Figure 4.13). Layer drift calculations were not possible, due to weak signals and the short duration of the layers.

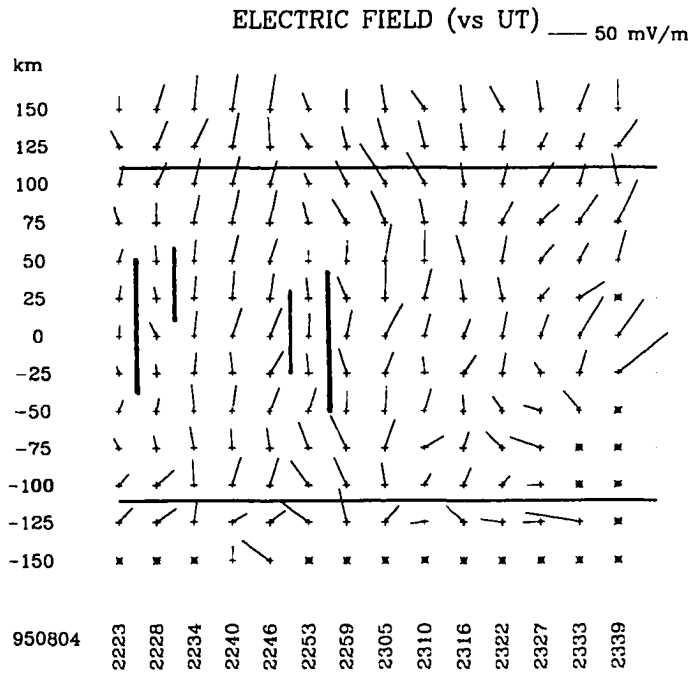

Figure 4.13 Relationship of the layers observed on 4 Aug 95 to the electric field (see Figure 4.5 for a description of the plot).

The layer observed on 14 Aug 95 was present at the start of the experiment, lasting from 2158 UT until 2226 UT. At that time the electric field was very weak, and remained so while the layer was present. The field did intensify to 30-50 mV/m to the SW at about 2345 UT (over an hour after the layer had disappeared), and remained in that

general condition until 0115 UT, when the signal became too weak to make further electric field calculations.. The layer was initially horizontal at an altitude of 110 km, but the last scan showed a downward tilt from 110 km at the layer's southern edge to 100 km at its northern boundary. The calculated drift for this layer was east at 5±25 m/s, and south at 70±35 m/s.

The final layer, observed in the course of this investigation, occurred on 15 Aug 95, from 2330 UT to 2346 UT. This was another case for which the electric field was quite weak and variable. Auroral precipitation occurred almost continuously prior to the layer being detected, but had disappeared by 2315 UT. Apparent layer drift was to the south, but signal strength was too weak to allow for analysis of the short-pulse spectra.

4.4 Discussion

4.4.1 General. Of the total of 13 layers observed over ten nights, four (occurring on 18 Jul 95 (second layer), 21 Jul 95, 14 Aug 95, and 15 Aug 95) were seen when the electric field strength was so low that the effect of the neutral wind on ion motion would be comparable to that of the electric field. None of them displayed downward motion, which would be expected if a layer is in the process of formation at a node in the structure of the atmospheric tide. Thus, it is likely that these four layers had been substantially formed prior to being observed, and were subsequently transported over the station by the action of the neutral wind. Whether the electric field, or the effect of the neutral wind, dominated the formation of these layers is a matter of pure speculation, since formation probably occurred away from the station prior to the time of observation. However, it is interesting to note that these four layers were indistinguishable from the other layers observed, in terms of altitude and horizontal extent.

The balance of this section is devoted to interpretation of those events for which the influence of the electric field could reasonably be expected to determine the motion of the metallic ions, i.e., the neutral wind could be taken to be negligible. Specific topics to

be discussed include: the altitude and time of occurrence of layers; layer drift; horizontal extent; and the connection of auroral precipitation to the observation of layers.

4.4.2 Altitude of Occurrence. Theory predicts that layers forming for electric fields directed to the SW should be found at lower altitudes than those forming for fields directed to the NW. Within the NW quadrant, the more northerly the field is directed, the higher is the altitude of convergence. Furthermore, layers formed by SW fields are expected to slowly drift downward at a decreasing rate, while those formed by NW fields tend to remain at the same altitude as long as the field direction remains unchanged. The observations support this general picture.

The difference in altitude for layers formed by NW versus SW electric fields is best illustrated by comparing the two layers seen on 16-17 Aug 94. The electric field was predominantly to the NW when the first layer was observed at an altitude of 110 km. The second layer appeared as the first disappeared, and the field turned to the SW. Its altitude was 100 km, lower than the first layer.

Of the three layers observed when the electric field was to the SW, two exhibited marked downward drift (22 May 95; first layer of 18 Jul 95). The third (i.e., the second layer of 16-17 Aug 94) was located at an altitude of 100 km, low enough that downward drift might be approaching zero due to increasing drag from the neutral atmosphere.

The layer observed on 19-20 Jul 95 is consistent with the theoretical prediction that increasingly northerly fields are associated with layer formation at higher altitudes. In this case, the electric field in the vicinity of the layer turns to the north as one moves southward along the geomagnetic meridian. Concurrently, the altitude of the layer increases, as expected.

The layers with the highest altitude (120 km) were seen on 4 Aug 95, when a strong electric field directed almost due north was present. Recall from Chapter 3, that the convergence altitude increases rapidly as a northwesterly field becomes more closely directed to due (magnetic) north, and that the layer formation mechanism becomes less

efficient, i.e., it takes a longer time for a layer to form. Thus, it is unlikely that these layers formed under the action of the observed field. Rather, it is suggested that these layers had formed at lower altitudes under conditions when the field was more westerly. Subsequently, they drifted into a region of increasingly northward electric field, where the layer was lifted upward. The observation of these layers over Sondrestrom, could be interpreted as a snapshot of this process.

As shown above, the relationship between electric field direction and the altitude at which layers were observed during this investigation are in general agreement with the theory discussed in Chapter 3. However, in conformity with earlier studies (see Chapter 1), it has been found that layers observed for electric fields to the NW were at lower altitudes than expected. In Chapter 3, it was suggested that this could be explained by a systematic error in the Banks-Kockarts collision frequency. To test this hypothesis, the value of the collision frequency (in terms of fractions of ν_{BK}) at the altitude of the layer has been determined for two cases (selected because in each, the electric field direction and altitude of the layer are well-defined). In the first case, the layer of 11 May 95, the layer altitude is 109 km, and the electric field is directed at ~41° west of magnetic north. For the second case considered, the layer of 19 Jul 95, the altitude is 105 km, and the field direction is ~52°. Figure 4.14 depicts a graphical solution for the collision frequency. As can be seen, a better fit to the data is achieved if the collision frequency is set between 0.1 and 0.2 times the Banks-Kockarts value. Since the ion-neutral collision frequency is proportional to the neutral density, this discrepancy could be due to a problem with the MSISE-90 model. However, this implies that the MSIS model underestimates density by nearly an order of magnitude, which does not seem likely. Rather, the trouble is more probably that the induced dipolar interaction, used in deriving the B-K collision frequency, does not adequately model the physics of ion-neutral collisions. Of course the evidence presented here is rather sparse, but is believed to be sufficiently compelling to warrant future study of this topic.

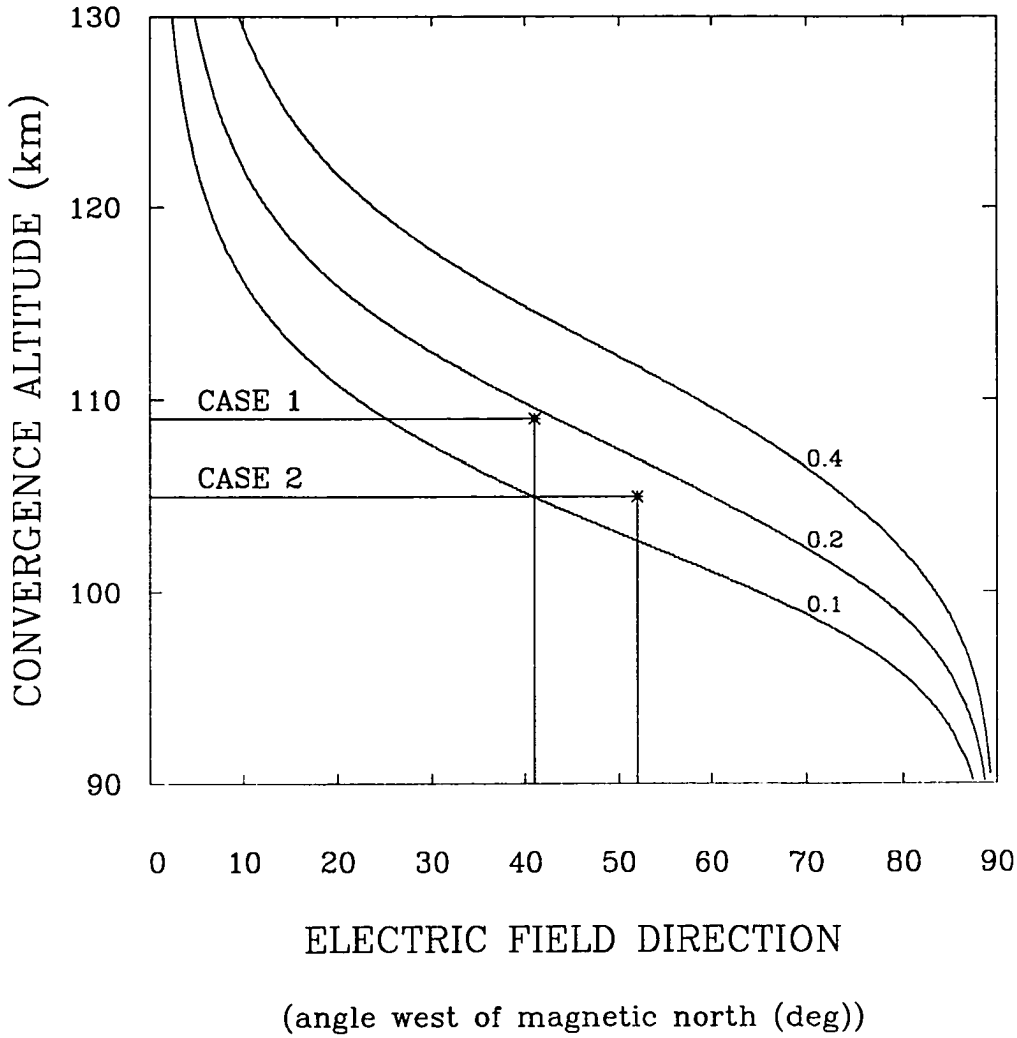

Figure 4.14 Estimation of the ion-neutral collision frequency for two cases (described in the text). The three curves give the theoretically predicted convergence altitude as a function of electric field direction, when different multiples of the Banks-Kockarts collision frequency are assumed (0.1, .0.2, and 0.4). An asterisk marks each estimate.

4.4.3 Time of Occurrence. One would expect that the time-of-day at which layers form is determined by the location of the station as it moves under the overall convection pattern; at times the station is under a NW or SW field, and at other times it is not. Such considerations drove the timing of the experiments conducted during this investigation. Indeed, of the 13 layers observed, only two persisted beyond 0100 UT (recall that all of the radar experiments spanned at least 2200 - 0300 UT). This theme is pursued further in the next chapter. Below, two other significant features in the data are discussed. These play an important part in motivating the development of a qualitative model of layer occurrence outlined in Chapter 5.

One feature, that stands out when reviewing days on which layers occur, is that there are many periods of time during which a NW or SW electric field is present, yet no layers are observed. As discussed in section 4.3.2, this was also seen to be the case on those days when layers were not seen at all. The implication is that metallic ions are sometimes not present in the vicinity of Sondrestrom, or at least have total abundances that are too low to produce layers detectable with our experiment. There is no reason to believe that this conclusion should not hold at all high-latitude locations. This implies that large-scale horizontal transport of ions must redistribute metallic ions, leading to "preferred" times and locations for layer formation. Subsequently, these layers may drift away, perhaps to be observed at a site remote from their point of origin.

A more subtle effect is associated with three of the nine layers which were observed under conditions when the electric field dominated the neutral wind. These three layers were seen at times when abrupt changes in the electric field structure occurred, from configurations not conducive to layer formation to ones for which layer formation would be expected. On 11 May 95 and 22 May 95, layers were observed as the field suddenly increased in strength. On 18 Jul 95, a layer was seen as the field direction swung from approximately due magnetic north to SW, while its magnitude remained relatively constant. In each of these cases the layer was present 20-30 minutes, disappearing while

favorable electric fields continued to remain. One interpretation of this effect is that what is being observed is the formation of a layer, followed by its drift from the field of view. A problem with this explanation is that the rate observed of "formation" is much faster than theoretically predicted (see Chapter 3). An alternate interpretation follows from thinking of changes in the observed electric field as arising from the motion of the station relative to the large-scale high-latitude convection pattern (this viewpoint is only a crude approximation, since the convection pattern is not fixed in time, due to changes in the IMF and to the fact that the geographic and geomagnetic poles do not coincide). This implies that a discontinuity in the electric field structure would approach Sondrestrom from geographic east at a speed of ~180 m/s (this corresponds to a velocity of ~140 m/s to the magnetic west, and ~110 m/s to the magnetic south). As shown in Chapter 3, theory predicts that layers should drift with a component to the magnetic west (if the electric field is directed in the NW or SW quadrant). If the drift velocity exceeds 140 m/s (which is quite likely on theoretical grounds, especially for fields directed to the NW), then a layer would tend to "pile up" along the discontinuity in the field structure. If this is the case, what is observed with the radar might simply be the transport of this layer over the station.

Whatever the precise interpretation of the observations might be, it appears that the horizontal transport of metallic ions must play a decisive role in determining the time (and location) of layer formation. This idea is revisited in the next chapter.

4.4.4 Horizontal Structure. For this scanning experiment, the field-of-view at the altitudes where layers were observed is ~200 km along the magnetic meridian, thus establishing an upper limit on determination of north-south extent. Horizontal structure in the magnetic east-west direction cannot be unambiguously assessed. Taking these limitations into account, the observations do indicate that the latitudinal extent of thin layers is often in the range of 50-150 km. This suggests that thin ion layers found at high latitudes might better be regarded as *patches* of ionization, rather than layers, since the term

layer connotes a structure of broad horizontal extent. However, this conclusion must be tempered by recalling that the density threshold for detection of the layers discussed here was high, ~$1x10^5$ cm^{-3}. Therefore, the extent of the layers may have been larger than reported here; the radar experiments may have just resolved the high density portions of more expansive layers. Even so, it would appear that the horizontal structure of thin metallic ion layers at high latitudes is patchy in nature, characterized by enhancements in the ion density as one moves along a layer.

4.4.5 Layer Drift. The theory outlined in Chapter 3, indicates that thin metallic ion layers should drift in a manner characterized by the direction of the electric field: for layers formed at the convergence altitude in a NW field, the drift should be due west; for layers formed with southerly electric fields the drift should be nearly aligned with the horizontal projection of the electric field. Unfortunately, the determination of the horizontal motion of thin layers proved to be more difficult than anticipated.

A crude estimate of the drift along the magnetic meridian was made by marking the apparent movement of a layer in sequential scans. However, the results of such analysis can be misleading in cases when the layer has relatively small horizontal scale and/or drift in the east-west direction is also occurring. Since the ion layers appear to have patchy horizontal structure, and theory predicts substantial westward drift velocity, the apparent drift velocities reported previously should be met with skepticism. A better way to measure layer drift is through the Doppler analysis, but this technique also had its limitations.

In order to apply the technique described in section 4.2.4 to calculate layer drift, two requirements must be met: the radar signal must be strong enough to yield power spectra well enough defined to conduct Doppler analysis; and the electric field must not vary much spatially (along the layer) or in time (between the two scans used to make the estimate). It was found that these conditions were met for only three layers. Calculated

layer drift for these cases is given in Table 4.5. The general direction of drift in each instance corresponded with that predicted by theory.

Table 4.5 Summary of Measured Layer Drifts.

LAYER DATE	ELECTRIC FIELD	EASTWARD DRIFT (m/s)	NORTHWARD DRIFT (m/s)
11 May 95	NW	-58 ± 35	-1 ± 25
22 May 95	SW	-95 ± 30	-83 ± 40
18 Jul 95 (1st)	SW	-5 ± 20	-100 ± 30

4.4.6 Auroral Connection. This investigation did not establish any clear causal relationship between the occurrence of thin ion layers, and the incidence auroral precipitation. For the limited cases studied, layers were seen before, during, and after auroral ionization was detected. Layers were also observed on nights for which no aurora was present during the time of the experiment. One event does rate special consideration here. The layer observed on 3-4 Aug 95 was sometimes superimposed on regions of auroral ionization. It seemed that the presence of auroral precipitation did not in any way disrupt the layer. This suggests a possible connection between thin ion layers and the observation of enhanced optical emissions, sometimes seen to emanate from thin horizontal layers within an auroral arc (Hallinan et al., 1985). This subject is beyond the scope of the present investigation, but merits future consideration.

4.5 Closure

The main findings of this observational investigation are as follows:

⇒ There is a strong suggestion that layers preferentially occur during the summer months. This is a new result, which has not been treated previously. An explanation for seasonality in layer occurrence is offered in Chapter 5.

⇒ As has been seen in earlier studies, layers are often not observed, even though favorable electric fields are present. Current theory cannot account for this feature in the data. This subject will be revisited in Chapter 5.

⇒ Layers forming in the evening over Sondrestrom tend to appear before 0100 UT.

⇒ Layers tend to be observed in conjunction with abrupt changes in the structure of the convective electric field.

⇒ Layers were observed to drift horizontally, as predicted by the theoretical development in Chapter 3.

⇒ As observed in earlier investigations, layers occurring in conjunction with northwesterly directed electric fields appeared at altitudes below that predicted by the current theory. Empirical measurements of the ion-neutral collision frequency suggest that the widely used induced-dipole model for the collision frequency is too large by a factor of about ten.

⇒ The horizontal structure (along the geomagnetic meridian) was found to be on the order of 50-150 km, consistent with the findings of Bristow and Watkins (1993).

CHAPTER 5
OCCURRENCE OF THIN METALLIC ION LAYERS

5.1 Introduction

The results of the observational program described in Chapter 4, suggest two generalizations concerning the occurrence of thin metallic ion layers at high latitudes, under the condition that the effect of the electric field dominates that of the neutral wind. First, it is quite clear that an electric field directed to the magnetic northwest or southwest is necessary, but not sufficient, for the occurrence of thin layers. Second, there is evidence of a seasonal variation in the rate of occurrence of thin layers, with more layers being observed during the summer months (in the Northern Hemisphere). The objective of this chapter is to put forward a plausible explanation for both of these effects.

When layers are not observed after the electric field has been directed to the NW or SW for a period of time, an obvious conclusion one can draw is that the population of metallic ions in the vicinity of the station is too low to permit formation of a detectable layer (alternately, times when layers do form could be associated with relative enhancements of the local ion population). In Chapter 2, it was shown that meteoric and relevant chemical processes (the sources and sinks of metallic ions) proceed slowly, typically with time scales on the order of days. On the other hand, theory predicts that ions can be efficiently lifted out of the background ion layer by northeasterly directed electric fields, and attain horizontal velocities of several hundred meters per second as they reach altitudes of reduced ion-neutral drag. This implies that transport governs the distribution of metallic ions. Ion transport is determined by the spatial and temporal structure of the convective electric field, indicating that an understanding of the occurrence of thin layers requires a careful analysis of the convection pattern over the entire polar region.

Similarly, seasonal variations in meteoric and chemical processes do not appear capable of explaining the increased rate of occurrence of thin layers during the summer. The influx of sporadic meteoroids peaks during the autumn months, while several major

meteor showers (e.g., the Geminid and Quadrantid showers) take place during the winter. Enhancement of metallic ion populations due to increased photoionizaton during the summer months has been shown to be insignificant (Whitehead, 1989), because the photoionization rates for metals are very low (Swider, 1969). However, if the average structure of the convection pattern varies with season, then one would expect the redistribution of ions through the transport process to also differ from season to season in some average sense. This might explain the seasonal effect in the occurrence of thin layers.

The above discussion suggests a working hypothesis that will be examined in this chapter: *the occurrence of thin ion layers (under geophysical conditions when the electric field dominates the neutral wind) is determined by the redistribution of metallic ions linked to the temporal and spatial structure of the convective electric field.* A rigorous test of this hypothesis would require the development of a detailed three-dimensional simulation of metallic ion transport, a project which is beyond the scope of this thesis. However, a qualitative evaluation is possible, one which draws upon a recently introduced model of high-latitude convective potentials (Weimer, 1995), and the theory of ion transport outlined in Chapter 3. This conceptual analysis will be seen to generally support the validity of the hypothesis, and also provides the basis for the future development of the three-dimensional simulation suggested by this thesis work.

5.2 An Electric Field Model

For this study, electric potentials obtained from a model devised by Weimer [1995] are used to calculate the electric field. Weimer's model is based upon *in situ* measurements of the electric field made from the DE-2 satellite between August 1981 and March 1983. These observations were related to measurements of the interplanetary magnetic field (IMF) provided by the ISEE 3 and IMP 8 satellites. The data were then sorted in one of two ways: by the angle of the IMF in the geocentric solar magnetospheric (GSM) Y-Z plane and the magnitude of the IMF's tangential component (the magnitude of the

vector sum of B_y and B_z); or by the IMF angle in the Y-Z plane and the dipole tilt angle, i.e., the angle between the dipolar axis and the GSM Z-axis. The latter method is of special interest for the present investigation, since the tilt angle is related to the season, so by construction Weimer's model allows one to produce average convection patterns (given the IMF angle) for summer and winter. The electric potential, as a function of magnetic local time (MLT) and corrected geomagnetic (CGM) latitude, was then determined using a least error fit of spherical harmonics. Figure 5.1 is a representative plot of a convective field generated using Weimer's model.

Although expressing the convective field in the CGM coordinate system is useful for many applications, for the present investigation the electric field in the geographic coordinate system is required. The coordinate conversion is accomplished using an algorithm developed by Gustafsson et al. [1992], yielding the electric potential as a function of geographic latitude and longitude at a specified universal time (UT) and altitude (250 km was selected for this study). The horizontal components of the electric field are calculated directly from the potential by differentiation. Recalling that the convective electric field is assumed to be orthogonal to the geomagnetic field, the vertical component is then found by solving $\mathbf{E} \circ \mathbf{B} = 0$.

Having obtained the electric field, one can use equations 3.4a-c to calculate the ion velocity. For example, Figure 5.2 shows examples of polar plots of the of the horizontal component of ion velocity, which have been calculated assuming no neutral wind, and that the altitude is such that **ExB** drift defines the velocity (a good assumption for altitudes greater than ~150 km). Notice that in each case the general shape of the flow field corresponds to the equipotential lines shown in Figure 5.1, but that there are slight differences in the specific shape of the fields as a function of UT. This is so because the orientation of the dipole axis with respect to the Sun changes with UT, which should lead to a variation in the coupling between the geomagnetic field and the IMF, and hence a difference in the convection pattern.

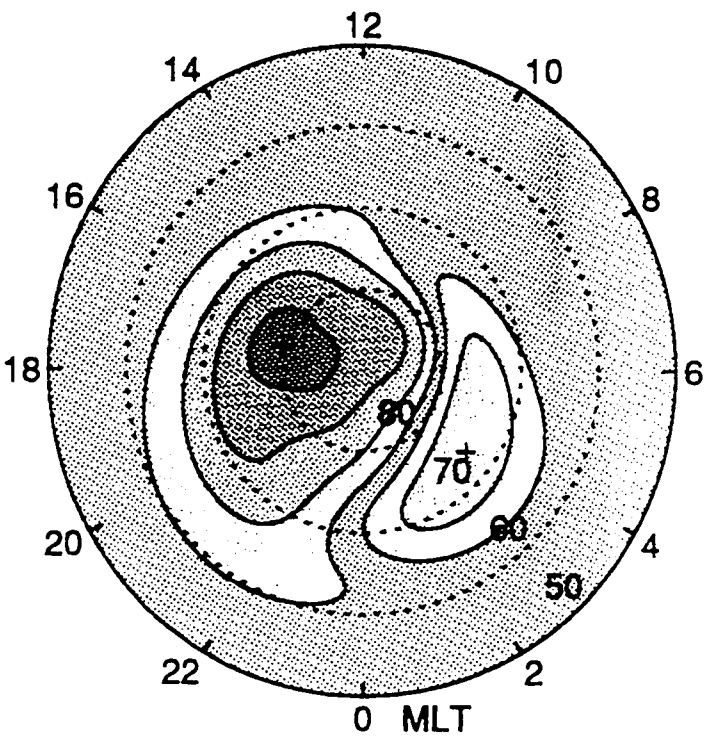

Figure 5.1 Example of the convective electric potential (from Weimer, 1995), plotted in terms of CGM latitude and MLT. Specific IMF conditions for this figure are: $3.5 < B_T < 5.2\ nT$; and IMF is directed along the +Y-axis (GSM), i.e., $B_z = 0$. The original figure is in color, and doesn't reproduce well here. The important thing to observe is the shape of the pattern, since it corresponds to streamlines for horizontal ion flow.

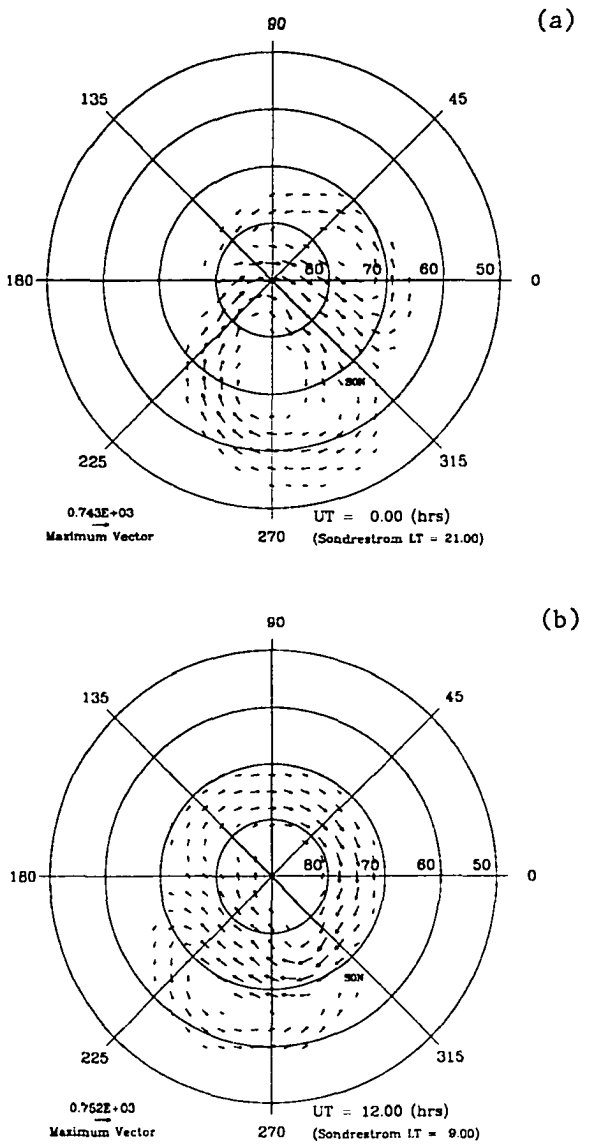

Figure 5.2 Geographic polar plot of the horizontal component of the ion velocity field arising from the electric field described by Figure 5.1. Fields are plotted for two different times: (a) 0000 UT; and (b) 1200 UT. The velocity has been calculated at an altitude 250 km, high enough that **ExB** drift defines the ion motion. Note that the speed associated with the maximum velocity arrow is in meters per second. The location of Sondrestrom is marked with "SON."

5.3 *Possible* Layer Occurrence

Recall that both theory and the observations indicate that a necessary, but not sufficient condition, for the occurrence of thin layers is an electric field directed to the magnetic NW or SW. One can get an idea of the regions at which layer formation is *possible* at a given UT by constructing a polar plot with areas of NW or SW fields identified, e.g., see Figure 5.3. When viewing Figure 5.3, it is important to note that these plots represent a snapshot in time, in this case 2100 UT. Nevertheless, there is a marked difference for IMF north versus IMF south, and a more subtle seasonal effect.

By overlaying a sequence of plots made for different times over the course of the day, one can see the daily extent of the region of possible layer occurrence, as is illustrated in Figure 5.4. For southward IMF, there is little difference in the region of possible layer occurrence between summer and winter. However, for northward IMF, the necessary field configuration extends ~5°-10° farther south during the summer. Figure 5.5 depicts the direction of the electric field over Sondrestrom for various seasons and IMF conditions. The remarkable feature here is the absence of favorable conditions for layer formation over Sondrestrom during the winter for IMF north.

The above analysis provides significant insight into the question of layer occurrence. As might be expected, the direction of the IMF plays a major role in defining the geographic extent of the region of possible layer formation. This is especially important at lower latitudes, which may fall completely outside of the zone of possible occurrence for certain IMF configurations, as was shown to be the case for Sondrestrom during the winter for IMF north. Similarly, the seasonal variation in layer occurrence at Sondrestrom may be explained by IMF-related differences in the average convection pattern. Since it is reasonable to assume that the probability of finding the z-component of the IMF to be positive is equal to that of finding it to be negative, the results shown in Figures 5.4 and 5.5 strongly suggest that layers are more likely to occur during the summer, consistent with the observations made during this investigation.

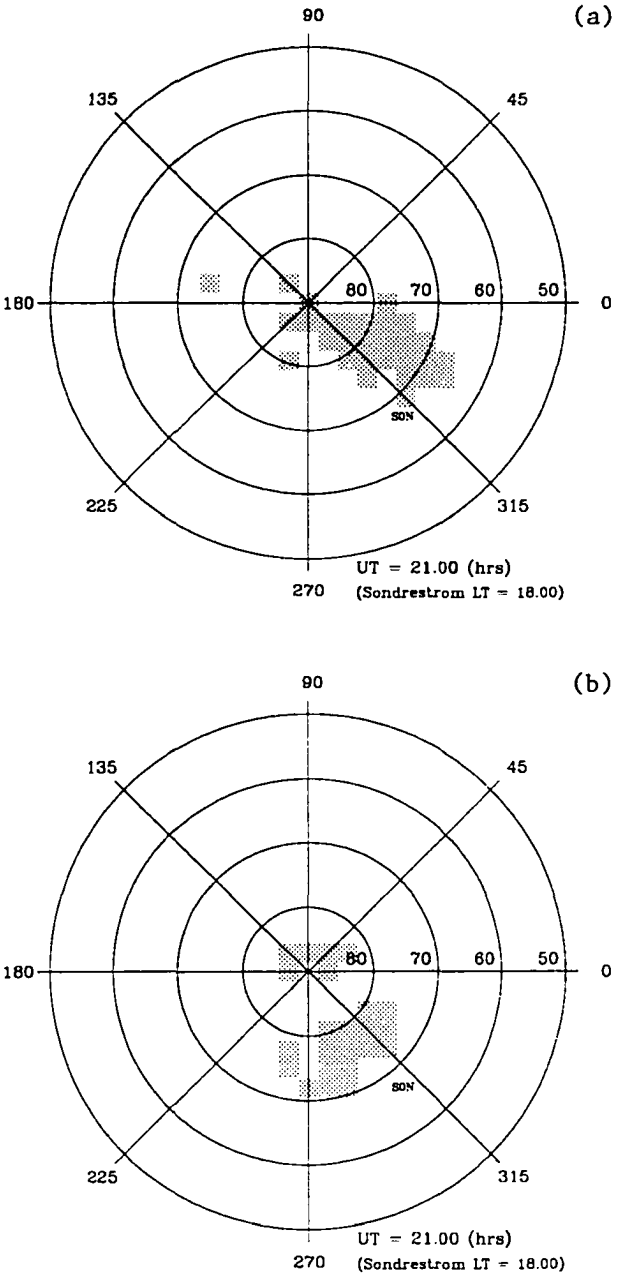

Figure 5.3 Geographic polar plot of regions of possible layer formation (shaded) at 2100 UT for: (a) summer, IMF-north; (b) winter, IMF-north; (c) summer, IMF-south; (d) winter, IMF-south.

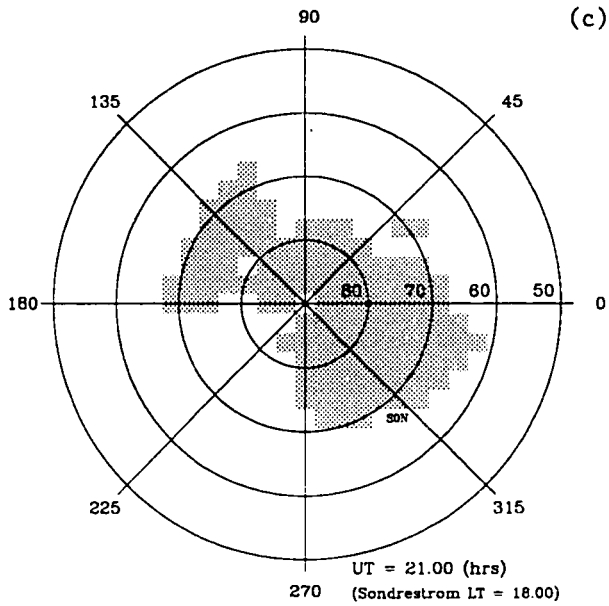

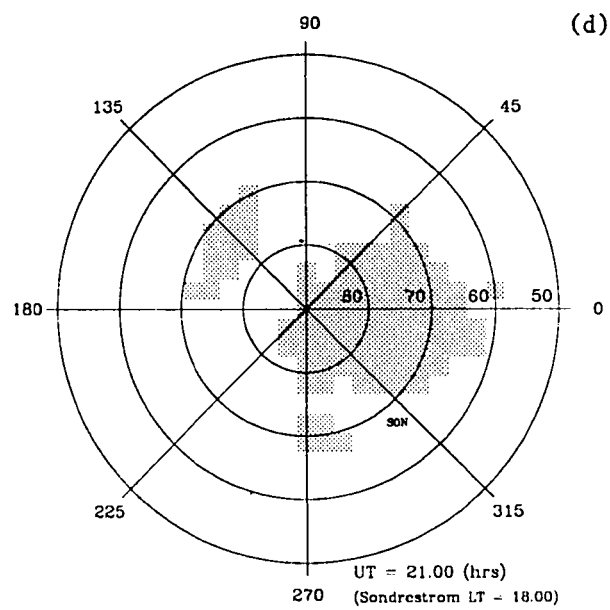

Figure 5.3 continuation.

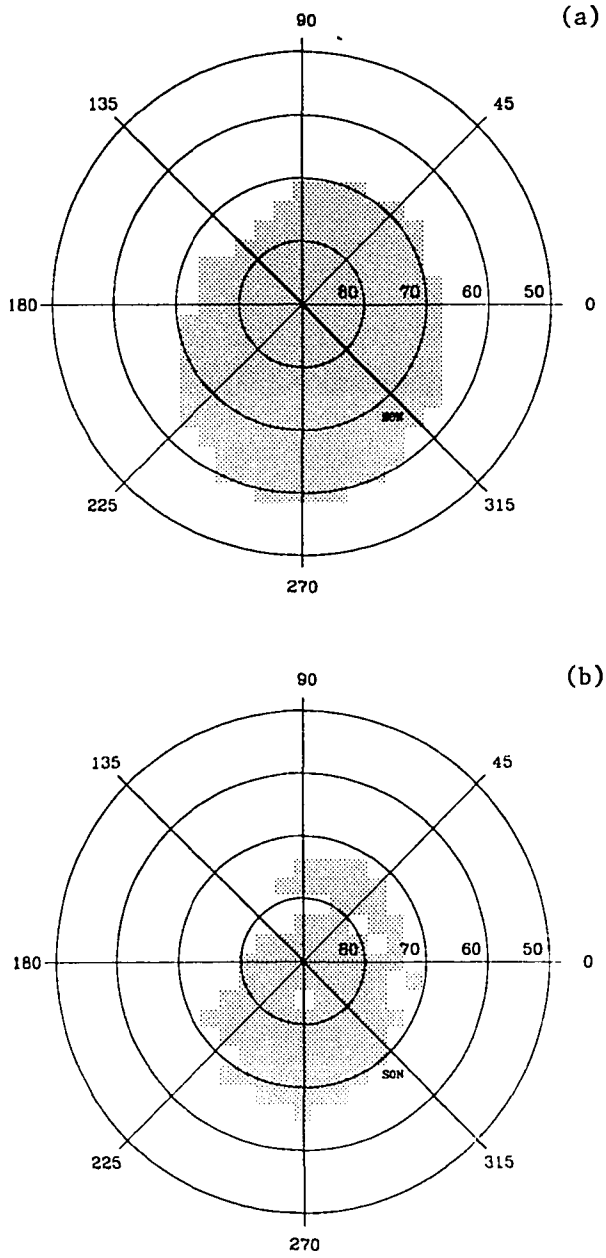

Figure 5.4 Geographic polar plot of regions of possible layer formation (shaded) over an entire day for: (a) summer, IMF-north; (b) winter, IMF-north; (c) summer, IMF-south; (d) winter, IMF-south.

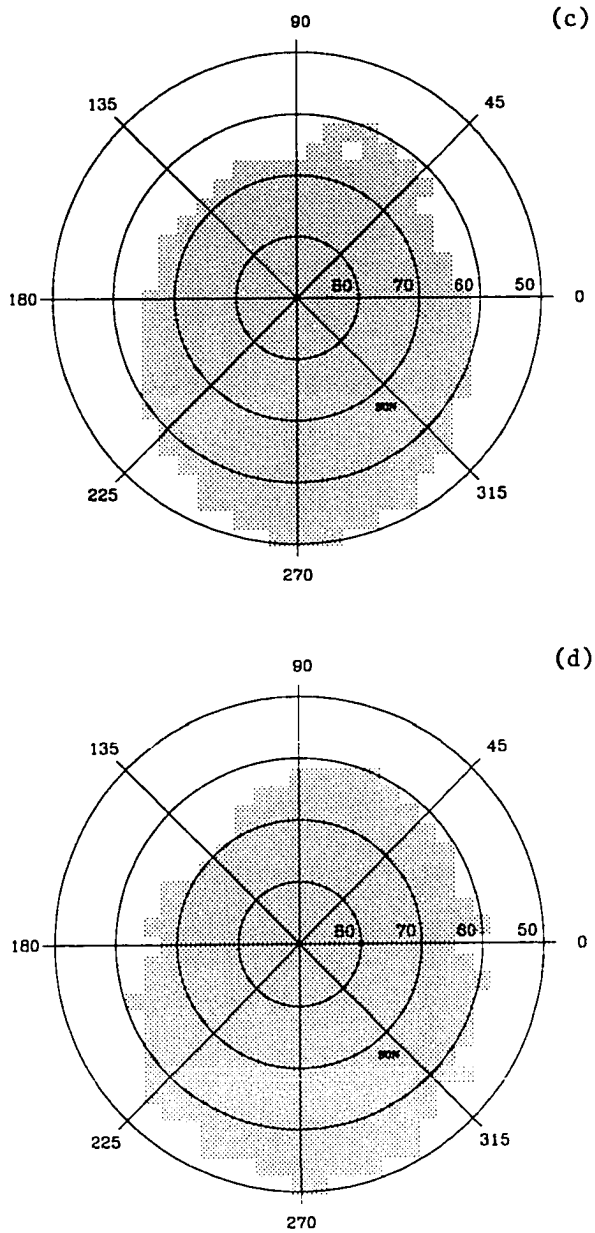

Figure 5.4 continuation.

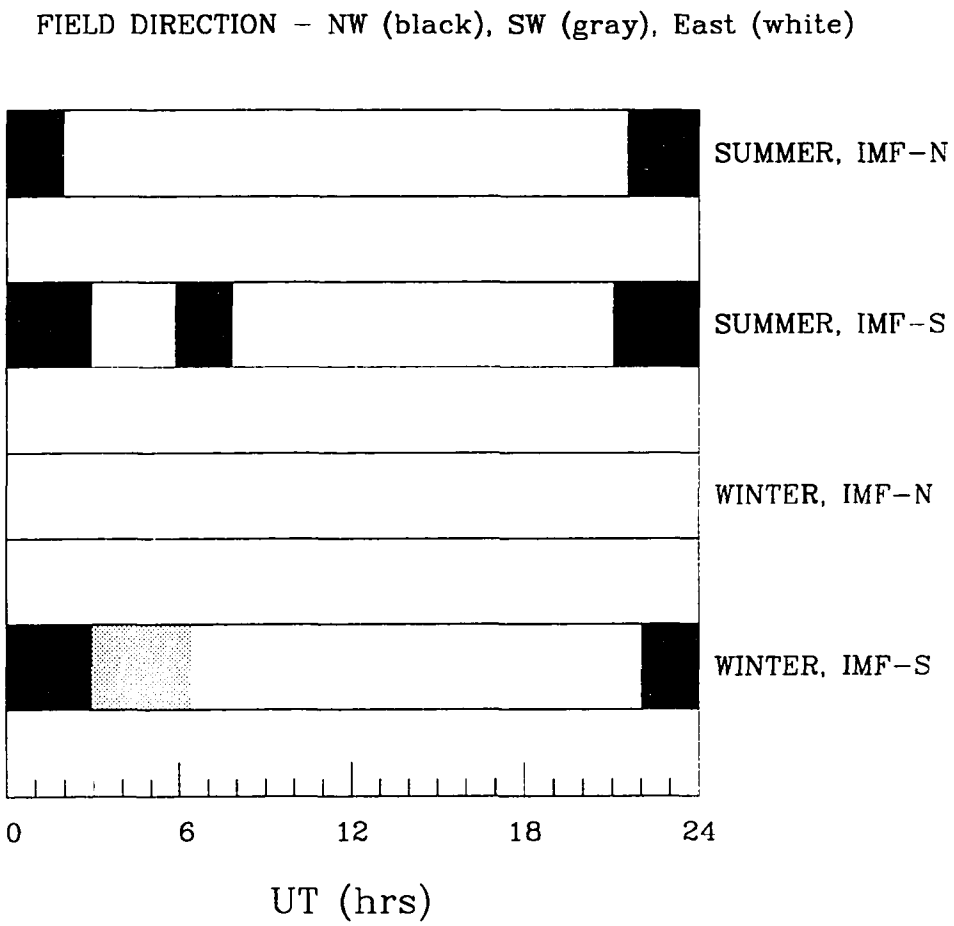

Figure 5.5 Model-derived direction of the electric field over Sondrestrom as a function of UT for various combinations of season and IMF direction.

5.4 Ion Transport and the Occurrence of Layers: Basic Concepts

In section 5.3, a plausible explanation for the seasonal variation in layer occurrence over Sondrestrom was put forward, based upon a simple evaluation of when and where the conditions necessary for layer formation (in terms of electric field direction) prevail. Of course, this approach cannot account for the failure to see layers whenever the correct conditions are present. By hypothesis, the redistribution of metallic ions by transport is responsible for providing enhancements to the local ion population, sufficient for formation of detectable layers. In this section, an argument is developed in support of this proposition.

As was shown in Chapter 3, when the electric field is directed to the magnetic NE, ions can be lifted up out of the broad background metallic layer which is centered at an altitude of ~95 km (fields to the SE also drive ions upward, for altitudes above the divergent null in the vertical velocity profile). Neglecting gravity (and the neutral wind), an ion subjected to such a field would move upward, but would be constrained to a surface normal to the geomagnetic field. Thus, as it moved upward it would also be moving poleward and to the magnetic west. However, consideration of equation 3.2 indicates that gravity is non-negligible at sufficiently high altitudes, where the ion velocity is given by

$$\mathbf{v} \approx \frac{\mathbf{E}\times\mathbf{B}}{B^2} + \frac{(\mathbf{g}\circ\mathbf{B})}{B^2\nu}\mathbf{B}, \tag{5.1}$$

where ν is the ion-neutral collision frequency. To better appreciate the effect of gravity, assume that the electric field is everywhere directed due east, and adopt a centered-dipole model for the geomagnetic field. In this case, an ion's trajectory will remain in the same meridional plane. Figure 5.6 shows the trajectory of an iron ion, initially at an altitude of 100 km and a dipole latitude of 60°, when the field strength is 50 mV/m. Gravity limits the rise of this ion to an altitude of ~300 km. Since a degree of latitude

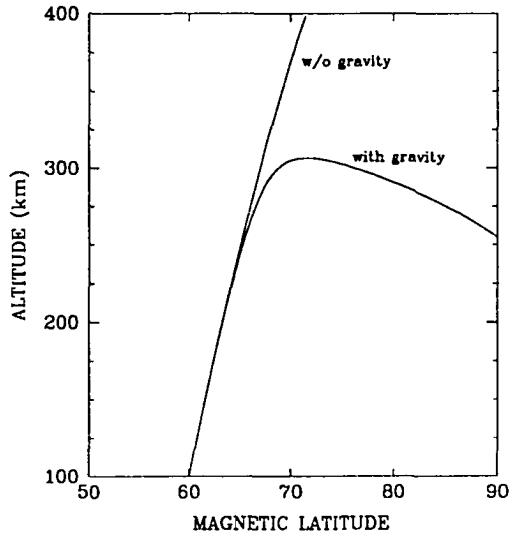

Figure 5.6 Trajectory of an ion in a centered-dipole magnetic field, and subject to an eastward electric field with a strength of 50 mV/m. Comparison of the curves illustrates the effect of neglecting gravity.

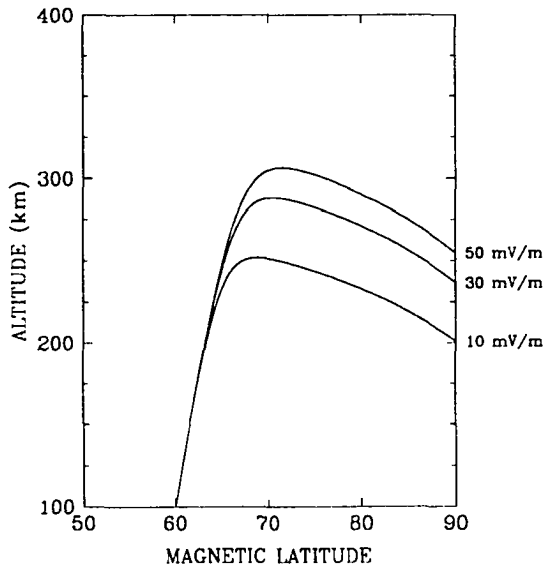

Figure 5.7 Influence of the electric field strength on the trajectory of an ion in a centered-dipole magnetic field. The electric field in each case is directed to the magnetic east.

corresponds to about 100 km in distance along the Earth's surface, it is apparent that the motion of the ion is very nearly horizontal over most of its path. Figure 5.7 shows the impact of varying the strength of the electric field; the maximum altitude attained by the ion is lower as field strength decreases, but this effect is not too dramatic. In Figure 5.8, the effect of the initial latitude is highlighted. For a given electric field strength, ions originating at lower latitudes rise to slightly higher altitudes than those starting more northward, but as they move farther north, their trajectories merge. Another feature displayed in Figure 5.8 is that ions north of 70° dipole latitude do not reach the F-region. This is a consequence of increasing magnetic inclination, which limits the contribution made by the electric field to the vertical component of the ion velocity, as can be understood from equation (5.2):

$$v_z \approx \frac{E_e}{B}\cos I - \frac{g}{\nu}\sin I, \tag{5.2}$$

recalling that E_e is the component of the electric field to the magnetic east, and I is the inclination.

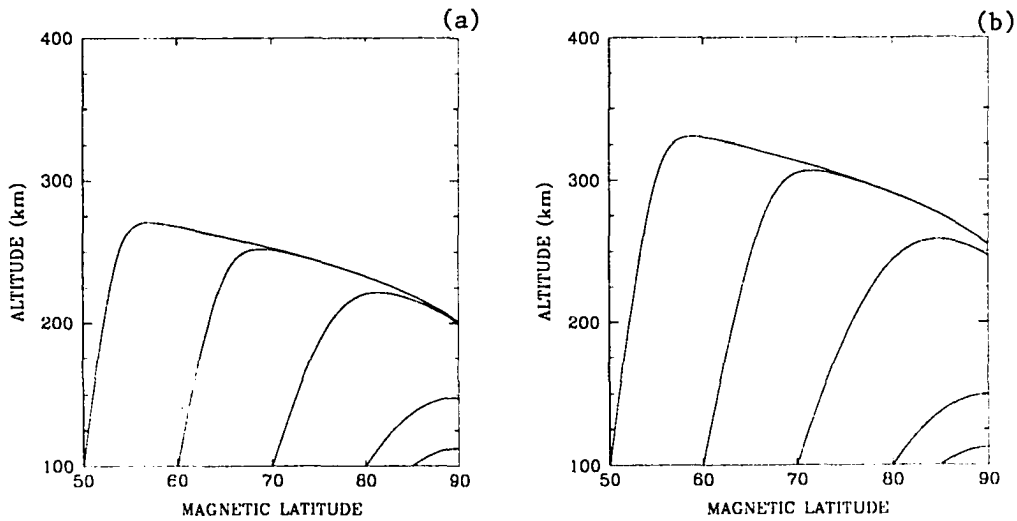

Figure 5.8 Ion trajectories in a centered-dipole magnetic field for different initial latitudes. The electric field is directed to the east with a strength of: (a) 10 mV/m; and (b) 50 mV/m.

From the elementary analysis provided above, one can draw three inferences. First, after being lifted into the F-region, ions move nearly horizontally. Second, as the ions are moving horizontally, they should be located within a stream, ~25 km in vertical extent, centered between altitudes of 225 and 300 km (these numbers were arrived at by comparing Figures 5.8a and 5.8b). Finally, at dipole latitudes exceeding ~70°, the electric field mechanism is not effective for lifting additional ions into the F-region, and those originating at lower latitudes will simply pass over this region, so long as the electric field remains unchanged. These conclusions find remarkable support in the satellite measurements of Fe^+ made using a mass spectrometer on board the *Atmospheric Explorer-C* during the period December 1973 through November 1978. Grebowsky and Pharo [1985] report that while measurements were made at altitudes ranging from 145 to 4300 km, most Fe^+ observations occurred between 250 and 310 km. Furthermore, as can be seen in Figure 5.9, most measurements of Fe^+ were made on the dayside at invariant latitudes

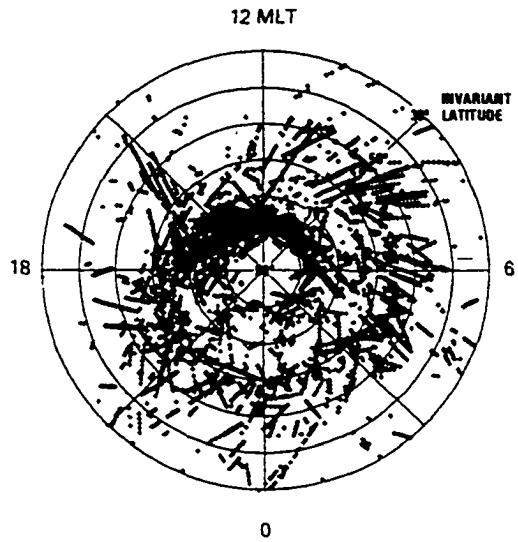

Figure 5.9 Plot of Fe^+ observations made in the F-region by a mass spectrometer onboard the AE-C satellite (from Grebowsky and Pharo, 1985). This represents measurements made from 1974 through 1978. Density threshold is 30 cm^{-3}. Note that no measurements were made poleward of an invariant latitude of 84°.

between 70° and 80° (note however that the satellite's orbit precluded measurements poleward of 84° invariant latitude, which accounts for the absence of observations near the pole). This too is consistent with the theoretical analysis given above; northeasterly electric fields tend to be found on the dayside, and one would expect the ion density to increase with increasing latitude, as ions from successive latitudes merge into the flow (recall Figure 5.8).

The simple model developed above can be extended to study how ions should "precipitate" from the F-region when encountering a westerly directed electric field. Assume that as the ions flow over the pole, the electric field abruptly changes direction to due magnetic west. This field, along with gravity, will force the ions downward, eventually forming a layer. Trajectories for ions initially at an altitude of 250 km (associated with uplift by a 50 mV/m electric field), and at 200 km (associated with a 10 mV/m uplifting field) are shown in Figure 5.10. Metallic ions flowing in the F-region, although

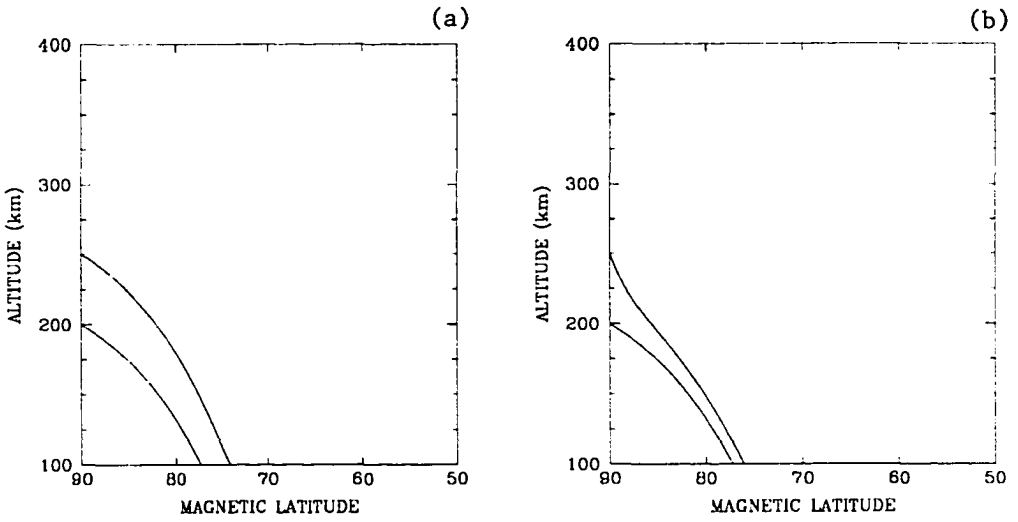

Figure 5.10 "Precipitation" of ions encountering a westward electric field as they cross the pole. A centered-dipole magnetic field is assumed. Electric field strengths is 50 mV/m in (a), and 10 in (b).

originating at dipole latitudes of 50°-70°, return to the lower E-region in a restricted range of latitudes, at quite high dipole latitudes: 74°-76° and 76°-77° for westerly field strengths of 50 mV/m and 10 mV/m, respectively. Most importantly, ions from the F-region are not available for layer formation at latitudes below approximately 75°, regardless of the electric field orientation. These results demonstrate a mechanism by which enhancements (and deficiencies) in the local metallic ion density can be created, supporting the contention that large-scale redistribution of metallic ions via horizontal transport is responsible for the failure to observe layers even when the electric field is properly directed.

5.5 Ion Transport and the Occurrence of Layers: A Case Study

Of course, the above discussion of the influence of horizontal transport on the occurrence of layers is highly idealized. The actual geomagnetic field is not generated by a centered dipole, as illustrated in Figure 5.11. Furthermore, the convective electric field exhibits complex temporal and spatial structure, one result of which is the introduction of a (magnetic) zonal component to the ion flow. Nevertheless, employing the conceptual framework devised in Section 5.4, one can make a qualitative assessment of at what time metallic ions, transported from regions of uplift on the dayside can be expected to precipitate over a given point (e.g., Sondrestrom) on the nightside. When dealing with a more realistic situation, the main points of the simple model to keep in mind are: (a) metallic ions in the F-region flow horizontally within a relatively narrow range of altitudes, until reaching a region where the electric field forces the stream downward; (b) precipitation should be restricted to a narrow band of magnetic latitudes (as suggested in Figure 5.10).

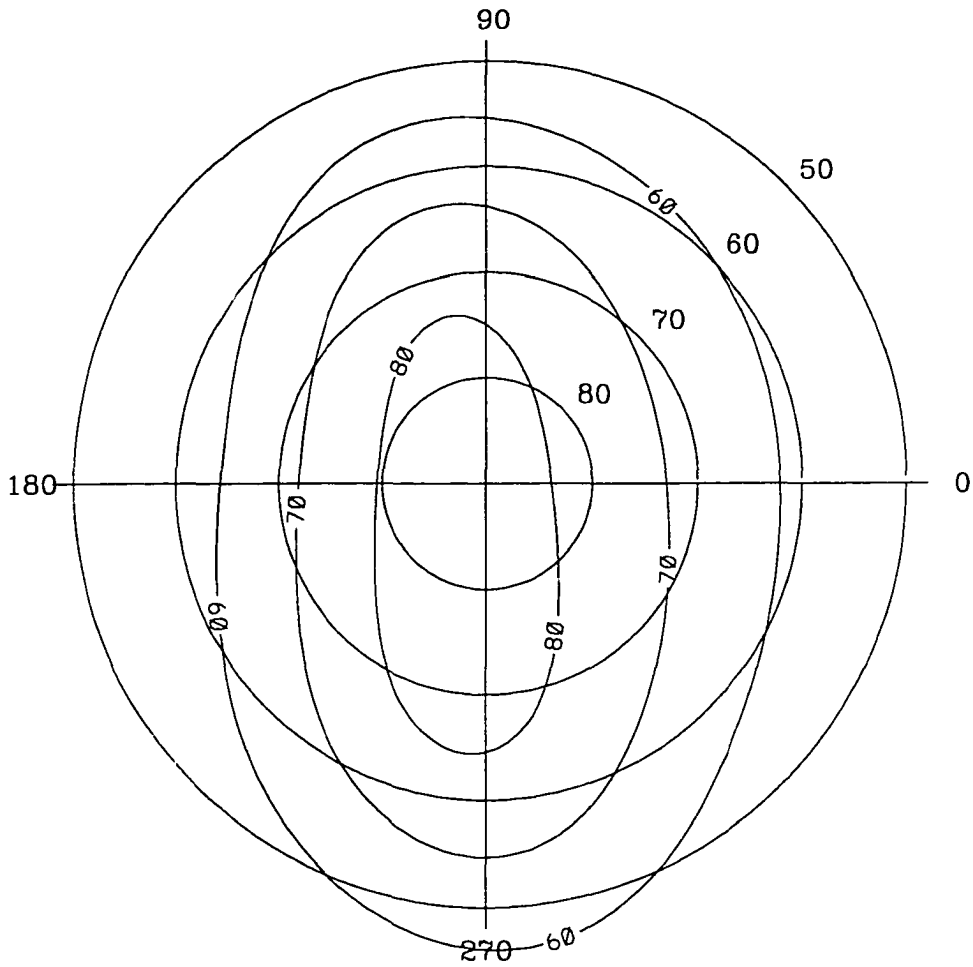

Figure 5.11 Geographic polar plot of contours of constant dip latitude (60°, 70°, and 80°) based on the DGRF/IGRF geomagnetic field model (epoch 1995).

For example, consider Figure 5.12, which describes the high-altitude (F-region) velocity for Fe^+ at one-hour intervals between 2200 UT and 0200 UT on a typical day during the summer months with the IMF directed southward. For regions where the of electric field has a (magnetic) easterly component, the velocity field depicted in Figure 5.12 is an excellent representation of the flow field for the ions. As ions enter shaded regions, corresponding to downward flow, the high-altitude velocity pattern only approximately depicts the flow field, because as the ions reach lower altitudes, their horizontal speed decreases, and the velocity changes direction in a systematic manner (as discussed in Chapter 3): it approaches due magnetic west, if the electric field is in the NW quadrant; and becomes aligned with the horizontal component of the electric field, if the field is directed to the SW.

With the above-mentioned qualifications in mind, assume that the velocity field does (approximately) represent the flow field. Treating the flow pattern in each plot in Figure 5.12 as fixed, an interesting question is: where will ions, flowing in the F-region precipitate in the shaded area? To obtain a rough answer, one can trace ion trajectories along the streamlines associated with the flow pattern. First assume that the ions entering the region of NW or SW electric fields are flowing in the F-region in an altitude range of 200-250 km. The average values of the ion velocity components, as they drop from the F-region to the altitude of layer formation, can be approximated by

$$\langle v_x \rangle \approx -\frac{E}{B} \tag{5.3a}$$

$$\langle v_y \rangle \approx -\frac{E}{B}\sin I \tag{5.3b}$$

$$\langle v_z \rangle \approx -\frac{E}{B}\cos I \tag{5.3c}$$

where the x-direction is to the local magnetic east, the y-direction is positive toward magnetic north, and the z-direction is positive upwards. Using these average values, the time required for ions to flow from the F-region to the layer altitude can be estimated by

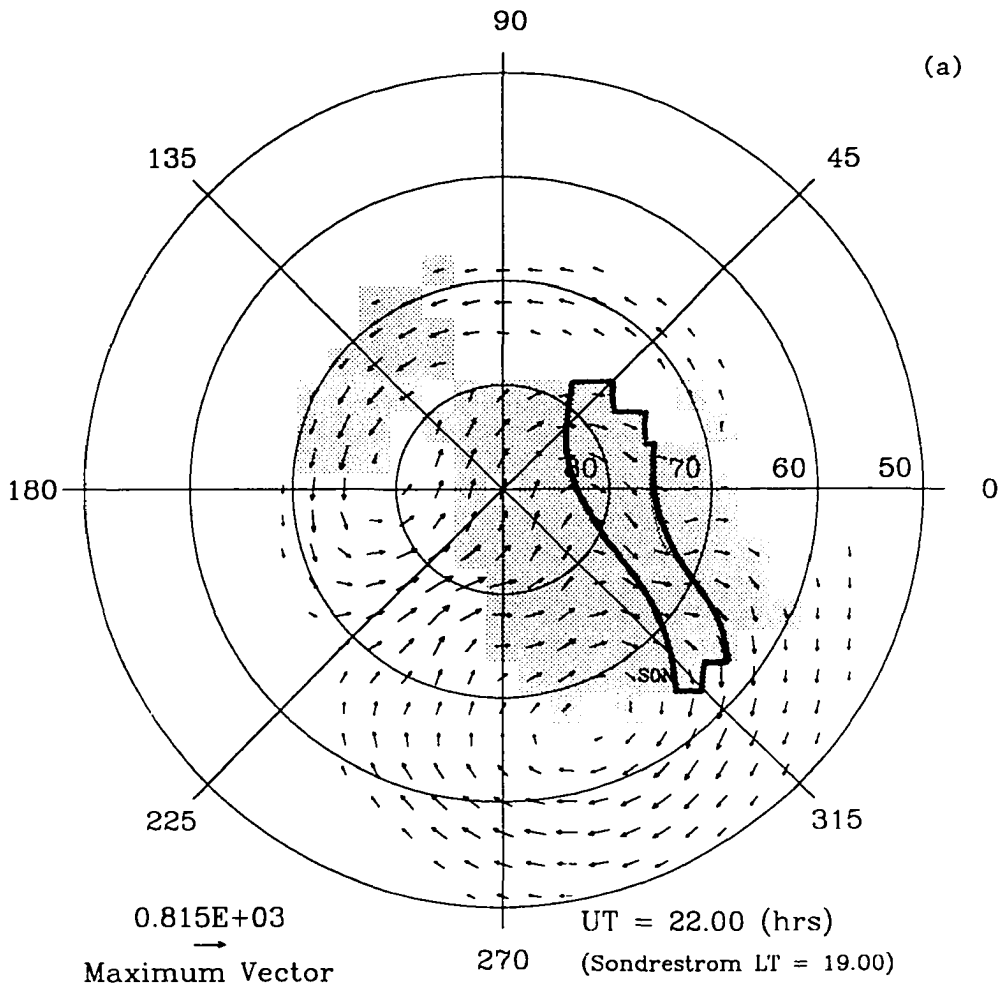

Figure 5.12 Typical ion flow patterns for IMF southward during the summer months. The velocity magnitudes are in m/s. Shaded areas correspond to regions where the electric field is directed to the NW or SW. The region of metallic ion deposition is indicated with heavy lines. The times of the plots are: (a) 2200 UT; (b) 2300 UT; (c) 0000 UT; (d) 0100 UT; and (e) 0200 UT.

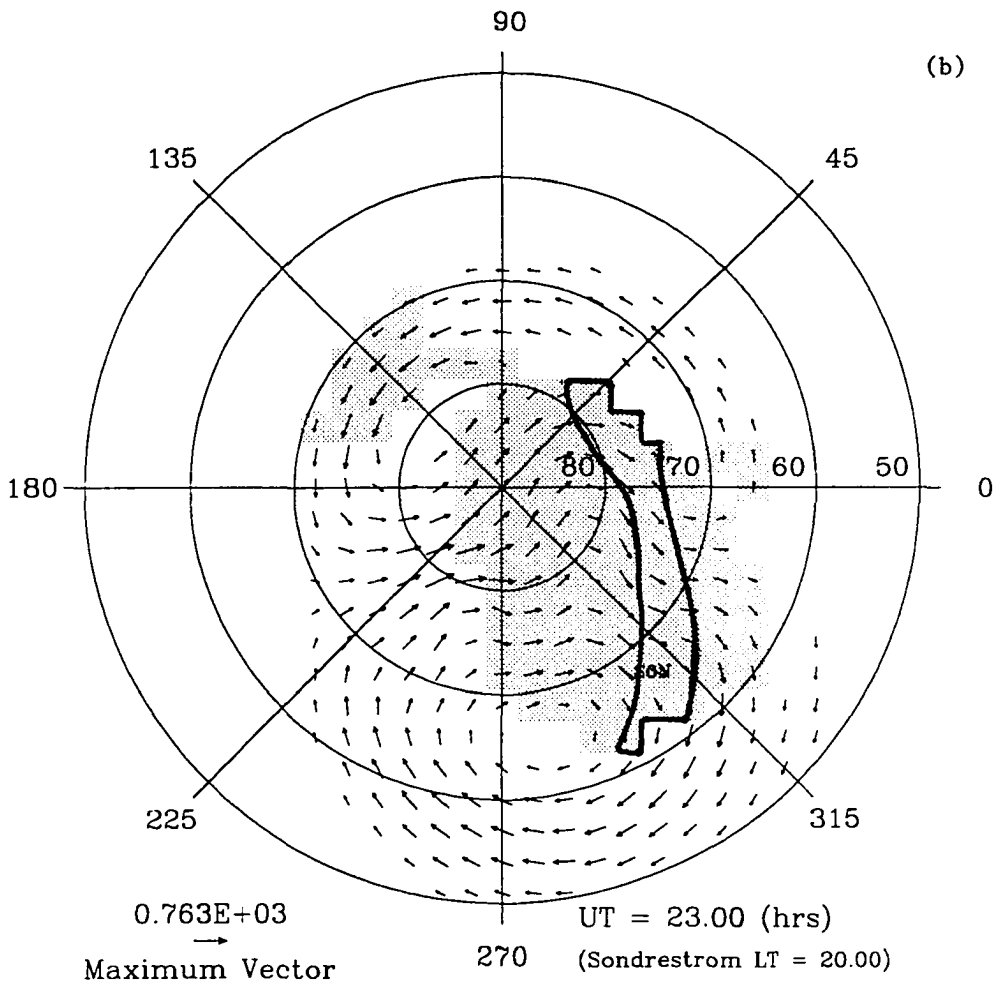

Figure 5.12 continuation.

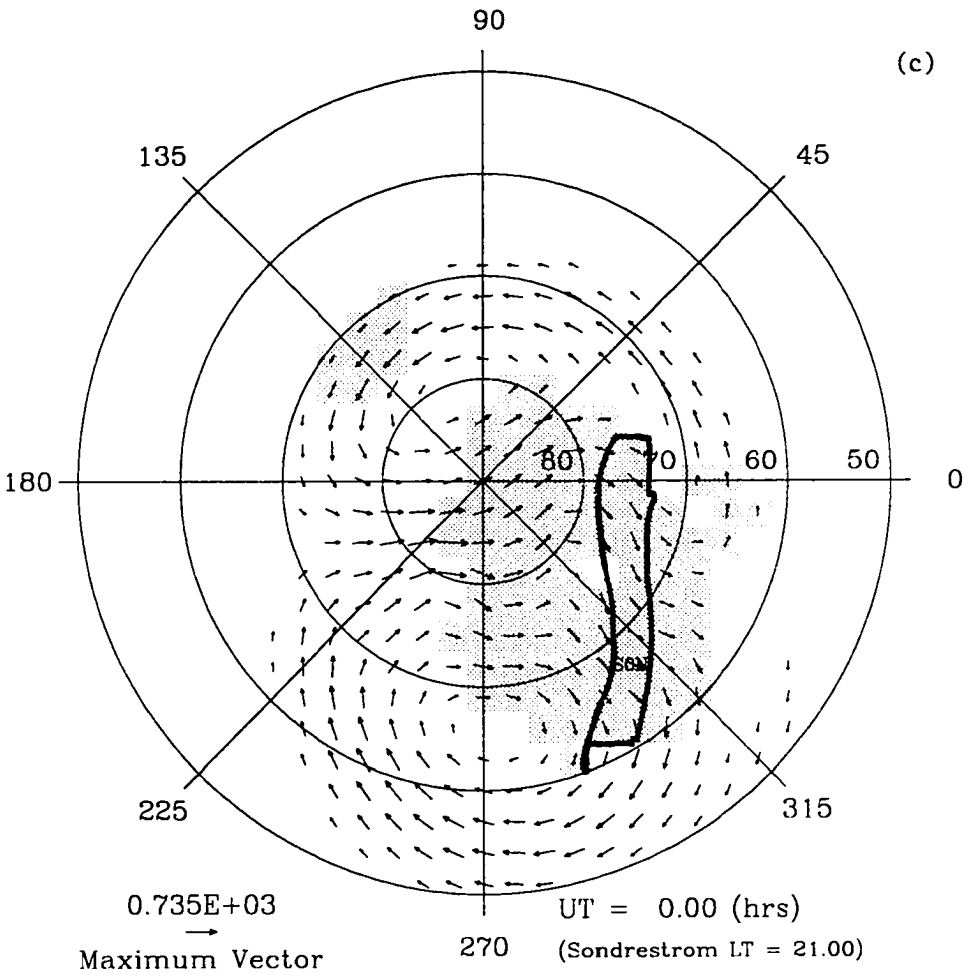

Figure 5.12 continuation.

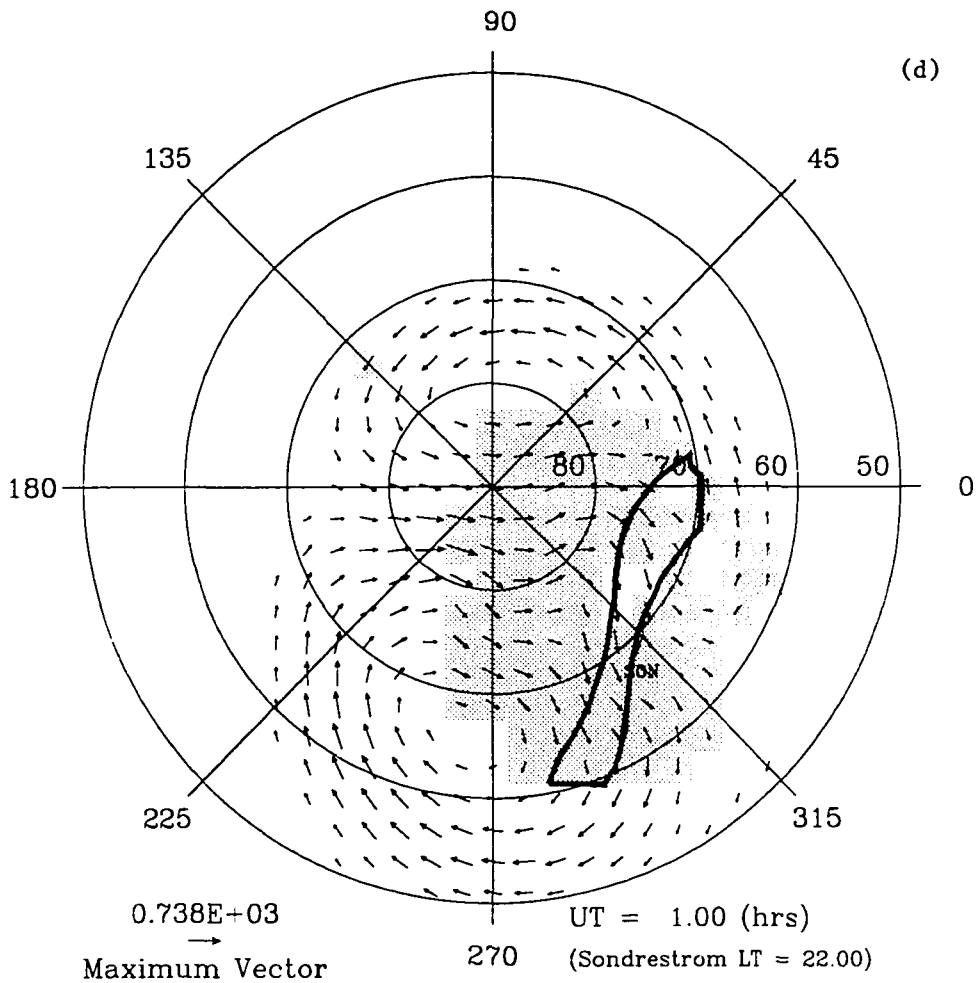

Figure 5.12 continuation.

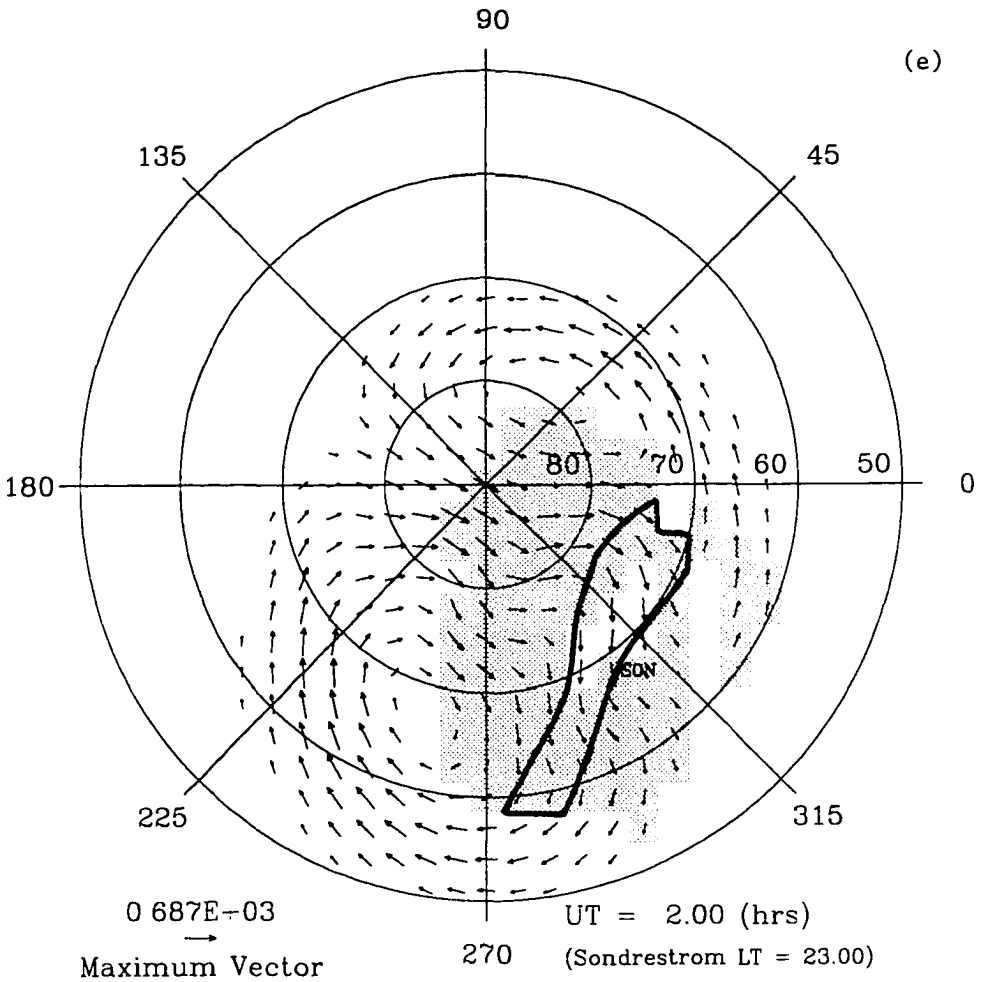

Figure 5.12 continuation.

$$\Delta t \approx \frac{\Delta z}{\langle v_z \rangle}, \tag{5.4}$$

and the horizontal distance traveled along the streamline in that time is

$$\Delta L \approx \Delta t \sqrt{\langle v_x \rangle^2 + \langle v_y \rangle^2}. \tag{5.5}$$

Substituting from equations (5.3) and (5.4) into equation (5.5) yields

$$\Delta L \approx \frac{\sqrt{1+\sin^2 I}}{\cos I} \Delta z. \tag{5.6}$$

For the inclination, use 85°, which by inspection is a reasonable average value of that parameter in the region of interest (recall Figure 5.11). Also, by inspection, the value of *E/B* is approximately 0.7 km/s. Calculated values of ion transit time, and the corresponding horizontal displacement are given in Table 5.1.

Table 5.1 Ion Transit Time and Horizontal Displacement for Two Initial Altitudes.

Initial Altitude	Transit Time, Δt	Horiz. Displacement, ΔL
250 km	41 min	2400 km
200 km	27 min	1600 km

By inspection of the plots in Figure 5.12, one sees that the flow pattern does not change much over intervals on the order of an hour. Since the calculated transit times are less than an hour, this gives some confidence that the assumption of a fixed flow pattern is acceptable. Thus, to see where ions entering the shaded region (location of NW or SW electric fields) are deposited at a given UT, simply measure along the streamlines for a distance of 1600 and 2400 km. The resulting region of deposition is indicated on each plot. Recalling Figure 5.11, notice that the area where ions precipitate at any given UT is limited, falling primarily within dip latitudes of 70° and 80°, as expected from the simplified analysis presented in section 5.4. Plots made for other times (see Figure 5.13) show a similar limitation in the extent of the deposition region.

The above analysis indicates ions would be deposited over Sondrestrom from 2200 through ~2400 UT. After ~2400 UT, the flow field is such that ions cannot make it to Sondrestrom. This suggests a relative enhancement of the local metallic ion population before midnight, which in turn implies a greater chance of detecting thin layers. On the other hand, after midnight the occurrence of layers would be inhibited by a relative shortage of ions, despite the presence of a "properly' directed electric field. Once again, it must be pointed out that this is only a crude estimate. Nonetheless, these conclusions have some observational support. Recall the layer observations reported in Chapter 4. On the days that layers were detected, the experiment ran until at least 0300 UT. Of the 13 layers seen, eight were observed before 2400 UT, and only two persisted after 0100 UT (and these vanished before 0145 UT). Although not conclusive, the simple analysis provided above and the somewhat sparse observational record together suggest a connection between large-scale metallic ion transport and the occurrence of thin layers.

5.6 Closure

In this chapter it has been argued that the temporal and spatial structure of the convective electric field can explain important features in the occurrence of thin metallic ion layers. An apparent decreased rate of occurrence during the winter (at Sondrestrom) may result from the tendency for properly directed fields to be absent over the station when the IMF is to the north. In addition, a plausible case was made that large-scale horizontal transport of metallic ions can result in enhanced local ion populations, which would increase the probability of formation of a detectable thin layer. Clearly, more work remains to be done before a complete understanding of the occurrence of thin layers is to be had. As mentioned in section 5.1, a full treatment of layer occurrence demands a detailed three-dimensional simulation of the process. The results of the analysis performed here both serve to motivate such an effort, and indicate a future line-of-attack.

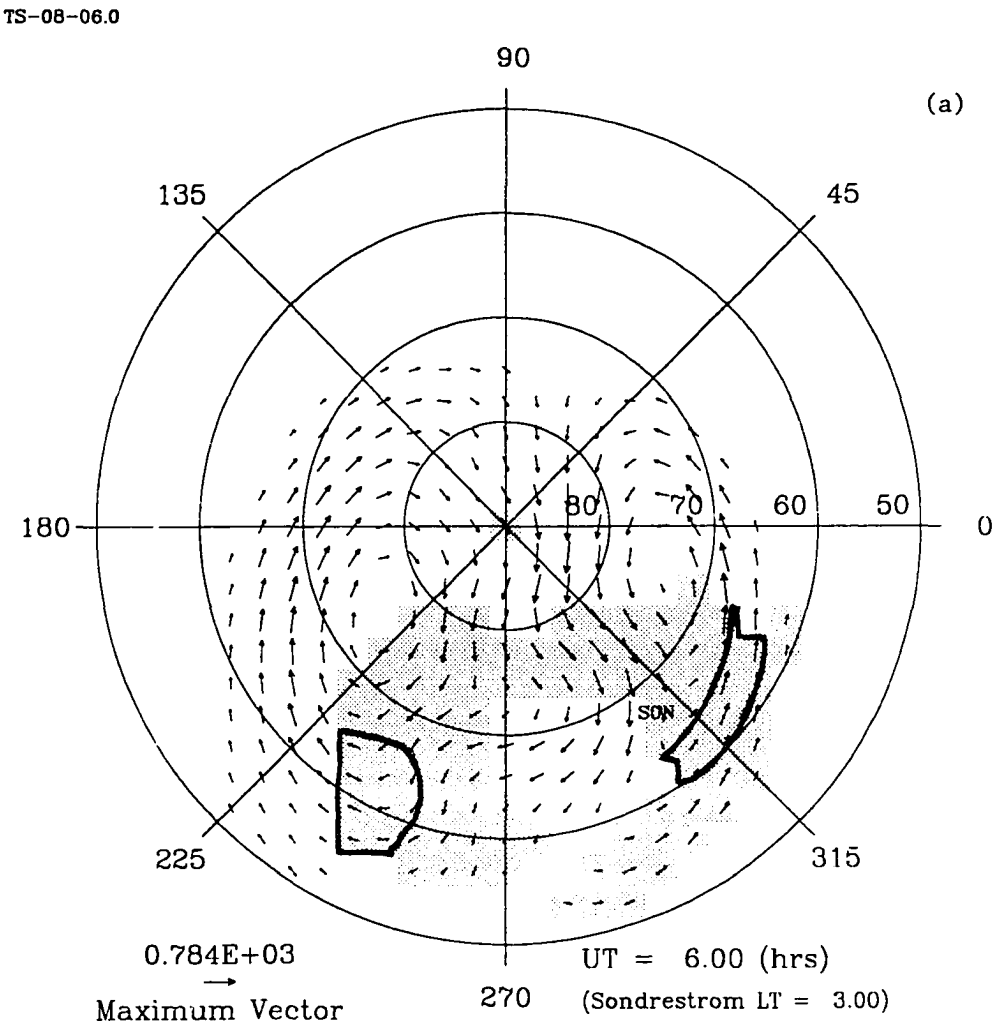

Figure 5.13 Examples of regions of ion deposition at: (a) 0600 UT; (b) 1200 UT; (c) 1800 UT. The flow pattern is for a typical day during the summer, with IMF south (the same conditions as in Figure 5.12).

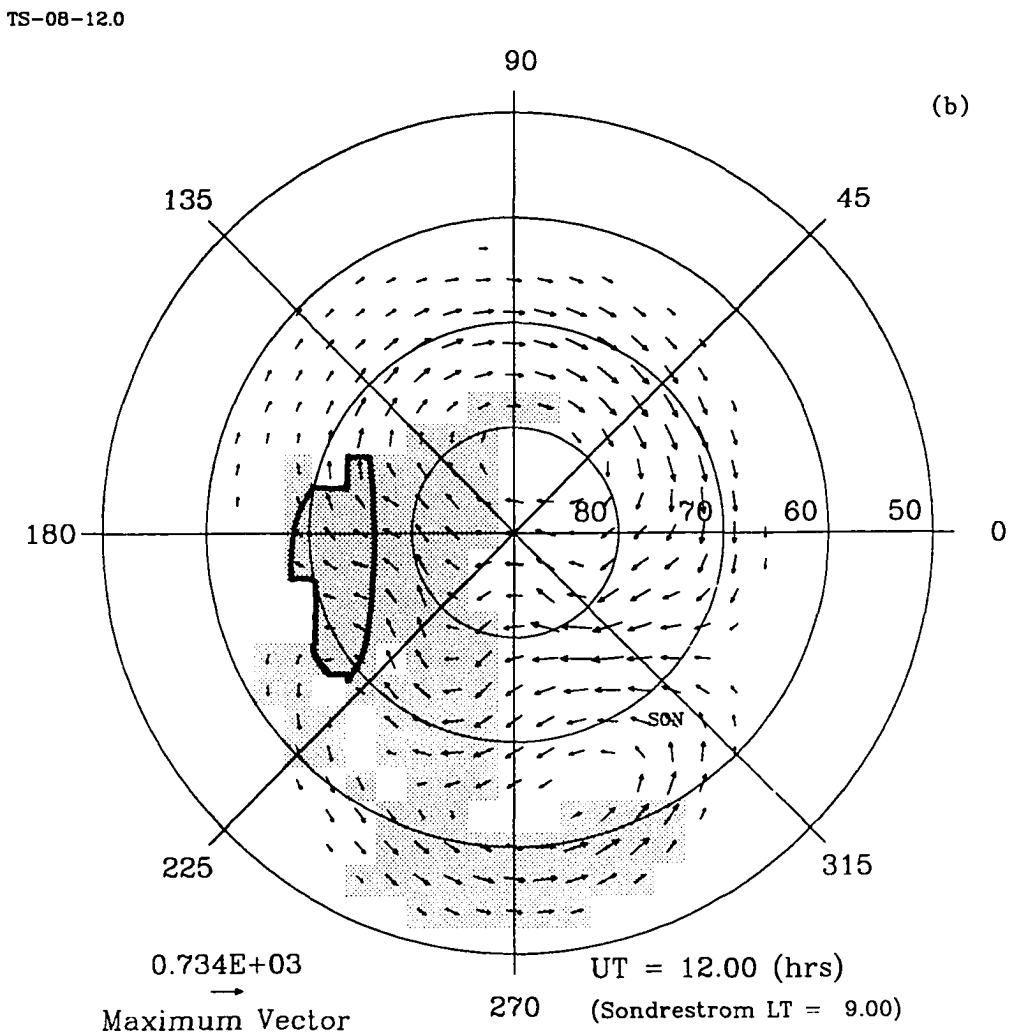

Figure 5.13 continuation.

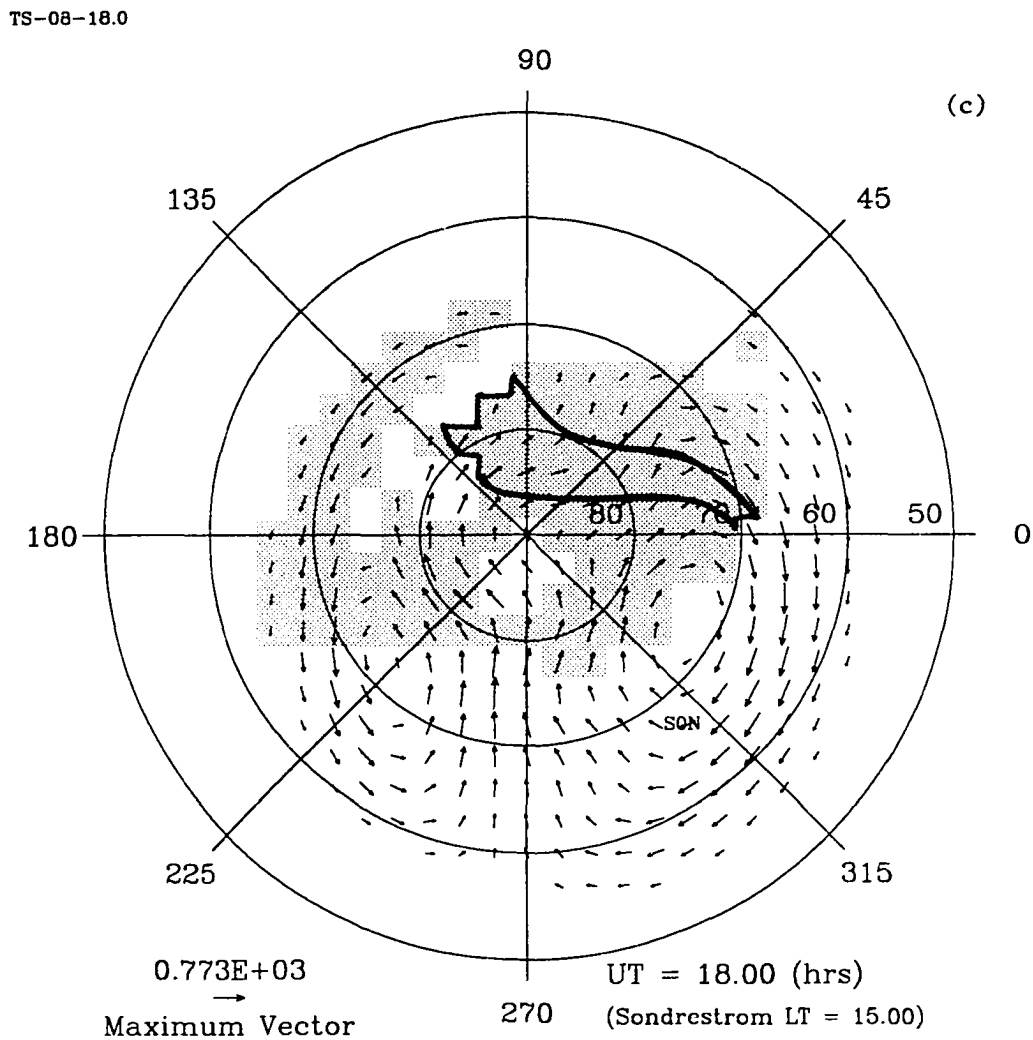

Figure 5.13 continuation.

CHAPTER 6
CONCLUSIONS

6.1 Summary

Thin metallic ion layers at high latitudes have been studied in earnest for only a relatively short time, starting with the theoretical work of Nygrén and his colleagues in 1984. In the following years, observational studies revealed two significant deficiencies in the theory: layers, present when fields are directed to the magnetic northwest, are typically 10-20 km lower than predicted; and layers often fail to appear despite the presence of electric fields which on a theoretical basis should lead to efficient layer formation. In addition, Nygrén's theory concerns itself only with the vertical motion of the metallic ions, a limitation also present in subsequent refinements of the theory made in 1991 by Bristow and Watkins, and Kirkwood and von Zahn. Thus, the theory is by design incapable of addressing questions relating to the horizontal drift of layers or the role of horizontal transport in determining occurrence of layers.

The chief tool used for studying thin ion layers at high latitudes is the incoherent-scatter radar, one of which is located in Norway, another at Sondrestrom in Greenland. The observational record, as discussed in Chapter 1, has been rather sparse. For the most part, the radars have been operated with the beam in a fixed direction, so that horizontal motion and structure of the layers cannot be determined. There had also been no systematic attempt to determine if there exists a seasonal variation in the rate of layer occurrence (as is seen at mid-latitudes).

This thesis describes a coupled theoretical and observational program aimed at clarifying a number of the poorly understood aspects of this interesting phenomenon. Significant advances in the theory of thin layers have been made by taking into account the horizontal transport of metallic ions, which is driven by the spatially and temporally varying convective electric field. Execution of a unique radar experiment at Sondrestrom, capable of simultaneously determining the electric field and layer characteristics

along the local geomagnetic meridian, has yielded new information about the horizontal extent and drift of thin layers as related to the structure of the electric field. Additionally, observations were made on a regular basis over the course of an entire year, revealing that layers tend to occur during the summer months. All experiments spanned 2200-0300 UT (some ran for more extended periods), but layers were almost exclusively observed prior to 0100 UT. When layers were observed, they exhibited great variability in terms of duration, apparent drift, and horizontal extent. As a generalization, the picture that emerges is one of patches of ionization drifting sometimes quite rapidly across the field-of-view.

The main conclusions of this thesis, drawn from a synthesis of the theoretical and observational work, can be formulated as answers to the scientific questions posed in Chapter 1, and are summarized in Table 6.1. In the next section, these conclusions are elaborated upon. In addition, several refinements to the theory of the formation of thin layers have been made. It has been shown that layer formation is extremely inefficient when the electric field is directed in the southeast quadrant, or is within 20° of due (magnetic) north in the northwest quadrant. Kirkwood and von Zahn [1991] suggested that variability in the direction of the electric field would tend to broaden and weaken thin layers formed in the northwest quadrant, thus reducing detectability of these layers. It has been demonstrated here via simulation that fluctuating field direction does not affect the thickness or density of thin ion layers. Finally, it has been widely believed (Bristow and Watkins, 1991; Kirkwood and von Zahn, 1991) that layers forming when the electric field is directed in the southwest quadrant should be broader than those forming for fields in the northwest quadrant. It has been shown in this thesis that this is only the case early in the evolution of a layer; after ~40 minutes a layer formed for in a southwesterly electric field has similar thickness and density to one formed for a northwesterly field.

Table 6.1 Main Conclusions.

Why aren't thin layers observed whenever the electric field is "properly" oriented?
Answer: This happens when the local ion population is insufficient for the formation of detectable layers. The local metallic ion population is determined by large-scale horizontal ion transport which itself is determined by the temporal and spatial structure of the convective electric field.

Why are layers observed at lower altitudes than predicted by current theory, when the electric field is directed to the northwest?
Answer: The altitude of layer formation depends upon the ion-neutral collision frequency. The induced-dipole model for the collision frequency, which is used in ionospheric studies, appears to yield values that are too large by a factor of approximately ten. This could account for the discrepancy between theory and observations.

To what extent do thin ion layers drift horizontally?
Answer: Theory suggests that layers in a NW electric field should drift due (magnetic) west with speeds on the order of hundreds of meters per second, while layers in SW fields should tend to drift parallel to the horizontal component of the electric field, with speeds under 100 m/s. The observations generally support this theoretical prediction.

What is the typical horizontal dimension of high-latitude thin ion layers?
Answer: Only the layer extent along the geomagnetic meridian could be observed in this study; this typically ranged from 50 to 150 km. Since the density threshold for layer detection was quite high, $\sim 10^5$ cm^{-3}, these observations could indicate either truly narrow layers, or patches of enhanced density in a broader, less dense thin layer.

Is there a seasonal variation in the occurrence of thin layers?
Answer: The observations strongly suggest that layers over Sondrestrom form more frequently during the summer months. This is probably attributable to a annual variation in the structure of the convective electric field, an effect which is most noticeable when the IMF is northward.

6.2 Discussion of the Main Conclusions

6.2.1 Failure of Layers to Occur. An electric field with strength greater than approximately 10 mV/m will normally dominate the effect of the neutral wind on ion motion. If such a field is directed to the magnetic northwest or southwest, a layer should form. That layers are not always observed when a "proper" electric field is present, is an indication of a localized deficiency in the metallic ion population (or conversely, the occurrence of layers could be attributable to an enhancement in the ion population). An evaluation of the meteoric deposition of metals and of metallic chemistry revealed that these processes proceed too slowly to affect the ion population on time-scales of less than several days. This suggests that large-scale horizontal transport of ions is responsible for determining whether a sufficient number of ions are present at a given place and time to form a detectable layer.

Based on simple conceptual arguments, it has been shown that metallic ions can be transported upward into the F-region from the background metal layer (formed by meteoroid ablation at altitudes between 90 and 100 km) by easterly directed electric fields which typically occur on the dayside. The effects of increasing geomagnetic inclination and gravity combine to force these ions, regardless of their initial latitude, into a stream with a nominal thickness of about 25 km, centered between altitudes of 225 and 300 km (this corresponds well with satellite observations of Fe^+ in the F-region reported by Grebowsky and Pharo [1985]), which flows nearly horizontally over the polar cap. When this stream of ions encounters an electric field with a westerly component it will be forced downward, and ions will be deposited in the E-region within a relatively narrow band of magnetic latitudes. The actual structure of the convective electric field dictates when and where the ions "precipitate" into the E-region, thus defining region(s) of enhanced ion population, and hence where layers are more likely to form. A demonstration of the above concept using a realistic model of the summertime convective field, predicted layer occurrence at Sondrestrom which agreed quite well with the observations.

6.2.2 Altitude of Layer Formation. The simple one-dimensional theory of layer formation shows that when the electric field is directed in the northwest quadrant, ions converge from above and below to form a layer at the altitude of a null in the vertical velocity profile. Once an ion-neutral collision frequency model is adopted, the altitude of convergence is a function only of the direction of the electric field, with the altitude decreasing as the electric field becomes more westerly directed. When the conventional collision frequency model (which assumes an induced dipolar interaction between ions and neutrals) is used, theoretically predicted layer altitudes are 10-20 km higher than those actually observed. Adoption of a collision frequency smaller by a factor of approximately ten, brings the theory and observation into agreement. Empirical estimates of the collision frequency were possible for two of the layers observed during this study. They exhibited the correct functional relationship between altitude and field direction, but had values between 0.1 and 0.2 times the standard model. Of course, it is dangerous to draw sweeping conclusions from two data points, nonetheless there is a strong suggestion that the collision frequency now used in ionospheric studies possesses a systematic error, at least when applied in the E-region.

6.2.3 Layer Drift. A theoretical analysis of layer drift indicates that in regions of northwesterly directed electric fields, layers should drift to the magnetic west, if they are located at the altitude of converge (a layer not at the altitude of convergence would drift vertically toward that altitude, with its horizontal drift velocity approaching due west). In southerly fields, layers tend to drift in the direction of the electric field (Pederson motion), due to the high collision frequency at the relatively low altitudes at which these layers form. The magnitude of the drift velocity is proportional to that of the electric field. For northwesterly fields with a magnitude of 50 mV/m, theoretically predicted drift velocities smoothly increase from ~50 m/s for a westerly field, to ~1000 m/s as the field direction approaches due magnetic north. For southerly fields the predicted drift velocity for a 50 mV/m field is ~50 m/s, regardless of the specific direction of the electric field. Experimental determination of the layer drift velocity was only possible for three

layers. In each case the direction of drift was in general agreement with that predicted by theory. Observed drift speeds ranged from ~60 to ~125 m/s. The results of this investigation suggest that advection is non-negligible when investigating the evolution of layer density at some location in the ionosphere. This is especially true for experiments conducted with the instrument pointed in a fixed direction, which as been the case in many of the studies done previously (recall Chapter 1).

6.2.4 Horizontal Extent. No theoretical prediction of the extent of thin layers was attempted in this study; such an effort must await the development of a three-dimensional simulation of metallic ion transport. However, the radar experiment was well-suited for determining the horizontal structure of the layers along the local geomagnetic meridian. It was found that the layers observed during this study had a typical width of 50-150 km. Since the density threshold for the experiment was ~10^5 cm^{-3}, the observed latitudinal extend could result from either layers that are indeed narrow, or from localized enhancements of the ion density on a broader layer of lower (undetectable) density. Whichever the case, the observations suggest that thin layers might be better thought of as thin *patches* of ionization.

6.2.5 Seasonal Variation of Occurrence. Observations were conducted at Sondrestrom monthly from August 1994 through August 1995, with the exception of April and June of 1995. The only months in which layers were observed were May, July, and August. This strongly suggests a seasonal dimension in the occurrence rate of thin layers (at least at Sondrestrom). Based on evaluation of convection patterns derived from Weimer's [1995] empirical model for high-latitude ionospheric electric potentials, it can be seen that on average during the winter months Sondrestrom is outside of the region of strong convective electric fields, when the IMF is directed southward. This implies a decreased likelihood of observing layers, which indeed was observed to be the case.

6.3 Future Work

The results of this investigation suggest several potentially fruitful directions that the study of thin ion layers might take. Some of these are discussed below.

First, the development of a detailed three-dimensional simulation of metallic ion transport would provide a tool necessary for advancing the conceptual model of layer occurrence outlined in Chapter 5. Coupled with a realistic model of the convective electric field, a better understanding of the temporal and spatial distribution of thin layers would be possible.

Second, evidence of a systematic error in the currently accepted theoretical model for the ion-neutral collision frequency demands immediate attention, since the collision frequency is a fundamental parameter in many aspects of ionospheric physics. A two-pronged approach is recommended: a theoretical reevaluation the interaction between ions and neutral molecules; and an extensive observational campaign to confirm the results obtained so far. This effort might well be the most important one to evolve from this thesis.

Finally, it would be interesting to investigate a possible connection between the apparent increased frequency of layer formation during the summer months at high latitudes, and the well-established tendency towards increased summertime layer occurrence at mid-latitudes. The seasonal effect at mid-latitudes has not yet been explained. It is possible that a complex linkage between the large-scale atmospheric circulation and the convective electric field could permit metallic ions to be transported from the polar regions to lower latitudes. This sort of "polar fountain" could serve to enhance the ion population at lower latitudes, thus leading to an increase in observations of layers. At this point this idea is purely speculative, but the results of this thesis imply that large-scale redistribution of metallic ions can play an influential role in determining the location and time of the occurrence of thin metallic layers.

References

Axford, W.I., The formation and vertical movement of dense ionized layers in the ionosphere due to neutral wind shears. J. Geophys. Res. **68**, 769-779, 1963.

Axford, W.I., Cunnold, D.M., The wind-shear theory of temperate zone sporadic E. Radio Sci. **1**, 191-198, 1966.

Baggaley, W.J., Steel D.I., The seasonal structure of ionosonde E_s parameters and meteoroid deposition rates. Planet. Space Sci. **32**, 1533-1539, 1984.

Banks, P.M., Kockarts, G., *Aeronomy Part A*, Academic Press, 1973.

Behnke, R.A., Vickrey, J.F., Radar evidence for Fe^+ in a sporadic-E layer. Radio Sci. **10**, 325-327, 1975.

Bowles, K.L., Observations of vertical incidence scatter from the ionosphere at 41 Mc/s. Phyys. Rev. Lett. **1**, 454-455, 1958.

Bristow, W.A., Watkins, B.J., Numerical simulation of the formation of thin ionization layers at high latitudes. Geoph. Res. Lett. **18**, 404-407, 1991.

Bristow, W.A., *The Formation and Characteristics of E-region Thin Ionization Layers at High Latitudes*. Doctoral thesis, University of Alaska Fairbanks, 1992,

Bristow, W.A., Watkins, B.J, Incoherent scatter observations of thin ionization layers at Sondrestrom. J. Atmos. Terr. Phys. **55**, 873-894, 1993.

Bronshten, V.A., *Physics of Meteoric Phenomena*, Reidel, 1983.

Brown, T.L., The chemistry of metallic elements in the ionosphere and mesosphere. Chem. Rev. **73**, 645-667, 1973.

Chimonas G., Axford, W.I., Vertical movement in temperate-zone sporadic E layers. J. Geophys. Res. **73**, 111-117, 1968.

Chimonas G., Enhancement of sporadic E by horizontal transport within the layer. J. Geophys. Res. **76**, 4578-4586, 1971.

Chiu, Y.T., Self-consistent electrostatic field mapping in the high-latitude ionosphere. J. Geophys. Res. **79**, 2790-2802, 1974.

Constantinides, E., Bedinger, J.F., Observed redistribution of E-region ionization by neutral winds. J. Atmos. Terr. Phys. **33**, 461-472, 1971.

de la Beaujardière, O., Wickwar, V., Leger,C., McCready, M., Baron, M., *The Software System for the Chatanika Incoherent-scatter Radar* (revised technical report for SRI project 8358). SRI International, Menlo Park, California, 1984.

Dougherty, J.P., Farley, D.T., The theory of incoherent scattering of radio waves by a plasma. Proc. Roy. Soc. (London) **A259**, 79-99, 1960.

Dungey, J.W., Effect of a magnetic field on turbulence in an ionized gas. J. Geophys. Res. **64**, 2188-2191, 1959.

Elford, W.G., Olsson-Steel, D., The height distribution of radio meteors: observations at 6 Mhz. J. Atmos. Terr. Phys. **50**, 811-818, 1988.

Evans, J.V., Theory and practice of ionospheric study by thomson scatter radar. Proc. IEEE **57**, 496-529, 1969.

Farley, D.T., A theory of electrostatic fields in a horizontally stratified ionosphere subject to a vertical magnetic field. J. Geophys. Res. **64**, 1225-1233, 1959.

Farley, D.T., Multiple-pulse incoherent-scatter correlation function measurements. Radio Sci. **7**, 661-666, 1972.

Fejer, J., Scattering of radiowaves by an ionized gas in thermal equilibrium. J. Geophys. Res. **65**, 2635-2636, 1960.

From, W.R., Whitehead, J.D., On the peculiar shape of sporadic E clouds. J. Atmos. Terr. Phys. **40**, 1025-1032, 1978.

Geller, M.A., Smith, L.G., Voss, H.D., Analysis of nighttime E-region winds and ionization production. Radio Sci. **10**, 335-345, 1975.

Gordon, W.E., Incoherent scattering of radio waves by free electrons with applications to space exploration by radar. Proc. IRE **46**, 1824-1829, 1958.

Gray, R.W., Farley, D.T., Theory of inchoerent-scatter measurements using compressed signals. Radio Sci. **8**, 123-131, 1973.

Greenberg, J.M., in *Comets* (ed. Wilkenning, L.L.), University of Arizona Press, 1982.

Greenwald, R.A., Weiss, W., Nielson, E., Thomson, N.R., STARE: A new radar auroral backscatter experiment in northern Scandinavia. Radio Sci. **10**, 357, 1978.

Grebowsky, J.M., Pharo, M.W., The source of midlatitude metallic ions at F-region altitudes. Planet. Space Sci. **33**, 807-812, 1985.

Gustafsson, G., Papitashvili, N.E., Papitashvili, V.O., A revised corrected geomagnetic coordinate system for epochs 1985 and 1990. J. Atmos. Terr. Phys. **54**, 1609-1631, 1992.

Hallinan, T.J., Stenbaek-Nielson, H.C., Deehr, C.S., Enhanced aurora. J. Geophys. Res. **90**, 8461-8475, 1985.

Harvey, G.A., Elemental abundance determination of meteors by spectroscopy. J. Geophys. Res. **73**, 3913, 1973.

Hedberg, A., Seasonal variations in the correlation of meteors and sporadic E. J. Atmos. Terr. Phys. **38**, 785-788, 1976.

Hedin, A.E., Extension of the MSIS thermospheric model into the middle and lower atmosphere. J. Geophys. Res. **96**, 1159-1172, 1991.

Hedin, A.E., Biondi, M.A., Burnside, R.G., Hernandez, G., Johnson, R.M., Killeen, T.L., Mazaudier, C., Meriwether, J.W., Salah, J.E., Sica, R.J., Smith, R.W., Spenser, N.W., Wickwar, V.B., Virdi, T.S., Revised global model of thermospheric winds using satellite and ground-based observations. J. Geophys. Res. **96**, 7657-7688, 1991.

Hess, G.C., Geller, M.A., Aeronomy Report 74. Aeronomy Laboratory, Department of Electrical and Computer Engineering, University of Illinois, Urbana, 1976.

Horowitz, J.L., *Radar Measurements of Electric Fields in the High-Latitude Ionosphere and other Topics in Auroral Physics*. Doctoral Thesis, University of California San Diego, 1976.

Hughes, D.W., Meteor spectra and meteoroid composition. Nature **244**, 538, 1973.

Hughes, D.W., "Meteors," in *Cosmic Dust* (ed. McDonnell, J.A.M.), John Wiley and Sons, pp. 123-185, 1978.

Hughes, D.W., McBride, N., The mass of meteor streams. Mon. Not. R. astr. Soc. **240**, 73-79, 1989.

Hughes, D.W., Stephenson, D.G., The diurnal variation in the mass distribution of sporadic meteors. Mon. Not. R. astr. Soc. **155**, 403-413, 1972.

Hunten, D.M., Turco, R.P., Toon, O.B., Smoke and dust particles of meteoric origin in the mesosphere and stratosphere. J. Atmos. Sci. **37**, 1342-1357, 1980.

Huuskonen, A., Nygrén, T., Jalonen, L., Bjørnå, N., Hansen, T.L., Brekke, A., Turunen, T., Ion composition in sporadic E layers measured by the EISCAT UHF radar. J. Geophys. Res. **93**, 14603-14610, 1988.

Istomin, V.G., Ions of extra-terrestrial origin in the earth ionosphere. Space Res. **3**, 209-220, 1963.

Kane T.J., Gardner, C.S., Structure and seasonal variability of the nighttime mesospheric Fe layer at midlatitudes. J. Geophys. Res. **98**, 16875-16866, 1993a.

Kane T.J., Gardner, C.S., Lidar observations of the meteoric deposition of mesospheric metals. Science **259**, 1297-1300, 1993b.

Kelley, J.D., *The Sondrestrom Incoherent-scatter Radar Facility—Research, Operation, and Coordination* (annual report for SRI Project 7117). SRI International, Menlo Park, California, 1990.

Kirkwood, S., Collis, P.N., Gravity wave generation of simultaneous auroral sporadic-E layers and sudden sodium layers. J. Atmos. Terr. Phys. **51**, 259-269, 1989.

Kirkwood, S., von Zahn, U., On the role of auroral electric fields in the formation of low altitude sporadic-E and sudden sodium layers. J. Atmos. Terr. Phys. **53**, 389-407, 1991.

Kresákova, M., Kresák, L., *Contr. Astr. Obs. Skalnate Pleso* **1**, 40, 1955.

Lebedinets, V.N., Manochina, A.V., Shushkova, V.B., Interaction of the lower thermosphere with the solid component of the interplanetary medium. Planet. Space Sci. **21**, 1317-1332, 1973.

Lovell, A.C.B., *Meteor Astronomy*, Oxford University Press, 1954.

Mason, B., *Handbook of Elemental Abundances in Meteorites*, Gordan and Breach, 1971.

Mathews, J.D., Bekeny, F.S., Upper atmospheric tides and the vertical motion of ionospheric sporadic layers at Arecibo. J. Geophys. Res. **84**, 2743-2750, 1979.

Mathews, J.D., Morton, Y.T., Zhou, Q., Observations of ions layes during the AIDA campaign. J. Atmos. Terr. Phys. **55**, 447-457, 1993.

Miller, K.L., Smith, L.G., Horizontal structure of midlatitude sporadic-E layers observed by incoherent scatter radar. Radio Sci. **10**, 271-276, 1975.

Miller, K.L., 1995

Mozer, F.S., Serlin, R., Magnetospheric electric field measurements with balloons. J. Geophys. Res. **74**, 4739-4754, 1969.

Narcisi, R.S., Bailey, A.D., Mass spectrometer measurements of positive ions at altitudes from 64 to 112 kilometers. J. Geophys. Res. **70**, 3687-3700, 1965.

Narcisi, R.S., "Composition Studies of the Lower Ionosphere," in *Physics of the Upper Atmosphere* (ed. Veriani, F.), Editrice Compositori Publisher, pp. 12-59, 1971.

Nicol, E.J., MacFarlane, J., Hawkes, R.L., Residual mass from atmospheric ablation of small meteoroids. Planet. Space Sci. **33**, 315-320, 1985.

Nygrén, T., Jalonen, L., Oksman, J., Turunen, T., The role of electric field and neutral wind direction in the formation of sporadic E-layers. J. Atmos. Terr. Phys. **46**, 373-381, 1984a.

Nygrén, T., Jalonen, L., Huuskonen, A., Turunen, T., Density profiles of sporadic E-layers containing two metal ion species. J. Atmos. Terr. Phys. **46**, 885-893, 1984b.

Olsson-Steel, D., Elford, W.G., The height distribution of radio meteors: observations at 2 Mhz. J. Atmos. Terr. Phys. **49**, 243-258, 1987.

Öpik, E.J., *Physics of Meteor Flight in the Atmosphere*, Interscience, 1958.

Piggott, W.R., Rawer, K., *URSI Handbook of Ionogram Interpretation and Reduction.* Elsevier Publishing Company, 1961.

Plane J.M.C., The chemistry of meteoric metals in the Earth's upper atmosphere. Int. Rev. Phys. Chem. **10**, 55-106, 1991.

Plane, J.M.C, "Laboratory studies of the chemistry of meteoric metals," in *Chemical Kinetics* (ed. Compton, G.G. and Hancock, G.), Elsevier, pp. 313-367, 1994.

Potter, D., *Computational Physics*, John Wiley and Sons, 1973.

Rees, M.H., *Physics and Chemistry of the Upper Atmosphere*, Cambridge University Press, 1989.

Rose, G., Schlegel, K., Rinnert, K., Kohl, H., Nielson, E., Dehmel, G., Friker, A., Lübken, F.-J., Lühr, H., Neske, E., Steinweg, A., The ROSE project. Scientific objectives and discussion of first results. J. Atmos. Terr. Phys. **54**, 657-667, 1992.

Sida, D.W., The production of ions and electrons by meteoritic processes. Mon. Not. R. astr. Soc. **143**, 37-47, 1969.

Sinno, K., On the time delay of the appearance of sporadic E following meteor activity. J. Atmos. Terr. Phys. **42**, 35-39, 1980.

Slattery, J.C., Friichtenicht, J.F., Ionization probability of iron particles at meteoric velocities. Astrophys. J. **140**, 235-244, 1967.

Swider, W., Processes for meteoric elements in the E-region. Planet. Space Sci. **17**, 1233-1246, 1969.

Smith, E.K., Temperate zone sporadic-E maps ($f_oE_s > 7$ Mhz). Radio Sci. **13**, 571-575, 1978.

Smith, L.G., Mechtly, E.A., Rocket observations of sporadic-E layers. Radio Sci. **7**, 367-376, 1972.

Southworth, R.B., Sekanina, Z., Physical and dynamical studies of meteors. NASA Contractor Report CR-2316, 16, 1973.

Steel, D.I., Elford, W.G., The height distribution of radio meteors: comparison of observations at different frequencies on the basis of standard echo theory. J. Atmos. Terr. Phys. **53**, 409-417, 1991.

Steinweg, A., Krankowsky, D., Lämmerzahl, P., Anweiler, B., Metal layers in the auroral E-region measured by mass spectrometers. J. Atmos. Terr. Phys. **54**, 703-714, 1992.

Swider, W., Processes for meteoric elements in the E-region. Planet. Space Sci. **17**, 1233-1246, 1969.

Trísková, L., On the seasonal variation in the temperate E_s occurrence. J. Atmos. Terr. Phys. **36**, 861-869, 1974.

Turunen, T., Nygrén, T., Huuskonen, A., Nocturnal high-latitude E-region in winter during extremely quiet conditions. J. Atmos. Terr. Phys. **55**, 783-795, 1993.

Turunen, T., Siién, J., Nygrén, T., Jalonen, L., Observation of a thin E_s-layer by the EISCAT radar, Planet. Space Sci. **33**, 1407-1416, 1985.

Weimer, D.R., Models of high-latitude electric potentials derived with a least error fit of spherical harmonic coefficients. J. Geophys. Res. **100**, 19595-19607, 1995.

Weiss, A.A., The distribution and orbits of sporadic meteors. Aust. J. Phys. **10**, 77, 1957.

Whitehead, J.D., The formation of the sporadic-E layer in the temperate zones. J. Atmos. Terr. Phys. **20**, 49-58, 1961.

Whitehead, J.D., Mixtures of ions in the wind-shear theory of sporadic-E. Radio Sci. **1**, 198-203, 1966.

Whitehead, J.D., Recent work on mid-latitude and equatorial sporadic-E. J. Atmos. Terr. Phys. **51**, 401-424, 1989.

Zbinden, P.A., Hidalgo, M.A., Eberhardt, P., Geiss, J., Mass spectrometer measurements of the positive ion composition in the D- and E-regions of the ionosphere. Planet. Space Sci. **23**, 1621-1642, 1975.